



**Politecnico
di Torino**

Department of Mechanical and Aerospace Engineering

Master Degree Course in Aerospace Engineering

Master's Degree Thesis

Parametrized numerical analysis of hypersonic flow field

SUPERVISORS:

prof. Domenic D'AMBROSIO
Salvatore ESPOSITO

STUDENT:

Alberto PALMIERI
(matr. 301528)

DECEMBER 2023

Abstract

Since the end of World War II the interest in high-velocity aerodynamic technologies has grown significantly and research in hypersonic flows has become a strategic field of study. These developments have led to the engineering of heat shields used atmospheric entry modules, providing thermal protection to the crew and space probes, but also to the design of scramjet propulsion system. Clearly the military industry has got a substantial support in the production of long range and high speed weapons, such as hypersonic cruise missiles. Experimental analysis remains a fundamental pillar in design and test processes of hypersonic technologies, however this approach requires appropriate testing facilities which have significant operational costs. Several numerical methods have been developed in the last decades in order to properly simulate high-supersonic and reacting flows, providing a reliable tool suitable to investigate hypersonic regime. In this work has been analysed the flow field around a cone-like axisymmetric shape, using the Siemens' commercial Computational Fluid Dynamics (CFD) code, STAR-CCM+. Firstly, a comprehensive theoretical background has been widely described with a focus on high temperature effects, which characterize hypersonic flow regime. Then, an essential code has been written in order to properly calculate air equilibrium condition at different temperatures and pressures. It allows to freely choose which chemical species must be included in the calculations; nevertheless its use has been limited to examine Earth's multispecies atmospheric models. This procedure allowed to identify the thermodynamic conditions, at equilibrium, under which the gas dissociation and ionization occur. Lastly, a proper parametric numerical study of the hypersonic flow field around a cone-like body has been completed. The physical model adopted in these simulations included a seven species air model. The computational domain also includes a large portion of cone's wake in order to highlight how plasma evolves as it is transported downstream. The parameters chosen for this analysis were the free stream air properties established by the standard Earth's atmosphere model and the free stream Mach number. A steady state numerical simulation has been carried out for each pair of altitude-Mach number, ensuring an appropriate convergence of the solution.

Contents

Abstract	iii
List of Figures	xi
List of Tables	xiii
List of Fundamental Physical Constants	xv
List of Symbols	xvii
List of Subscripts and Superscripts	xxi
List of Acronyms	xxiii
Introduction	1
1 Physical models and general theoretical framework	3
1.1 Thermodynamic principles	3
1.1.1 Perfect and real gas models	4
1.1.2 Dalton's law and other state equation forms	5
1.1.3 First and second laws of thermodynamics	8
1.1.4 Reciprocity relations and specific heat capacities	9
1.1.5 Classification of gases	10
1.1.6 Gibbs free energy and equilibrium in multicomponent gas	12
1.2 Statistical thermodynamic description	16
1.2.1 Energy modes	16
1.2.2 States, macrostates and microstates	18
1.2.3 The Boltzmann distribution	19
1.2.4 Thermodynamic properties	19
1.2.5 Equilibrium constant	24
1.2.6 Heat of formation, sensible heat and standard state	25
1.3 Non-equilibrium	27
1.3.1 Chemical non-equilibrium	27
1.3.2 Damköler number	29
1.3.3 Vibrational non-equilibrium	29
1.4 General formulation of governing equation in hypersonic flows	30
1.4.1 Navier-Stokes equations	31
1.4.2 Navier-Stokes for non-equilibrium and reacting flow	31

2	Air models	35
2.1	Classification	35
2.1.1	Five species air model	36
2.1.2	Seven species air model	37
2.1.3	Nine species air model	38
2.1.4	Eleven species air model	40
2.1.5	Thirteen species air model	42
2.1.6	Numerical method	43
2.2	Single element-made species equilibrium behaviour	44
2.3	Air models chemical equilibrium analysis	54
2.3.1	Temperature-Pressure analysis	54
2.3.2	Results and observations	54
3	Computational fluid dynamic simulation	65
3.1	Geometry	65
3.1.1	Meshing operations	66
3.1.2	Mesh refinement	66
3.2	Physical model selection	69
3.2.1	Complex chemistry, multi-component gas, chemical reactions and transport properties	69
3.2.2	Boundary conditions	70
3.2.3	Initial condition	71
3.3	Simulation cases	71
4	Simulation results	75
4.1	Global parameters	75
4.1.1	Post-shock conditions	75
4.1.2	Maximum pressure, temperature and density	80
4.1.3	Drag coefficient	80
4.1.4	Stand-off distance	82
4.2	Reacting flow	83
4.2.1	Ions formation	83
4.2.2	Polynomial comparison	84
4.3	Limitations of numerical model	84
5	Conclusions	93
A	Standard Earth's atmosphere models	95
A.1	Geo-potential and geometric altitudes	95
A.2	Atmosphere composition	97
A.3	Physical characterization of the Earth's atmosphere	97
A.3.1	Vertical temperature gradient	97
A.3.2	Pressure	99
A.3.3	Density	100
B	Thermochemical properties	105
B.1	Chemical mechanism file format	105
B.2	Thermodynamic properties	105
B.2.1	Seven coefficients polynomials	105
B.2.2	Nine coefficients polynomials	106
B.3	Input file examples	106

Bibliography

109

List of Figures

1.1	qualitative representation of the inter-molecular force variation [1, adapted].	4
1.2	real gas behaviour compared to ideal gas using Van der Waals equation of state for molecular nitrogen and oxygen.	6
1.3	sign convention for heat and work exchanges between a generic closed thermodynamic system and the surroundings [1, adapted].	8
1.4	degrees of freedom for a molecule [1].	16
1.5	energy modes [1].	17
1.6	qualitative representation of number of microstates over macrostates [1]. . .	18
1.7	non-dimensional molar heat capacity at constant pressure of N_2 [16, 10]. . .	22
1.8	non-dimensional molar heat capacity at constant pressure of NO [16, 10]. .	22
1.9	non-dimensional molar heat capacity at constant pressure of Ar [16].	23
1.10	non-dimensional molar heat capacity at constant pressure of O^+ [16].	23
2.1	chemical equilibrium at $p = 1$ bar for N_2, N mixture.	45
2.2	chemical equilibrium at $p = 1$ bar for N_2, N, N^+, e^- mixture.	46
2.3	chemical equilibrium at $p = 1$ bar for N_2, N, N_2^+, e^- mixture.	47
2.4	chemical equilibrium at $p = 1$ bar for N_2, N, N_2^+, N^+ mixture.	48
2.5	chemical equilibrium at $p = 1$ bar for O_2, O mixture.	49
2.6	chemical equilibrium at $p = 1$ bar for O_2, O, O^+, e^- mixture.	50
2.7	chemical equilibrium at $p = 1$ bar for O_2, O, O_2^+, e^- mixture.	51
2.8	chemical equilibrium at $p = 1$ bar for O_2, O, O_2^+, O^+, e^- mixture.	52
2.9	chemical equilibrium at $p = 1$ bar for Ar, Ar^+, e^- mixture.	53
2.10	chemical equilibrium at $p = 1$ bar for five species air model, initial molar fraction, $\chi_{N_2} = 0.79, \chi_{O_2} = 0.21$	55
2.11	chemical equilibrium at $p = 1$ bar for seven species air model, initial molar fraction, $\chi_{N_2} = 0.79, \chi_{O_2} = 0.21$	56
2.12	chemical equilibrium at $p = 1$ bar for nine species air model, initial molar fraction, $\chi_{N_2} = 0.79, \chi_{O_2} = 0.21$	57
2.13	chemical equilibrium at $p = 1$ bar for eleven species air model, initial molar fraction, $\chi_{N_2} = 0.79, \chi_{O_2} = 0.21$	58
2.14	chemical equilibrium at $p = 1$ bar for thirteen species air model, initial molar fraction, $\chi_{N_2} = 0.78, \chi_{O_2} = 0.21, \chi_{Ar} = 0.01$	59
2.15	dissociated species at equilibrium condition for the thirteen species air model.	60
2.16	main ionized species at equilibrium condition for the thirteen species air model.	61
2.17	NO and NO^+ at equilibrium condition for the thirteen species air model. .	62
2.18	plasma at equilibrium condition for the thirteen species air model.	63
3.1	side view of the cone-like geometry [21].	65
3.2	CAD geometry.	66

3.3	full domain starting mesh.	67
3.4	mesh refined at nose ($M_\infty = 14$, $Z_a = 30$ km).	67
3.5	mesh refinement level at nose ($M_\infty = 14$, $Z_a = 30$ km).	68
3.6	mesh refined in the cone wake ($M_\infty = 14$, $Z_a = 30$ km).	68
3.7	mesh refinement level in the cone wake ($M_\infty = 14$, $Z_a = 30$ km).	68
3.8	full domain with boundary conditions.	70
3.9	nose domain with boundary conditions.	70
3.10	initial velocity field ($M_\infty = 8$, $Z_a = 30$ km).	72
4.1	post-shock pressure ratio at different Mach numbers and altitudes.	76
4.2	post-shock temperature ratio at different Mach numbers and altitudes.	76
4.3	post-shock density ratio at different Mach numbers and altitudes.	77
4.4	maximum pressure at different Mach numbers and altitudes.	77
4.5	maximum temperature at different Mach numbers and altitudes.	78
4.6	maximum density at different Mach numbers and altitudes.	78
4.7	wall pressure distribution for $M = 16$ and $Z_a = 20$ km.	79
4.8	wall temperature distribution for $M = 16$ and $Z_a = 20$ km.	79
4.9	maximum wall temperature at different Mach numbers and altitudes.	80
4.10	drag coefficient at different Mach numbers and altitudes.	81
4.11	drag coefficient on modified scale.	81
4.12	simulation shock stand-off distances at different Mach numbers and altitudes.	82
4.13	NO^+ maximum number density at different Mach numbers and altitudes.	84
4.14	maximum NO^+ plasma frequency at the outlet at different Mach numbers and altitudes.	85
4.15	NO , NO^+ molar fraction and temperature along stagnation streamline for simulation case $M_\infty = 16$ and $Z_a = 20$ km.	86
4.16	NO (solid) and NO^+ (dashed) molar fractions at longitudinal symmetry axis at $Z_a = 20$ km and varying Mach number.	87
4.17	NO (solid) and NO^+ (dashed) molar fractions at longitudinal symmetry axis at $Z_a = 30$ km and varying Mach number.	87
4.18	NO (solid) and NO^+ (dashed) molar fractions at longitudinal symmetry axis at $Z_a = 50$ km and varying Mach number.	88
4.19	NO (solid) and NO^+ (dashed, not displayed, molar fraction lower than 1×10^{-8}) molar fractions at longitudinal symmetry axis at $Z_a = 70$ km and varying Mach number.	88
4.20	species molar fraction along stagnation streamline for $M_\infty = 16$ and $Z_a = 20$ km.	89
4.21	comparison of maximum NO^+ number density using different thermodynamic properties polynomials $Z_a = 20$ km (BR - Burcat [4]; GP - Gupta [11]; MB - McBride [16]).	89
4.22	comparison between heat capacity polynomial fits of N_2 [16, 11, 4].	90
4.23	Mach number, $M_\infty = 16$ and $Z_a = 20$ km.	90
4.24	temperature, $M_\infty = 16$ and $Z_a = 20$ km.	91
4.25	pressure, $M_\infty = 16$ and $Z_a = 20$ km.	91
4.26	NO^+ number density, $M_\infty = 16$ and $Z_a = 20$ km.	91
4.27	electron number density, $M_\infty = 16$ and $Z_a = 20$ km.	92
4.28	electron number density, $M_\infty = 14$ and $Z_a = 50$ km.	92
A.1	Earth's atmospheric structure [25].	96
A.2	temperature vertical distribution [18].	101
A.3	pressure vertical distribution [18].	101

A.4	density vertical distribution [18].	102
A.5	extended temperature vertical distribution [17].	102
A.6	extended pressure vertical distribution [17].	103
A.7	extended density vertical distribution [17].	103

List of Tables

2.1	initial composition of air models at 298.15 K.	35
2.2	five species air model, formation matrix.	36
2.3	seven species air model, formation matrix.	37
2.4	nine species air model, formation matrix.	39
2.5	eleven species air model, formation matrix.	40
2.6	thirteen species air model, formation matrix.	42
3.1	simulation cases.	73
3.2	standard atmosphere free-stream boundary conditions.	74
A.1	dry, clean air composition near sea level [18].	98
A.2	temperatures and vertical temperature gradients [17, 18].	99

List of Fundamental Physical Constants

Constant	Symbol	Value	Unit (SI)
Earth's gravitational normal acceleration constant [17, 18]	g_0	9.80665	m s^{-2}
reduced Planck constant	\hbar	1.054×10^{-34}	J s
Boltzmann constant	k_B	$1.380\,649 \times 10^{-23}$	J K^{-1}
dry air molar mass [18]	\mathcal{M}_0	28.964 420	kg kmol^{-1}
Avogadro constant	N_A	$6.022\,57 \times 10^{23}$	mol^{-1}
dry air gas constant [18]	R_0	287.052 87	$\text{J kg}^{-1} \text{K}^{-1}$
effective Earth's radius [12]	r_0	$6.356\,766 \times 10^6$	m
universal gas constant	\mathcal{R}	8.31432	$\text{J mol}^{-1} \text{K}^{-1}$
Stefan-Boltzmann constant	σ	$5.670\,37 \times 10^{-8}$	$\text{W m}^{-2} \text{K}^{-4}$

List of Symbols

Symbol	Description	Unit (SI)
A	pre-exponent of Arrhenius modified eq.	$\text{cm}^3 \text{mol}^{-1} \text{s}^{-1}$
β	temperature exponent of Arrhenius modified eq.	-
C	concentration	kmol m^{-3}
c	mass fraction	-
χ	mole fraction	-
C_p	molar heat capacity for a constant pressure process	$\text{J kmol}^{-1} \text{K}^{-1}$
c_p	specific heat capacity for a constant pressure process	$\text{J kg}^{-1} \text{K}^{-1}$
C_v	molar heat capacity for a constant volume process	$\text{J kmol}^{-1} \text{K}^{-1}$
c_v	specific heat capacity for a constant volume process	$\text{J kg}^{-1} \text{K}^{-1}$
Da	Damköhler number	-
ε	energy of a particle	J
\mathcal{E}_a	activation energy of Arrhenius modified eq.	J kmol^{-1}
G	Gibbs free energy	J
\mathcal{G}	molar Gibbs free energy	J kmol^{-1}
γ	heat capacity ratio	-
g_a	local gravitational acceleration	m s^{-2}
$\Delta_f \mathcal{H}$	molar enthalpy of formation	J kmol^{-1}
$\Delta_f h$	specific enthalpy of formation	J kg^{-1}
\mathcal{H}	molar enthalpy	J kmol^{-1}
h	specific enthalpy	J kg^{-1}
Z_a	geo-potential altitude	m

Symbol	Description	Unit (SI)
z_a	geometric altitude	m
k	reaction rate	$\text{cm}^3 \text{mol}^{-1} \text{s}^{-1}$
K_c	concentration equilibrium constant	kmol m^{-3} or adimensional
Kn	Knudsen number	-
K_p	pressure equilibrium constant	Pa or adimensional
k_t	thermal conductivity	$\text{W m}^{-1} \text{K}^{-1}$
Φ	heat flux	W m^{-2}
M	Mach number	-
\mathcal{M}	molar mass	kg kmol^{-1}
M	mass	kg
η	mole-mass ratio	kmol kg^{-1}
$\hat{\mu}$	chemical potential	J mol^{-1}
μ	dynamic viscosity	$\text{kg m}^{-1} \text{s}^{-1}$
\mathcal{V}	molar volume	$\text{m}^3 \text{mol}^{-1}$
\mathcal{N}	number of moles	mol
n	number density	m^{-3}
N	number of particles	-
ν	stoichiometric mole number	-
p	pressure	Pa
Φ_g	gravity potential	$\text{m}^2 \text{s}^{-2}$
Q	heat	J
q	specific heat	J kg^{-1}
Re	Reynolds number	-
R	gas constant	$\text{J kg}^{-1} \text{K}^{-1}$
ρ	density	kg m^{-3}
S	entropy	J K^{-1}
\mathcal{S}	molar entropy	$\text{J K}^{-1} \text{kmol}^{-1}$
s	specific entropy	$\text{J K}^{-1} \text{kg}^{-1}$
x	space coordinate	m
\hat{i}	unit vector	-
t	time	s

Symbol	Description	Unit (SI)
τ	characteristic time	s
T	temperature	K
H	enthalpy	J
U	internal energy	J
\mathcal{U}	molar internal energy	J kmol ⁻¹
u	specific internal energy	J kg ⁻¹
V	volume	m ³
v	specific volume	m ³ kg ⁻¹
\mathbf{v}	velocity vector	m s ⁻¹
v	velocity component	m s ⁻¹
W	work	J
w	specific work	J kg ⁻¹

List of Subscripts and Superscripts

Symbol	Description
elr	electronic mode
e	element
eq	equilibrium
b	backward (reaction rate)
f	forward (reaction rate)
∞	free stream condition
0	ground state energy level
<i>ie</i>	<i>i</i> -th element
<i>js</i>	<i>j</i> -th species
irrev	irreversible process
<i>is</i>	<i>i</i> -th species
prd	product(s)
rct	reactant(s)
ref	reference state or value
rev	reversible process
rtn	rotational mode
vbr	vibrational mode
sens	sensible energy
s	species
o	standard state or value
trn	translational mode

List of Acronyms

Acronym	Description
CAD	Computer-Aided Design
CFD	Computational Fluid Dynamics
COESA	Committee on Extension to the Standard Atmosphere
DOF	Degree of Freedom
ICAO	International Civil Aeronautical Organization
MSL	Mean Sea Level
N-S	Navier-Stokes equations
NACA	National Advisory Committee for Aeronautics
STAR-CCM+	Computational Fluid Dynamics software developed by Siemens Digital Industries Software (Simulation of Turbulent flow in Arbitrary Regions - Computational Continuum Mechanics)

Introduction

Compressible flows are generally characterized by their Mach number, a non-dimensional parameter that measure velocity magnitude compared to the speed of sound. Focussing only on *supersonic* flows, which means that the free stream Mach number is greater than one, hypersonic regime, commonly speaking, involves flows that has a Mach number greater than five. Conversely to subsonic and supersonic flows, that have a rigorous definition and different behaviours, in hypersonic flow regime are considered phenomenon that are not relevant at relatively low supersonic Mach numbers, for example multi-component reacting gasses and high temperature phenomenon. Numerical approaches are usually cheaper than direct measurements but they are also more challenging since the models used are extremely complex. This thesis work is subdivided as follows:

- in the first chapter a general theoretical background is presented, with a main focus on high temperature effect and reacting flows;
- the second chapter describes the air models commonly used and provides a detailed description of their chemical equilibrium condition and plasma production;
- in the third chapter a numerical modelling approach using STAR-CCM+ is reported with an application example on a test geometry;
- the fourth chapter reports numerical results of all simulated cases.

Chapter 1

Physical models and general theoretical framework

This first proper chapter aims to briefly develop some fundamental concepts of thermodynamics and gas dynamics that are relevant in the description in high Mach number and high temperature flow field. Firstly, all necessary thermodynamic variables are introduced, in the second place chemical equilibrium and non-equilibrium for reacting flows are explained. Finally, a complete and general system of equation that describe a multi-chemical reacting gaseous mixture are reported at the end of this part. Furthermore, the high temperature effects, that surely have repercussions on hypersonic dynamics, are widely take into consideration. The main bibliographic references consulted while writing this chapter are [10, 1, 8, 26, 9, 5].

1.1 Thermodynamic principles

The notion of *thermodynamic system* refers to a specific portion of space, delimited by an abstract enclosure, that divide anything inside of it from the surrounding environment. Whatever is contained by this conceptual closed surface is considered part of the system itself. Systems can exchange matter and/or energy (classically heat and work, but also radiation), therefore they can be classified as follows:

Isolated systems: neither energy nor matter can be exchanged;

Closed systems: only energy can be exchanged;

Open systems: both matter and energy can be exchanged.

The thermodynamic system considered in this work is a homogeneous mixture of different gaseous species. The state of a given system in a specific point in time is totally determined when all its *state variables* (e.g. temperature T , pressure p , internal energy U , enthalpy H , entropy S , ...). More specifically, *thermodynamic equilibrium* is a peculiar state where each of its state variable do not change with time: in this case the thermodynamic state of the system is fully determined by knowing two of its state variables¹. Indeed, in a more formal way, all state variables are not independent. For this reason a general *equation of state* can be written as follows:

$$f(p, V, T) = 0.$$

¹this consideration is related to the Gibbs phase rule.

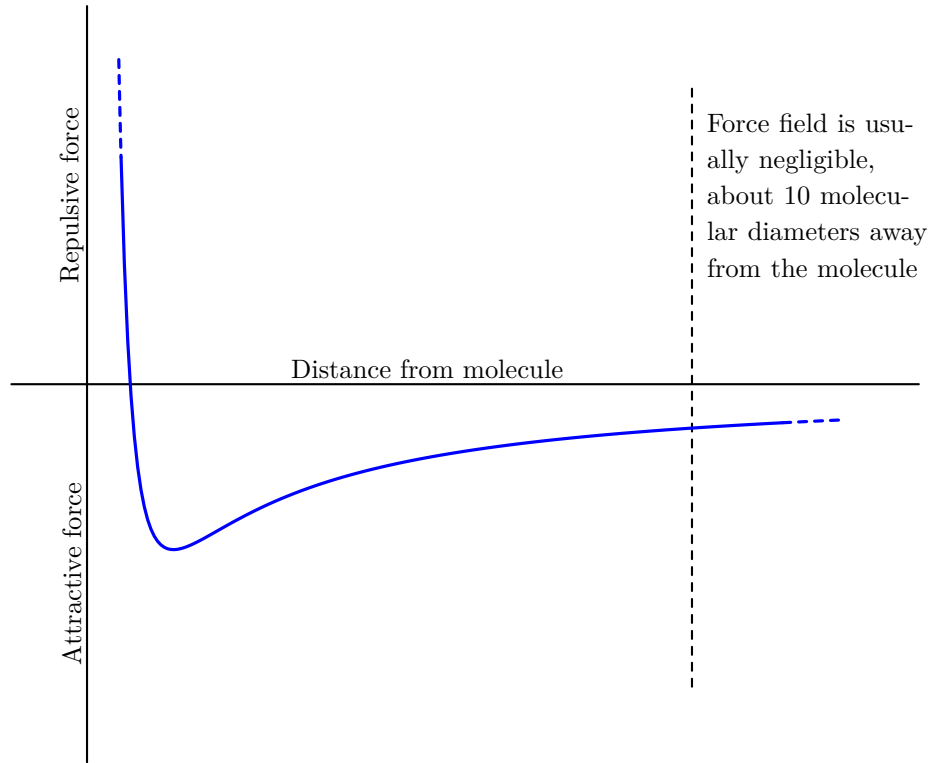


Figure 1.1: qualitative representation of the inter-molecular force variation [1, adapted].

The form of the equation of state depends on the properties of the specific substance that were considered.

1.1.1 Perfect and real gas models

Usually, a so called *perfect gas*, is a gaseous mixture whose behaviour, always considering an equilibrium state of the system, is described by the *perfect-gas* state equation:

$$pV = \mathcal{N}\mathcal{R}T. \quad (1.1)$$

By definition, inside a perfect gas inter-molecular forces do not play an important role, for that reason can be neglected. Inter-molecular forces are the result of electromagnetic phenomenons that take place between subatomic components of a particle. A schematic representation of the force field of an isolated particle is shown in figure 1.1. Conversely, in a *real gas* inter-molecular forces must be taken into consideration. Equation (1.1) becomes inaccurate when a gas has extremely high pressure and/or low temperature (obviously higher of its critical value). A more accurate equation of state that take into account real gas effects is the following:

$$\left[p + a \left(\frac{\mathcal{N}}{V} \right)^2 \right] \left(\frac{V}{\mathcal{N}} - b \right) = \mathcal{R}T \quad (1.2)$$

where

$$a = \frac{27}{64} \frac{\mathcal{R}^2 T_c^2}{p_c}$$

$$b = \frac{1}{8} \frac{\mathcal{R} T_c}{p_c}$$

indicating with the c subscript the *critical point* values of the specific substance considered (e.g. critical point of molecular nitrogen gas has $T_c \approx 126$ K and $p_c \approx 3.39 \times 10^6$ Pa whereas molecular oxygen gas $T_c \approx 155$ K and $p_c \approx 5.05 \times 10^6$ Pa). Equation (1.2) improves equation (1.1) introducing two additional factors that rectify the macroscopic state variables: the former correction is due to the intermolecular force effect that cause a reduction in the measurable effective pressure (for this reason it is incremented by a pressure-correction factor), the latter correction consider the volume of the particles and subtract it from the measured volume. In figure 1.2 can be observed that, as it has been foretold earlier, under certain condition of temperature and pressure the equation (1.1) is not accurate. Using the equation (1.1) is a reasonable approximation for a generic hypersonic flow inside Earth's atmosphere:

- the gas downstream of a shock wave has an increase in both pressure and temperature compared to free flow conditions;
- free flow pressure decreases monotonically with the rising of altitude.

For these reasons the lower right part of plots in figure 1.2 is hardly achievable.

1.1.2 Dalton's law and other state equation forms

Equation (1.1) is generic and does not take into account what the actual components of the gas considered are, obviously when the gas is composed of at least two different gaseous species. Considering a fixed volume V and temperature T condition, the *partial pressure* of the i -th chemical specie is defined as follows:

$$p_{is} := \frac{\mathcal{N}_{is} \mathcal{R} T}{V},$$

where \mathcal{N}_{is} is the number of moles of the i -th species. It follows that

$$\sum_{is} p_{is} = \frac{\mathcal{R} T}{V} \sum_{is} \mathcal{N}_{is} = \frac{\mathcal{N} \mathcal{R} T}{V} = p,$$

therefore

$$\sum_{is} p_{is} = p, \tag{1.3}$$

which it is known as *Dalton's law*.

Equation (1.1) can be written in different forms, involving also others physical quantities. This means that it is better to use one specific variable rather than another depending on the context. Some common physical quantities are the following:

- the concentration of i -th species, $C_{is} := \mathcal{N}_{is}/V$:

$$p_{is} = C_{is} \mathcal{R} T;$$

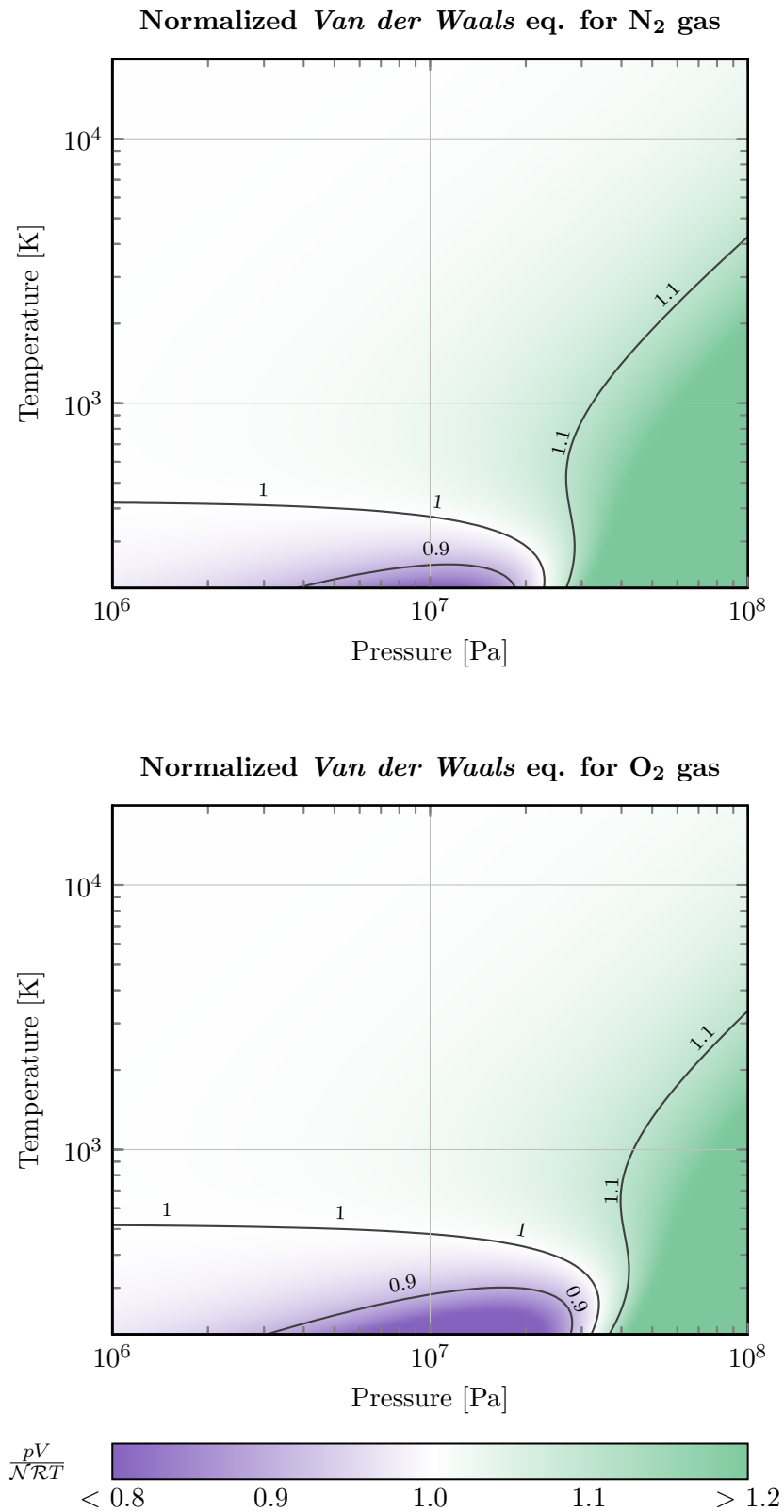


Figure 1.2: real gas behaviour compared to ideal gas using Van der Waals equation of state for molecular nitrogen and oxygen.

- the mole molar volume of the i -th species, $\mathcal{V} := V/\mathcal{N}_{is}$:

$$p_{is}\mathcal{V} = \mathcal{R}T;$$

- the specific volume of i -th species, $v_{is} := V/M_{is}$, and the density of i -th species, $\rho_{is} := v_{is}^{-1}$:

$$p_{is}v_{is} = R_{is}T, \quad p_{is} = \rho_{is}R_{is}T,$$

where

$$R_{is} = \frac{\mathcal{R}}{\mathcal{M}_{is}};$$

- the mole-mass ratio of the i -th species, $\eta := \mathcal{N}_{is}/M$:

$$p_{is}v = \eta_{is}\mathcal{R}T;$$

- the number density of the i -th species, $n_{is} := N_{is}/V = \mathcal{N}_{is}N_A/V$:

$$p_{is} = n_{is}k_B T;$$

where

$$k_B = \frac{\mathcal{R}}{N_A}$$

is the *Boltzmann constant*.

Other two non-dimensional variables should be mentioned:

- the mole fraction, $\chi := \mathcal{N}_{is}/\mathcal{N} = p_{is}/p$;
- the mass fraction, $c := M_{is}/M = \rho_{is}/\rho$.

Both of them have the same property, which arise from their definition:

$$\sum_{is} \chi_{is} = 1, \quad \sum_{is} c_{is} = 1.$$

From the ratio between equation (1.1) for the i -th chemical species and the same one but for the entire gaseous mixture, it is possible to get the following formulation:

$$\chi_{is} = c_{is} \frac{R_{is}}{R} = c_{is} \frac{\mathcal{M}}{\mathcal{M}_{is}},$$

which lead to

$$R = \sum_{is} c_{is} R_{is} = \frac{1}{\sum_{is} \chi_{is}/R_{is}};$$

$$\mathcal{M} = \sum_{is} \chi_{is} \mathcal{M}_{is} = \frac{1}{\sum_{is} c_{is}/\mathcal{M}_{is}}.$$

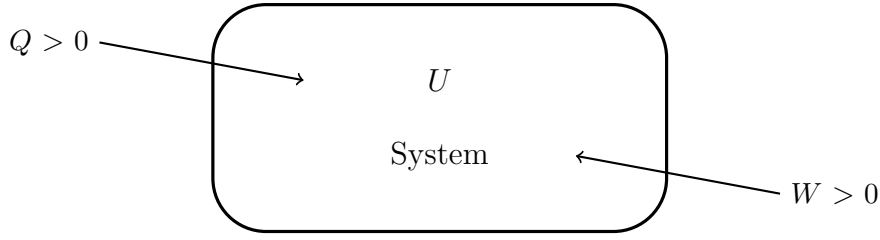


Figure 1.3: sign convention for heat and work exchanges between a generic closed thermodynamic system and the surroundings [1, adapted].

1.1.3 First and second laws of thermodynamics

Considering two generic equilibrium states of a system, the former (1) and the latter (2), the *first law* asserts that the variation of internal energy of the considered system, $\Delta U = U_2 - U_1$, is equal to the net heat and work exchanged between the system and the rest of the universe (in a broad sense):

$$\Delta U = \Delta Q + \Delta W,$$

or using specific quantities

$$\Delta u = \Delta q + \Delta w.$$

Usually the first law of thermodynamics is written by using differential operators:

$$du = \delta q + \delta w, \quad (1.4)$$

where the operator δ is commonly known as imperfect (or inexact) differential, meaning that its integral evaluation depends on its specific integration path $\gamma_{1,2}$. Integrating equation (1.4) between the initial state 1 and the final state 2 through the path $\gamma_{1,2}$ leads to the following form:

$$u_2 - u_1 = \int_{\gamma_{1,2}} \delta q + \int_{\gamma_{1,2}} \delta w.$$

The *second law* of thermodynamics asserts that for isolated systems always holds this expression:

$$ds \geq 0;$$

the equal symbol is valid if and only if *reversible processes* occur inside the system itself. A reversible process occurs when each state of the thermodynamic system between the initial and final states is an equilibrium state. Clearly this kind of transformations are extremely idealized but they allow to obtain relevant equations. A more generic form of the previous equation is the following:

$$ds = \frac{\delta q_{\text{rev}}}{T} + ds_{\text{irrev}}. \quad (1.5)$$

Thus, a reversible process satisfy

$$ds = \frac{\delta q_{\text{rev}}}{T}.$$

Considering a closed thermodynamic system, the following equivalence statements apply to reversible processes:

$$\begin{aligned}\delta q_{\text{rev}} &= T ds; \\ \delta w_{\text{rev}} &= -p dv.\end{aligned}$$

These formulations combined in equation (1.4) lead to

$$du = T ds - p dv \quad (1.6)$$

and

$$dh = T ds + v dp \quad (1.7)$$

where the specific enthalpy h is defined as $u + pv$.

1.1.4 Reciprocity relations and specific heat capacities

As seen previously, when equilibrium condition is reached the thermodynamic state of a system is defined by two (independent) state variables. For this reason is possible to write that $u = u(T, v)$ and $s = s(T, v)$. Using equation (1.6) it possible to get this first reciprocity equation:

$$\frac{\partial u}{\partial v} = -p + T \frac{\partial p}{\partial T}. \quad (1.8)$$

Similarly, writing that $h = h(T, p)$ and $s = s(T, p)$ the second reciprocity relation can be easily obtained:

$$\frac{\partial h}{\partial p} = v - T \frac{\partial v}{\partial T}. \quad (1.9)$$

For a perfect gas both u and h are function of temperature only, this because

$$\begin{aligned}\frac{\partial u}{\partial v} &= 0; \\ \frac{\partial h}{\partial p} &= 0;\end{aligned}$$

(these results can be derived following a comprehensive mathematical procedure found in B. Grossman's lecture notes [10]). Specific heats for gases are defined based on what kind of thermodynamic transformation undergone by the gas itself. They quantify the change in energy, per unit of mass, as the temperature increases by a unit value. For a *constant volume transformation*

$$\Delta q = \int_1^2 \frac{\partial u}{\partial T}(T, v) dT = \int_1^2 c_v(T, v) dT, \quad (1.10)$$

while for a *constant pressure transformation*

$$\Delta q = \int_1^2 \frac{\partial h}{\partial T}(T, p) dT = \int_1^2 c_p(T, p) dT. \quad (1.11)$$

A previously written, for perfect gasses both the specific heat capacities depends only from the temperature. There are important significant relations between this two specific heat capacities:

- the *heat capacity ratio*, γ

$$\gamma := \frac{c_p}{c_v}; \quad (1.12)$$

- the following equation, taken directly from Anderson's textbook [1],

$$c_p - c_v = \left(\frac{\partial u}{\partial v} + p \right) \frac{\partial v}{\partial T} \quad (1.13)$$

tells that exist a relation between the two specific heat capacities. Also, this expression works for both perfect and real gasses and, furthermore, in reacting mixtures: it is a general mathematical relation. Assuming as valid the perfect and non-reacting gas state equation (1.1), the equation (1.13) becomes

$$c_p - c_v = R$$

that is a well known result.

1.1.5 Classification of gases

It is possible to identify different categories of gases; this kind of differentiation is based on how gases behave in different thermodynamic conditions. The nomenclature used in this classification may be different depending on the scientific or technical field of study. Anderson's textbook [1] proposes the following arrangement.

Calorically perfect gas

A calorically perfect gas behaves as described by equation (1.1) in equilibrium conditions (as a consequence of being a perfect gas). A further hypothesis consist in assuming both the specific heat capacities as constants that depend on the chemical nature of the gas itself. Thus equations (1.10) and (1.11) degenerate in a much simpler equation:

$$h = c_p T,$$

$$u = c_v T.$$

Since c_p and c_v are constant, also their ratio γ and their difference R still also constant regardless of the thermodynamic state of the system.

Thermally perfect gas

In this case the equation (1.1) still holds, but both specific heat capacities are no longer constant: both of them are function of temperature. As written in section 1.1.4 in a

perfect gas h and u depend only from T , thus for a thermally perfect gas

$$dh = c_p(T) dT,$$

$$du = c_v(T) dT.$$

Since equation (1.1) holds, and for what is written in section 1.1.4, γ and $c_p - c_v$ still constant.

Chemically reacting mixture of perfect gases

For a chemically reacting mixture of perfect gases it is necessary to specify if the mixture has reached the chemical equilibrium condition or not. For a generic *non-equilibrium* state of a reacting mixture made up of n species it is possible to write that

$$h = f_h(T, p, \mathcal{N}_1, \mathcal{N}_2, \dots, \mathcal{N}_n);$$

$$u = f_u(T, p, \mathcal{N}_1, \mathcal{N}_2, \dots, \mathcal{N}_n);$$

$$c_p = f_{c_p}(T, p, \mathcal{N}_1, \mathcal{N}_2, \dots, \mathcal{N}_n);$$

$$c_v = f_{c_v}(T, p, \mathcal{N}_1, \mathcal{N}_2, \dots, \mathcal{N}_n).$$

Clearly the evolution of the gaseous mixture in general is a time-dependent process and each number of particles of the i -th species depend on how the fluid has evolved in previous time steps. The chemical equilibrium condition does not depend on time: as a thermodynamic equilibrium condition the state of the system is uniquely defined by two state variables:

$$h = f_h(T, p);$$

$$u = f_{1,u}(T, p) = f_{2,u}(T, v);$$

$$c_p = f_{c_p}(T, p);$$

$$c_v = f_{1,c_v}(T, p) = f_{2,c_v}(T, v).$$

As a mixture of perfect gases, equation (1.1) still holds. R in this case is no more a constant but depend on the mixture composition.

Real gas

Finally, this last scenario considers a real gas (Anderson further simplifies this case considering a non reacting gas), therefore equation (1.1) is no longer valid and more complex state equations should be used (e.g. equation (1.2)). Now specific heat capacities are not only temperature dependent but they need another state variable to be fully defined:

$$h = f_h(T, p);$$

$$u = f_{1,u}(T, p) = f_{2,u}(T, v);$$

$$c_p = f_{c_p}(T, p);$$

$$c_v = f_{1,c_v}(T, p) = f_{2,c_v}(T, v).$$

1.1.6 Gibbs free energy and equilibrium in multicomponent gas

The *Gibbs free energy*, G , is a thermodynamic variable defined as follows:

$$G = H - TS. \quad (1.14)$$

Considering a generic non-equilibrium process for what has been written previously, the Gibbs free energy of a reacting multispecies mixture depends not only from two independent thermodynamic state variables (as pressure and temperature) but also by how the mixture is composed:

$$G = f_G(T, p, \mathcal{N}_1, \mathcal{N}_2, \dots, \mathcal{N}_n).$$

where n is the number of chemical species involved in the process. Then, its differential is the following:

$$dG = \frac{\partial G}{\partial T} dT + \frac{\partial G}{\partial p} dp + \sum_{is} \frac{\partial G}{\partial \mathcal{N}_{is}} d\mathcal{N}_{is}. \quad (1.15)$$

Differentiating equation (1.14) leads to this result:

$$dG = dH - T dS - S dT.$$

Since

$$dS = \frac{dH}{T} - \frac{V}{T} dp + dS_{\text{irrev}},$$

than

$$dG = V dp - S dT - T dS_{\text{irrev}}. \quad (1.16)$$

Comparing equations (1.15) and (1.16), the partial derivatives of G have a clearer meaning:

$$\begin{aligned} \frac{\partial G}{\partial T} &= -S; \\ \frac{\partial G}{\partial p} &= V; \\ \sum_{is} \frac{\partial G}{\partial \mathcal{N}_{is}} d\mathcal{N}_{is} &= -T dS_{\text{irrev}}. \end{aligned}$$

From the last equation can be pointed out the *chemical potential*:

$$\hat{\mu}_{is} = \frac{\partial G}{\partial \mathcal{N}_{is}}. \quad (1.17)$$

Now, the change in entropy caused by irreversible processes that occur in a thermodynamic transformation can be quantified. This equation,

$$dS_{\text{irrev}} = -\frac{1}{T} \sum_{is} \hat{\mu}_{is} d\mathcal{N}_{is}, \quad (1.18)$$

allows to assert that if the thermodynamic transformation is reversible ($dS_{\text{irrev}} = 0$), then the chemical equilibrium is reached in each succession of states of the system. Equation (1.18) is a key equation for chemical equilibrium calculation, however it can be rewritten in a more functional way. Since G is an extensive variable, introducing its molar quantity \mathcal{G} , it follows that the Gibbs free energy of the entire gaseous mixture can be written as follows:

$$G = \sum_{is} \mathcal{G}_{is} \mathcal{N}_{is}.$$

Thus

$$\frac{\partial G}{\partial \mathcal{N}_{is}} = \mathcal{G}_{is}$$

and in equilibrium conditions equation (1.18) becomes

$$\sum_{is} \mathcal{G}_{is} d\mathcal{N}_{is} = 0. \quad (1.19)$$

Now, the *stoichiometric mole number*, ν , is introduced: it indicates how many moles of a chemical species is involved in a specific reaction. If ν_{is} is positive means that the i -th species is a product, otherwise a reactant. Therefore a generic chemical reaction can be written as an algebraic statement,

$$\sum_{is} \nu_{is} A_{is} = 0,$$

where A_{is} is a generic chemical species. It can be observed that $d\mathcal{N}_{is}$ and ν_{is} are somehow connected; indeed for a generic process that involve n species can be shown that

$$\frac{dN_1}{\nu_1} = \frac{dN_2}{\nu_2} = \dots = \frac{dN_n}{\nu_n} = d\xi$$

where ξ is a non-dimensional number which is a common factor that express the degree of advancement of the chemical reaction. Hence, equation (1.19) finally becomes

$$\sum_{is} \nu_{is} \mathcal{G}_{is} = 0. \quad (1.20)$$

It is relevant to say that for a given process, all the quantities involved in equation (1.20) are known. For stoichiometric mole numbers it is quite obvious (since the chemical reactions involved are fully recognized in the considered process) whereas \mathcal{G}_{is} is derived from experimental data. From the definition of Gibbs free energy (in an extensive way), equation (1.14) can also be written for a single species of the mixture and “normalized” with the number of moles of the same chemical species:

$$\mathcal{G}_{is} = \mathcal{H}_{is} - T\mathcal{S}_{is}. \quad (1.21)$$

Similarly to equation (1.7)

$$d\mathcal{H}_{is} = T d\mathcal{S}_{is} + \nu_{is} dp_{is}$$

the molar entropy for the i -th species can be derived as follows:

$$d\mathcal{S}_{is} = \frac{d\mathcal{H}_{is}}{T} - \mathcal{R} \frac{dp_{is}}{p_{is}}.$$

Since a thermally perfect gas is considered both molar internal energy and molar enthalpy differentials can be written in the following form:

$$d\mathcal{U}_{is} = \mathcal{C}_{v, is}(T) dT;$$

$$d\mathcal{H}_{is} = \mathcal{C}_{p, is}(T) dT;$$

and it ends to

$$d\mathcal{S}_{is} = \mathcal{C}_{p, is} \frac{dT}{T} - \mathcal{R} \frac{dp_{is}}{p_{is}}. \quad (1.22)$$

The integration of equation (1.22) is an easy task and, considering an arbitrary initial reference state, it is possible to get that

$$\mathcal{S}_{is} = \int_{T_{ref}}^T \mathcal{C}_{p, is}(T) \frac{dT}{T} - \mathcal{R} \ln\left(\frac{p_{is}}{p_{ref}}\right) + \mathcal{S}_{is, ref}. \quad (1.23)$$

Being that the entropy of a mixture can be expressed as the sum of the entropy of the i -th species multiplied by its molar fraction,

$$\mathcal{S} = \sum_{is} \chi_{is} \mathcal{S}_{is},$$

the entropy for a generic multicomponent mixture can be written:

$$\mathcal{S} = \sum_{is} \chi_{is} \left[\int_{T_{ref}}^T \mathcal{C}_{p, is}(T) \frac{dT}{T} - \mathcal{R} \ln\left(\frac{p_{is}}{p_{ref}}\right) \right] + \mathcal{S}_{ref}. \quad (1.24)$$

Now, it is possible to substitute equation (1.23) inside equation (1.21):

$$\mathcal{G}_{is} = \mathcal{H}_{is} - T \left[\int_{T_{ref}}^T \mathcal{C}_{p, is}(T) \frac{dT}{T} - \mathcal{R} \ln\left(\frac{p_{is}}{p_{ref}}\right) + \mathcal{S}_{is, ref} \right].$$

Can be observed that

$$\mathcal{G}_{is} = \mathcal{G}_{is}(T, p),$$

since a thermally perfect gas mixture is involved, both \mathcal{G}_{is} and the integral in dT are only temperature dependent. For this reason it is possible to separate the contribution of temperature and pressure:

$$\mathcal{G}_{is}(T, p_{is}) = \mathcal{H}_{is}(T) - T \left[\int_{T_{ref}}^T \mathcal{C}_{p, is}(T) \frac{dT}{T} - \mathcal{R} \ln\left(\frac{p^\circ}{p_{ref}} \frac{p_{is}}{p^\circ}\right) + \mathcal{S}_{is, ref}(T_{ref}) \right];$$

$$\mathcal{G}_{is}(T, p_{is}) = \mathcal{H}_{is}(T) - T \left[\int_{T_{ref}}^T \mathcal{C}_{p, is}(T) \frac{dT}{T} - \mathcal{R} \ln \left(\frac{p^\circ}{p_{ref}} \right) + \mathcal{S}_{is, ref}(T_{ref}) \right] + T \mathcal{R} \ln \left(\frac{p_{is}}{p^\circ} \right),$$

where the superscript \circ refers to the standard state pressure which, usually, it is 1 bar for gaseous species. The previous equation can be written in a more convenient way

$$\mathcal{G}_{is}(T, p_{is}) = \mathcal{G}_{is}^\circ(T) + T \mathcal{R} \ln \left(\frac{p_{is}}{p^\circ} \right) \quad (1.25)$$

Substituting equation (1.25) into equation (1.20) leads to

$$\sum_{is} \nu_{is} \left[\mathcal{G}_{is}^\circ(T) + T \mathcal{R} \ln \left(\frac{p_{is}}{p^\circ} \right) \right] = 0.$$

Finally, the equilibrium constant K_p can be defined rearranging the previous equation:

$$K_p(T) := \prod_{is} p_{is}^{\nu_{is}} = (p^\circ)^{\sum_{is} \nu_{is}} \exp \left(-\frac{\Delta \mathcal{G}^\circ(T)}{\mathcal{R}T} \right) \quad (1.26)$$

where

$$\mathcal{G}^\circ(T) = \sum_{is} \nu_{is} \mathcal{G}_{is}^\circ(T).$$

Example:

Consider nitrogen dissociation reaction,



where M is a generic third body that is not involved in the process. The equilibrium constant of the reaction is known:

$$K_p(T) = p^\circ \exp \left(-\frac{2\mathcal{G}_{\text{N}}^\circ(T) - \mathcal{G}_{\text{N}_2}^\circ(T)}{\mathcal{R}T} \right).$$

Therefore, the chemical composition of a mixture evaluated at some thermodynamic state of equilibrium identified by T_* and p_* should satisfy the following non-linear system of two equation:

$$\begin{cases} p_{\text{N}_2} + p_{\text{N}} = p_* \\ p_{\text{N}}^2 p_{\text{N}_2}^{-1} = K_p(T_*). \end{cases}$$

Should be noted that equilibrium constants are a function of temperature only; nevertheless, pressure plays also a role in defining the concentration in a reacting mixture. As will be discussed later, the Gibbs free energy “functions” are defined as data fits of experimental data (see appendix B).

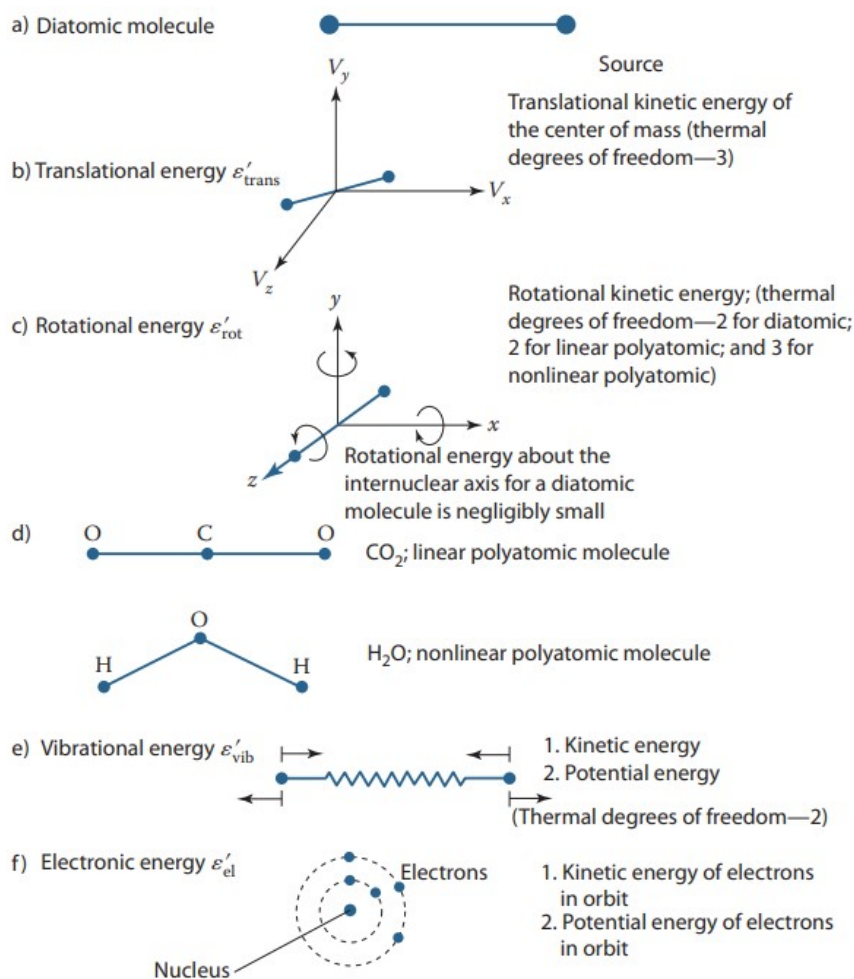


Figure 1.4: degrees of freedom for a molecule [1].

1.2 Statistical thermodynamic description

This section aims to introduce some useful concepts of statistical thermodynamics. A gas can be seen as a generic system of which can be measured its macroscopic thermodynamic variables, such as temperature, pressure, internal energy, ... At the same time it is possible to zoom in and see that each particle has a certain number of *degrees of freedom* DOF. To every degree of freedom is associated a specific *energy mode*.

1.2.1 Energy modes

Consider a diatomic molecule, such as nitrogen gas in its standard state N_2 , and count the number of degrees of freedom of the molecule (figure 1.4):

- it can translate in space and its kinematics could be described using three Cartesian components, hence the DOF is three;
- in a three-dimensional space rotation movements also involve three DOF but with some exceptions. Particles composed of one atom only do not involve any rotational DOF. Linear molecules (e.g. $\text{N}_2, \text{NO}, \text{CO}_2, \text{HCN}, \dots$) have two rotational DOFs. Non-linear polyatomic molecules (e.g. H_2O) have three rotational DOFs;

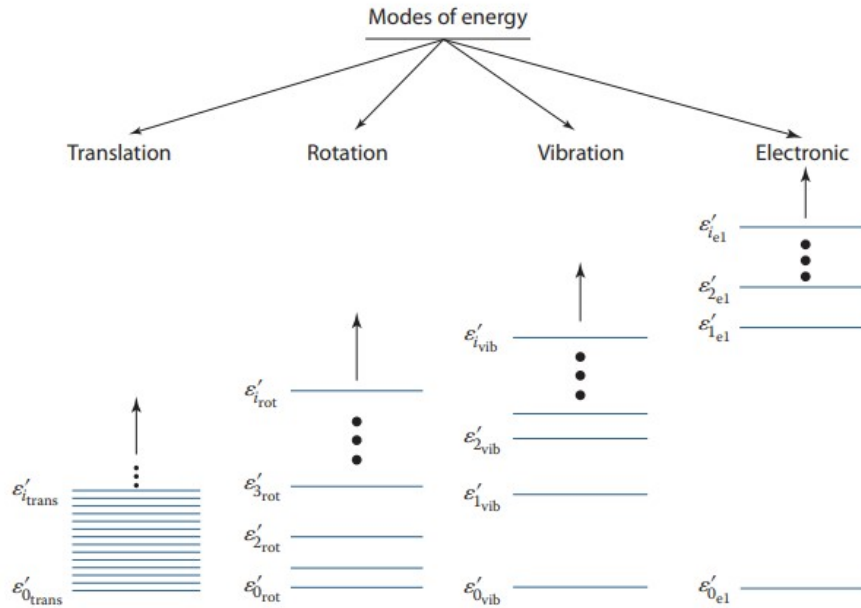


Figure 1.5: energy modes [1].

- all the atoms of a molecule are vibrating around their relative equilibrium position. In this specific case, nitrogen atoms vibrate with respect to each other and the covalent bond that join the two atoms can be modelled as a spring, hence there are two DOFs. Bigger molecules which involve more atomic species and multiple bonds need a more elaborate description, since they involve more than two DOFs.
- finally, also the movement of electrons around atomic nuclei constitute a sort of DOFs. Its description is even more complex and can not be modelled as a mechanical system as it has been done for the previous DOFs.

Thus, it is possible to classify each degree of freedom of the particle based on what kind of mode is involved:

- translation;
- rotation;
- vibration;
- electronic.

From an energetic point of view, the energy of a molecule ε' is the sum of all these four energy modes (figure 1.5):

$$\varepsilon' = \varepsilon'_{\text{trn}} + \varepsilon'_{\text{rtn}} + \varepsilon'_{\text{vbr}} + \varepsilon'_{\text{elr}}.$$

As it has been previously mentioned, species that are made of only an atom have both rotational and vibrational energy mode equal to zero. All energy modes are *quantized*, this means that each mode can reach only specific energy levels; in other words only few discrete levels are allowed. The lowest energy level is called *ground state* and it is defined as follows:

$$\varepsilon'_0 = \varepsilon'_{0\text{trn}} + \varepsilon'_{0\text{vbr}} + \varepsilon'_{0\text{elr}},$$

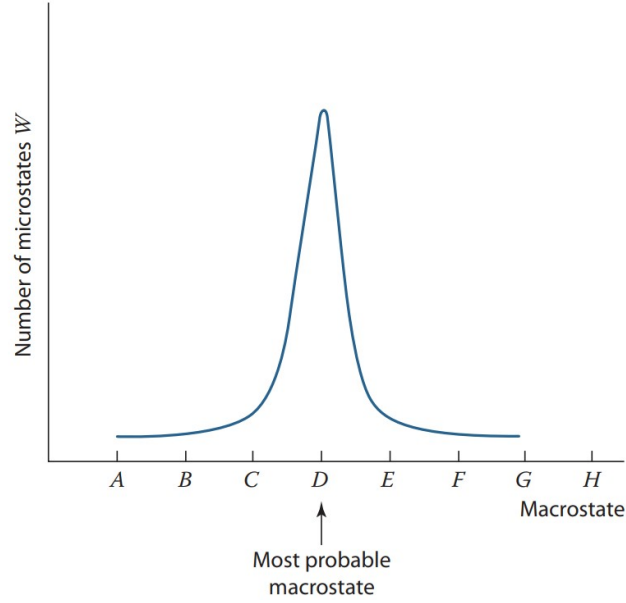


Figure 1.6: qualitative representation of number of microstates over macrostates [1].

it is the energy of an hypothetical particle that has reach the absolute zero temperature and for this reason each ground state energy could be also named as *zero-point energy* (note that $\varepsilon'_{0\text{rtn}} = 0$).

1.2.2 States, macrostates and microstates

Consider a system made of N indistinguishable particles. With the notation N_j indicates the number of particles of the system with energy level ε'_j . A first consideration is the following:

$$N = \sum_j N_j.$$

The energy of the system is

$$U' = \sum_j \varepsilon'_j N_j.$$

It can be noted that N_j change in time, this is due to collisions that happen between the molecules. The term *macrostate* indicate a specific distribution of N_j and the macrostate that occurs for most of the time, *most probable macrostate*, indicates the system configuration at thermodynamic equilibrium. A result of quantum mechanics is that for each energy level ε'_j can exist a certain amount of *distinguishable states*. In other words, g_j (called statistical weight) represents how many states have the energy level ε'_j . This means that if N_j indicates the distribution of energy levels throughout the system regardless what the statistical weight are, the same macrostate can have different *microstates*. The key aspect in order to find the most probable macrostate is to quantify the number of microstates for each macrostate. Since statistical thermodynamics assumes that all microstates have the same probability of occurring, the most probable macrostate is the one that have more microstates (figure 1.6).

1.2.3 The Boltzmann distribution

For temperature far above absolute zero the most probable distribution (so the most probable macrostate), N_j^* , is well described by the Boltzmann distribution

$$N_j^* = N \frac{g_j \exp\left[-\varepsilon'_j/(k_B T)\right]}{\sum_j g_j \exp\left[-\varepsilon'_j/(k_B T)\right]} = N \frac{g_j \exp\left[-\varepsilon_j/(k_B T)\right]}{\sum_j g_j \exp\left[-\varepsilon_j/(k_B T)\right]} \quad (1.27)$$

where

$$\varepsilon'_j = \varepsilon'_0 + \varepsilon_j$$

hence ε_j is the energy level evaluated net of ground state. Defining

$$Q := \sum_j g_j \exp\left[-\varepsilon_j/(k_B T)\right] \quad (1.28)$$

as the *partition function*, equation (1.27) becomes

$$N_j^* = N \frac{g_j \exp\left[-\varepsilon_j/(k_B T)\right]}{Q}. \quad (1.29)$$

Clearly, most of the mathematical steps and crucial observations have been omitted for simplicity, however equation (1.29) describes how the particles of the system are distributed throughout the energy levels in thermodynamic equilibrium condition (e.g. assigned temperature and volume in order to completely describe equilibrium condition).

1.2.4 Thermodynamic properties

The link between statistical description and the well-known macroscopic model is, in terms of sensible quantities,

$$U = \sum_j \varepsilon_j N_j.$$

From equation (1.28), follows that

$$\sum_j g_j \varepsilon_j \exp\left[-\varepsilon'_j/(k_B T)\right] = k_B T^2 \frac{\partial Q}{\partial T}.$$

Hence, the internal energy of the system is

$$U = N k_B T^2 \frac{\partial \ln Q}{\partial T},$$

in terms of molar quantities

$$\mathcal{U} = \mathcal{R} T^2 \frac{\partial \ln Q}{\partial T},$$

or per mass unit

$$u = R T^2 \frac{\partial \ln Q}{\partial T}. \quad (1.30)$$

Therefore, it is necessary a model to properly represent ε'_j . From the quantum mechanic theory, some relevant results are reported below:

- the translational energy mode is

$$\varepsilon'_{\text{trn}} = \frac{\pi^2 \hbar^2}{2m} \sum_{i=1}^3 \frac{n_i^2}{a_i^2}$$

where n_i are quantum numbers (they are integers, e.g. $n_i = 1, 2, \dots$), a_i represents linear dimensions of the system and m the mass of a single particle of the system;

- the rotational energy mode for a diatomic molecule is

$$\varepsilon'_{\text{rtn}} = \frac{\hbar^2}{2I} J(J+1),$$

where J is the rotational quantum number ($J = 1, 2, \dots$) and I the moment of inertia;

- for the vibrational energy mode (again, for a diatomic molecule only), the simpler model is the so called *harmonic oscillator*,

$$\varepsilon'_{\text{vbr}} = 2\pi\hbar \left(n + \frac{1}{2} \right) \nu,$$

where n still a quantum number and, as the previous modes, it can assume integer values and ν is the fundamental vibration frequency of the molecule (it changes from species to species);

- for the electronic energy mode there is not a concise and direct formulation as it was with the above-mentioned.

In terms of sensible energy levels, what it is written above becomes

$$\varepsilon_{\text{trn}} \approx \frac{\pi^2 \hbar^2}{2m} \sum_{i=1}^3 \frac{n_i^2}{a_i^2};$$

$$\varepsilon_{\text{rtn}} = \frac{\hbar^2}{2I} J(J+1);$$

$$\varepsilon_{\text{vbr}} = 2\pi n \hbar \nu;$$

$$\varepsilon_{\text{elr}} = \varepsilon'_{\text{elr}} - \varepsilon'_{0\text{elr}}.$$

From the definition of partition function (equation (1.28)) follows that

$$Q = Q_{\text{trn}} Q_{\text{rtn}} Q_{\text{vbr}} Q_{\text{elr}}.$$

Skipping to final results, it is possible to write the partition functions for each mode:

$$\begin{aligned} Q_{\text{trn}} &= \left(\frac{mk_B T}{2\pi\hbar^2} \right)^{\frac{3}{2}} V; \\ Q_{\text{rtn}} &= \frac{2Ik_B T}{\hbar}; \\ Q_{\text{vbr}} &= \frac{1}{1 - \exp\left(-\frac{2\pi\hbar\nu}{k_B T}\right)}. \end{aligned} \quad (1.31)$$

The partition function for the electronic energy mode, for the reason seen just above, can not be written explicitly:

$$Q_{\text{elr}} = \sum_{l=0}^{+\infty} g_l \exp\left(-\frac{\varepsilon_l}{k_B T}\right).$$

From equation (1.30), since partition function for three modes are known (equation (1.31)), it is possible to write that for a diatomic gas

$$\begin{aligned} u_{\text{trn}} &= \frac{3}{2} RT; \\ u_{\text{rtn}} &= RT; \\ u_{\text{vbr}} &= \frac{\vartheta/T}{\exp(\vartheta/T) - 1} RT; \end{aligned}$$

with

$$\vartheta := \frac{2\pi\hbar\nu}{k_B T}$$

which is called *characteristic temperature of vibration* of the molecule. Therefore, diatomic species have the following specific internal energy expression:

$$u = \frac{3}{2} RT + RT + \frac{\vartheta/T}{\exp(\vartheta/T) - 1} RT + u_{\text{elr}}.$$

Atomic species have not the rotational and vibrational contribution, clearly,

$$u = \frac{3}{2} RT + u_{\text{elr}}.$$

Now specific heat capacities can be written in a more explicit form:

Diatomic molecule

$$\begin{aligned} \frac{c_v}{R}(T) &= \frac{5}{2} + \left\{ \frac{\vartheta/(2T)}{\sinh[\vartheta/(2T)]} \right\}^2 + \frac{1}{R} \frac{\partial u_{\text{elr}}}{\partial T}; \\ \frac{c_p}{R}(T) &= \frac{7}{2} + \left\{ \frac{\vartheta/(2T)}{\sinh[\vartheta/(2T)]} \right\}^2 + \frac{1}{R} \frac{\partial u_{\text{elr}}}{\partial T}; \end{aligned}$$

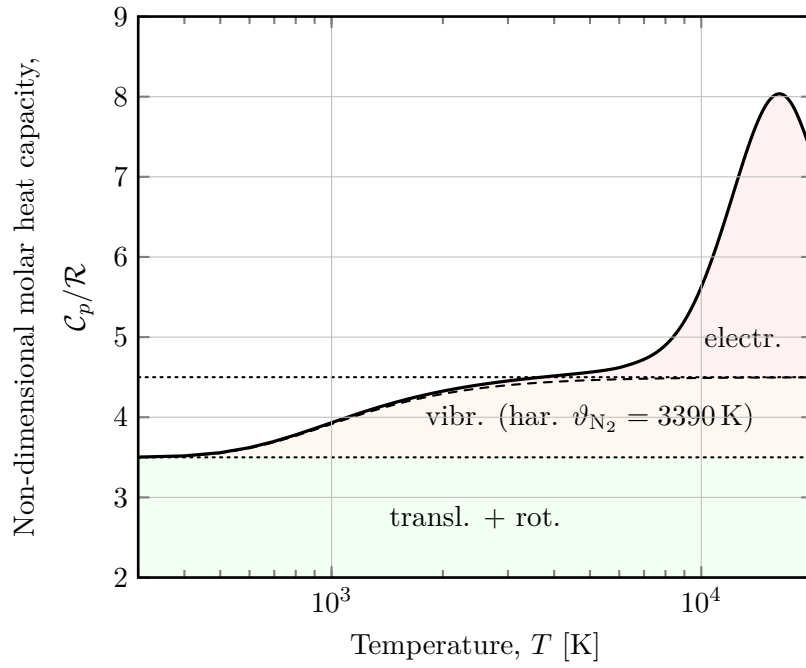


Figure 1.7: non-dimensional molar heat capacity at constant pressure of N_2 [16, 10].

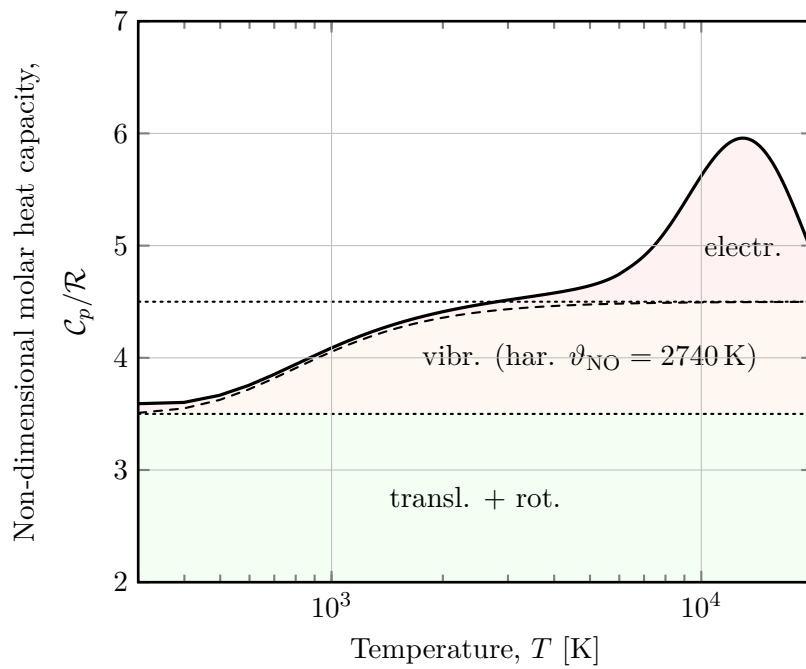


Figure 1.8: non-dimensional molar heat capacity at constant pressure of NO [16, 10].

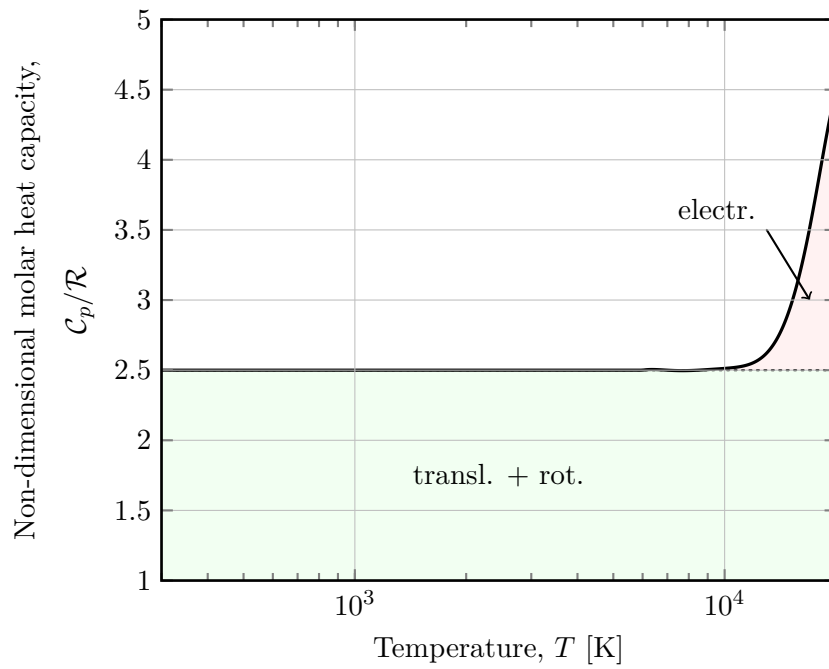


Figure 1.9: non-dimensional molar heat capacity at constant pressure of Ar [16].

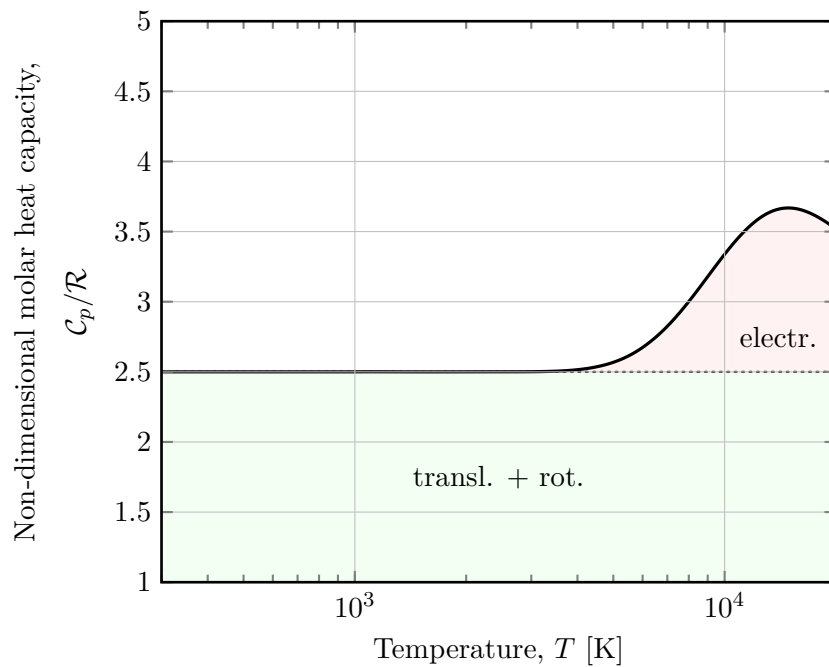


Figure 1.10: non-dimensional molar heat capacity at constant pressure of O^+ [16].

Monoatomic species

$$\frac{c_v}{R}(T) = \frac{3}{2} + \frac{1}{R} \frac{\partial u_{\text{elr}}}{\partial T};$$

$$\frac{c_p}{R}(T) = \frac{5}{2} + \frac{1}{R} \frac{\partial u_{\text{elr}}}{\partial T}.$$

Should be noted that this model is consistent with the thermally perfect gas classification, where internal energy and specific heat capacities were only temperature-dependent. Furthermore, the vibrational term reaches the limit value of RT for $T \rightarrow +\infty$, which is the energy associated to vibrational mode from the classical theory: in fact, the *principle of equipartition of energy* says that at each DOF is associated a specific amount of energy per particle

$$\frac{1}{2}k_B T.$$

Hence, a diatomic molecule mixture from a classical perspective has

$$u_{\text{vbr}} = RT$$

which represent the limiting value that can be reach by the harmonic oscillator model presented above.

1.2.5 Equilibrium constant

The constant equilibrium presented in equation (1.26) has a deeper meaning, in fact can been shown that it comes out from the statistical thermodynamic theory, summarily introduced in the past section. A chemically reacting mixture is taken now into consideration. The practical example reported by Anderson [1] uses generic names to indicate chemical species, so, consider the following reaction:



Should be noted that each species particle has its proper energy level sets, distributions, ground state, ... Since an isolated system in considered, it is possible to write this two equations:

- the energy is constant

$$U_{\text{system}} = \sum_i U^i = \text{const}, \quad i = A, B, AB, \dots;$$

- the number of the i -th nuclei component also remains constant:

$$N_i = \sum_j N_j^i = \text{const}, \quad i = A, B, AB, \dots$$

Where the superscript indicate the chemical species. In the case exemplified:

$$\begin{aligned} U^A + U^B + U^{AB} &= \text{const}; \\ N_A &= \sum_j N_j^A + \sum_j N_j^{AB} = \text{const}; \\ N_B &= \sum_j N_j^B + \sum_j N_j^{AB} = \text{const}. \end{aligned}$$

Since ground levels differ from species to species can be defined $\Delta\varepsilon_0$ as

$$\Delta\varepsilon_0 = \left(\varepsilon'_0\right)_{\text{products}} - \left(\varepsilon'_0\right)_{\text{reactants}},$$

or, more concisely,

$$\Delta\varepsilon_0 = \sum_{is} \nu_{is} \left(\varepsilon'_0\right)_{is}.$$

In equation (1.32) $\Delta\varepsilon_0$ is the following expression:

$$\Delta\varepsilon_0 = \left(\varepsilon'_0\right)_{AB} - \left(\varepsilon'_0\right)_A - \left(\varepsilon'_0\right)_B.$$

Calling back equations (1.27), (1.28) and (1.29), it is possible to write that

$$\frac{N_{AB}}{N_A N_B} = \exp\left(-\frac{\Delta\varepsilon_0}{k_B T}\right) \frac{Q_{AB}}{Q_A Q_B}.$$

Should be noted that partition functions depend on temperature, but also from the volume of the system (equation (1.31)). In section 1.1.2 different form of equation (1.1) were derived, hence it is possible to write that

$$\frac{N_{AB}}{N_A N_B} = \frac{p_{AB}}{p_A p_B} \frac{k_B T}{V},$$

which leads to

$$\frac{p_{AB}}{p_A p_B} = \frac{V}{k_B T} \exp\left(-\frac{\Delta\varepsilon_0}{k_B T}\right) \frac{Q_{AB}}{Q_A Q_B} := K_p(T).$$

The volume V cancels out with the one inside Q , precisely in Q_{trn} , and therefore K_p is only function of temperature. In a general form

$$K_{p, is}(T) = \left(\frac{k_B T}{V}\right)^{\sum_{is} \nu_{is}} \exp\left(-\frac{\Delta\varepsilon_0}{k_B T}\right) \prod_{is} Q_{is}^{\nu_{is}} \quad (1.33)$$

which has the same meaning of equation (1.26).

1.2.6 Heat of formation, sensible heat and standard state

Expressions like *sensible energy levels* and *standard state* have been widely used in previously written paragraphs, but a rigorous definition of what is their actual meaning has not been provided yet.

Sensible energy: consider a kilogram of gas whose enthalpy is h . The existence of a ground energy level u_0 allows the following writing:

$$h = h_{\text{sens}} + u_0,$$

or in terms of internal energy u

$$u = u_{\text{sens}} + u_0.$$

Standard state: it is a thermodynamic state used as reference in order to evaluate other physical properties. For gases the standard pressure p° is 1 bar (old publications, such as [11], uses 1.013 25 bar as reference pressure). In order to fully describe the standard state it has been defined a standard temperature, T° , whose value is 298.15 K. Since thermodynamic properties are temperature dependent, the notation $(\dots)^\circ(T)$ explicitly indicate that the generic property (\dots) is evaluated at standard pressure.

Consider a generic thermodynamic process that involves a enthalpy variation. For a reacting, multispecies gaseous mixture

$$h = \sum_{is} c_{is} h_{is}.$$

Since

$$(h_{\text{sens}})_{is} = h_{is} - (u_0)_{is} = R_{is}T + \underbrace{(u_{\text{trn}})_{is} + (u_{\text{rtn}})_{is} + (u_{\text{vbr}})_{is} + (u_{\text{elr}})_{is}}_{(u_{\text{sens}})_{is}},$$

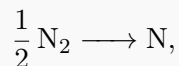
at the end of this hypothetical process

$$\Delta h = \Delta h_{\text{sens}} + \Delta u_0, \quad (1.34)$$

and the quantity Δu_0 can not be measured directly. Now it is necessary to define a new quantity called *standard heat of formation* at standard temperature, $\Delta_f \mathcal{H}_{298.15 \text{ K}}^\circ$, which is the enthalpy variation between a chemical species and its primitive elements in their standard state per mole ($\Delta_f h_{298.15 \text{ K}}^\circ$ is referred to mass unit).

Example:

The formation of atomic nitrogen is described by this reaction:



Should be noticed that N_2 is the form in which pure nitrogen is combined in standard state, hence $(\Delta_f \mathcal{H}_{298.15 \text{ K}}^\circ)_{\text{N}_2} = 0 \text{ J kmol}^{-1}$.

The evaluation of Δu_0 is possible knowing the enthalpy of formation at absolute zero, $\Delta_f h_{0 \text{ K}}^\circ$, which is a tabulated data [11]. Ultimately it is possible to rewrite equation (1.34) as follows:

$$\Delta h = \Delta h_{\text{sens}} + \Delta_f h_{0 \text{ K}}^\circ. \quad (1.35)$$

1.3 Non-equilibrium

The previous sections widely described equilibrium condition for a perfect gas, giving also more information about equilibrium constants, which are a prerequisite to the continuation of this theoretic chapter. In this work two “types” of non-equilibrium are of interest:

Chemical non-equilibrium chemical reactions need a certain amount of time, called *reaction rate* k , in order to achieve their equilibrium;

Vibrational non-equilibrium as it will be explained later, energy transfer between molecules also takes time to happen, particularly vibrational modes, and to reach internal energy equilibrium.

This consideration are crucial in hypersonic flows because it is characterized by strong variations of thermodynamic variables due to shock-waves.

1.3.1 Chemical non-equilibrium

The dissociation of nitrogen is described by the following expression



and it is taken as example for this discussion. In this context it is common to use the notation $[\text{N}_2]$ to indicate the concentration of diatomic nitrogen (C_{N_2}), $[\text{N}]$ indicates C_{N} and so on. Equation (1.36) can be seen as combination of a forward reaction and a backward reaction

Forward reaction:



Backward reaction:



The terms k_f and k_b are respectively the *forward* and *backward reaction rates* of equations (1.37) and (1.38). Focussing on equation (1.37) it is possible to write that

$$\begin{aligned} \frac{d[\text{N}_2]}{dt} &= -k_f [\text{N}_2] [\text{M}]; \\ \frac{d[\text{N}]}{dt} &= 2k_f [\text{N}_2] [\text{M}]; \end{aligned}$$

while for equation (1.38)

$$\begin{aligned} \frac{d[\text{N}_2]}{dt} &= k_b [\text{N}]^2 [\text{M}]; \\ \frac{d[\text{N}]}{dt} &= -2k_b [\text{N}]^2 [\text{M}]. \end{aligned}$$

For a generic reaction, the change in product concentrations is given by this equation

$$\frac{d[X_{is}]}{dt} = (\nu_{js})_{\text{prd}} k_{is}(T) \prod_{js} [X_{js}]^{\alpha_{js}},$$

while for reactants

$$\frac{d[X_{is}]}{dt} = -(\nu_{js})_{\text{rct}} k_{is}(T) \prod_{js} [X_{js}]^{\alpha_{js}};$$

in this case ν_{prd} and ν_{rct} are considered in absolute value and not with a positive sign if it is related to products and negative for reactants. These are also called *laws of mass action* limited to the i -th reaction mechanism. The α_{js} term, in general, is not related to the j -th stoichiometric number but it depends on the overall reaction mechanism. As pointed out in [26], when the process is made of a “elementary, simple, single-step reaction”, it is true that

$$\alpha_{js} = \nu_{js}.$$

In the end, combining forward and backward reactions, it is possible to write the net rates for equation (1.36):

$$\begin{aligned} \frac{d[N_2]}{dt} &= k_b [N]^2 [M] - k_f [N_2] [M]; \\ \frac{d[N]}{dt} &= 2k_f [N_2] [M] - 2k_b [N]^2 [M]. \end{aligned}$$

At equilibrium both net reaction rates should be equal to zero:

$$\begin{aligned} k_b [N]_{\text{eq}}^2 [M]_{\text{eq}} - k_f [N_2]_{\text{eq}} [M]_{\text{eq}} &= 0; \\ k_f [N_2]_{\text{eq}} [M]_{\text{eq}} - k_b [N]_{\text{eq}}^2 [M]_{\text{eq}} &= 0. \end{aligned}$$

It is clear that both equation are the same:

$$\frac{[N]_{\text{eq}}^2}{[N_2]_{\text{eq}}} = \frac{k_f}{k_b}$$

From equation (1.1) follows that

$$K_p = \left(\frac{p_N^2}{p_{N_2}} \right)_{\text{eq}} = \mathcal{R}T \frac{[N]_{\text{eq}}^2}{[N_2]_{\text{eq}}} = \mathcal{R}T \frac{k_f}{k_b} = \mathcal{R}T K_c,$$

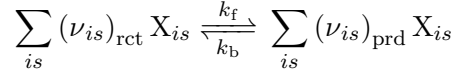
hence

$$K_c = \left(\frac{1}{\mathcal{R}T} \right)^{\sum_{is} \nu_{is}} K_p.$$

It is now clear that k_f and k_b are bonded with the equilibrium constant. Therefore only one of the two should be known. Finally, for equation (1.36) the complete laws of mass action are

$$\begin{aligned} \frac{d[N_2]}{dt} &= -k_f [M] \left\{ [N_2] - \frac{1}{K_c} [N]^2 \right\}; \\ \frac{d[N]}{dt} &= 2k_f [M] \left\{ [N_2] - \frac{1}{K_c} [N]^2 \right\}. \end{aligned}$$

In a general form, an arbitrary chemical reaction



the net rate, given by the law of mass action, is

$$\frac{d[X_{is}]}{dt} = \sum_{is} \left\{ (\nu_{is})_{\text{prd}} - (\nu_{is})_{\text{rct}} \right\} \left\{ k_f \prod_{js} [X_{js}]^{(\nu_{js})_{\text{rct}}} - k_b \prod_{js} [X_{js}]^{(\nu_{js})_{\text{prd}}} \right\}. \quad (1.39)$$

Usually, the forward chemical rate constants can be found in literature [11, 19] as experimental results. Chemical reaction rates are in the so called *Arrhenius modified* form:

$$k_f = AT^\beta \exp\left(\frac{\mathcal{E}_a}{RT}\right). \quad (1.40)$$

1.3.2 Damköler number

Sometimes it is useful to define a parameter that allows to describe roughly the chemical non-equilibrium. The Damköler number can be defined as follows:

$$Da := \frac{\tau_{\text{fluid}}}{\tau_{\text{chemistry}}} \quad (1.41)$$

where τ_{fluid} is the characteristic time of the fluid itself (its magnitude can be ratio between a length and a velocity that distinguish the flow regime, like those used in the Reynolds number) and $\tau_{\text{chemistry}}$ is the one that represent the chemical reaction characteristic time that occurs in the flow field. Two extreme scenarios can be identified:

- $Da \rightarrow 0$: all the chemical reaction are too slow to produce any measurable change in the chemical species of the mixture. This condition is known as *frozen flow*;
- $Da \rightarrow +\infty$: all the chemical reaction are extremely quick if compared with the characteristic time of the flow field and equilibrium composition is reached in any location of the domain.

As example, imagine a infinitesimal control volume ad observe what happens to the molecules inside of it as it is transported by the flow: if a frozen flow is considered all the composition of the gas contained in the control volume will remain constant although all thermodynamic variables changes in the advection process. If $Da \rightarrow +\infty$ as soon as the control volume moves causing changes in therms of thermodynamic state variables inside of it, the mixture reaches immediately its new equilibrium state. Actually, in hypersonic regime none of these condition really happens, it is possible to say that in most of the cases $\tau_{\text{chemistry}} = \mathcal{O}(\tau_{\text{fluid}})$ with is classifiable as non-equilibrium.

1.3.3 Vibrational non-equilibrium

Similarly to chemical non-equilibrium it is possible to analyse vibrational non-equilibrium. As it has previously seen gas particles have different degrees of freedom and when they collide may happen that a transition in terms of energy level occurs. Considering only the vibrational energy levels and assuming that transitions happens between the adjoining ones, for the i -th vibrational energy level holds that

$$\frac{dN_i}{dt} = k_{i+1,i}N_{i+1} + k_{i-1,i}N_{i-1} - k_{i,i+1}N_i - k_{i,i-1}N_i \quad (1.42)$$

where $k_{j,j}$ is the vibrational rate for the i -th and j -th levels. It is clear that for an harmonic oscillator model

$$k_{i-1,i} = k_{i,i-1} \exp\left(-\frac{2\pi\hbar\nu}{k_B T}\right).$$

Since the harmonic oscillator model assumes that vibrational energy levels are equally spaced, equation (1.42) becomes

$$\frac{dN_i}{dt} = k_{0,1} \left\{ -iN_i + (i+1)N_{i+1} + \exp\left(-\frac{2\pi\hbar\nu}{k_B T}\right) [-(i+1)N_i + iN_{i-1}] \right\}. \quad (1.43)$$

Equation (1.43) can be rewritten in terms of sensible internal energy, becoming both concise and meaningful:

$$\frac{du_{\text{vbr}}}{dt} = \frac{(u_{\text{vbr}})_{\text{eq}} - u_{\text{vbr}}}{\tau_{\text{vbr}}} \quad (1.44)$$

where

$$\tau_{\text{vbr}} = \left\{ k_{0,1} \left[\exp\left(-\frac{2\pi\hbar\nu}{k_B T}\right) \right] \right\}.$$

Equation (1.44), also called *vibrational rate equation*, describes how internal energy varies in a non-equilibrium regime. The exchange of energy between gas molecules can be explained with two mechanism:

vibration-translation transfer (V-T transfer): it is the most feasible process of energy exchange between molecules. The relaxing time for diatomic species, $\tau_{\text{vbr}}^{\text{V-T}}$, can be derived by experimental data and it follows

$$\tau_{\text{vbr}}^{\text{V-T}} p = C_1 \exp\left[\left(\frac{C_2}{T}\right)^{1/3}\right]$$

where C_1 and C_2 derive from laboratory measurements;

vibration-vibration transfer (V-V transfer): it is another mechanism allowing vibrational energy exchanges, which is more complex than the model seen in equation (1.44).

1.4 General formulation of governing equation in hypersonic flows

This final section condensates all the theoretical aspects of reacting mixture and high-temperature effects on gases providing a set of partial differential equation which describe hypersonic flow-fields. This formulation it is fundamentally an adjustment of traditional Navier-Stokes equations (N-S) that takes into account gaseous multispecies flows and chemical reactions. This kind of model obviously is based on a continuum description of the fluid and it is not always a reasonable model choice (see appendix A). Anyway, continuum fluid models are reliable for $Kn \lesssim 1 \times 10^{-2}$, where Kn is the *Knudsen number*, which is defined as the ratio between free molecular path and a characteristic flow-field length.

1.4.1 Navier-Stokes equations

Continuum fluid description is based on three conservation laws:

- mass;
- momentum;
- energy.

In absence of mass injections, volume forces (e.g. gravity) and energy sources the N-S can be written as follows:

$$\frac{\partial}{\partial t} \rho + \frac{\partial}{\partial x_i} (\rho v_i) = 0; \quad (1.45)$$

$$\frac{\partial}{\partial t} (\rho v_i) + \frac{\partial}{\partial x_j} (\rho v_i v_j) = -\frac{\partial}{\partial x_i} p + \frac{\partial}{\partial x_j} \tau_{ij}; \quad (1.46)$$

$$\frac{\partial}{\partial t} (\rho E) + \frac{\partial}{\partial x_i} (\rho v_i E) = -\frac{\partial}{\partial x_i} (p v_i) + \frac{\partial}{\partial x_j} (\tau_{ij} v_j) + \frac{\partial}{\partial x_i} \Phi_i; \quad (1.47)$$

where τ is the stress tensor, which, for Newtonian fluid, is modelled as follows

$$\tau_{ij} = \mu \left(\frac{\partial v_i}{\partial x_j} + \frac{\partial v_j}{\partial x_i} \right) + \delta_{ij} \lambda \frac{\partial v_k}{\partial x_k},$$

with λ as another viscosity coefficient that, according with Stokes' hypothesis, is

$$\lambda = -\frac{2}{3}\mu.$$

The variable E is the specific total internal energy,

$$E = u + \frac{1}{2} \|\mathbf{v}\|^2,$$

and Φ is the heat flux:

$$\Phi_i = -k_t \frac{\partial T}{\partial x_i}$$

with k as thermal conductivity. Equations (1.45), (1.46) and (1.47) describe the flow-field of a generic viscous fluid in absence of external forces and sources of any kind; however the way in which they are written do not allows to clearly explicit high-temperature effects and reacting processes.

1.4.2 Navier-Stokes for non-equilibrium and reacting flow

In case of non-equilibrium reacting flow, it is necessary to improve the model adding further equation to the main set previously presented.

Species source term

Since in a reacting flow some chemical species may be generated while other may be vanished, a new source term must be introduced:

$$\Omega_{is}^{\text{ch}} = \mathcal{M}_{is} \frac{d[X_{is}]}{dt}$$

where $\frac{d[X_{is}]}{dt}$ follows directly from equation (1.39).

Mass diffusion

In this case two new terms should be defined. First, a *diffusion velocity*

$$\mathbf{w}_{is} = \mathbf{v}_{is} - \mathbf{v}$$

where \mathbf{v}_{is} is a velocity only referred to the i -th species. After that, it is possible to define the species-mass diffusive flux referred to the i -th species,

$$\mathbf{J}_{m, is} = \rho \mathbf{w}_{is};$$

it is dependent on concentration, pressure and temperature gradient:

$$\mathbf{J}_{m, is} = -\rho_{is} \left\{ \sum_{js} D_{is, js} [\nabla \chi_{js} - (c_{js} - \chi_{js}) \nabla \ln p] + D_{T, is} \nabla \ln T \right\}$$

where $D_{is, js}$ is the multi-component diffusion coefficient of the i -th species in the j -th species and $D_{T, i}$ is the thermal diffusion coefficient of the i -th species.

Vibrational non-equilibrium source term

In this case equation (1.44) must be integrated into the system of equation as source term in order to include vibrational non-equilibrium, assuming V-T transfer mechanism only.

Energy diffusion

Energy is also transported as diffusion process of the i -th species. It results in a heat flux in which each species has a contribution:

$$\Phi_D = \sum_{is} h_{is} \mathbf{J}_{m, is}.$$

Transport properties

Since for a multicomponent gas is made of multiple species with different viscosities, the viscosity of the mixture can be approximated with the Wilke's rule,

$$\mu = \sum_{is} \frac{\chi_{is} \mu_{is}}{\sum_{js} \chi_{js} \phi_{is, js}}$$

with

$$\phi_{is, js} = \frac{1}{8} \left(1 + \frac{\mathcal{M}_{is}}{\mathcal{M}_{js}} \right)^{-1/2} \left[1 + \left(\frac{\mu_{is}}{\mu_{js}} \right)^{1/2} \left(\frac{\mathcal{M}_{js}}{\mathcal{M}_{is}} \right)^{1/4} \right]^2$$

or with the Mathur-Saxena method as suggest in [7]:

$$\mu = \frac{1}{2} \left[\sum_{is} \chi_{is} \mu_{is} + \left(\sum_{is} \frac{\chi_{is}}{\mu_{is}} \right)^{-1} \right].$$

Dynamic viscosity for each individual species can be found as least-squares fits [24, 11]. Similarly, also thermal conductivity uses the same averaging formula:

$$k_t = \frac{1}{2} \left[\sum_{is} \chi_{is} k_{tis} + \left(\sum_{is} \frac{\chi_{is}}{k_{tis}} \right)^{-1} \right],$$

where k_{tis} is the thermal conductivity of the i -th species, which can be obtained by curve fits [11]. Finally, diffusion coefficients D_{is,j_s} and $D_{T,i}$ are better described in [11] where their curve fits can be found.

Finally, the system of equation for non-equilibrium, reacting flow-field is the following:

$$\begin{aligned} \frac{\partial}{\partial t} \rho + \frac{\partial}{\partial x_i} (\rho v_i) &= 0; \\ \frac{\partial}{\partial t} (\rho v_i) + \frac{\partial}{\partial x_j} (\rho v_i v_j) &= -\frac{\partial}{\partial x_i} p + \frac{\partial}{\partial x_j} \tau_{ij}; \\ \frac{\partial}{\partial t} (\rho E) + \frac{\partial}{\partial x_i} (\rho v_i E) &= -\frac{\partial}{\partial x_i} (p v_i) + \frac{\partial}{\partial x_j} (\tau_{ij} v_j) + \frac{\partial}{\partial x_i} \left(-k_t \frac{\partial T}{\partial x_i} + \sum_{is} h_{is} \mathbf{J}_{m,is} \cdot \hat{\mathbf{i}}_{x_i} \right); \\ \frac{\partial}{\partial t} (\rho u_{\text{vbr},is}) + \frac{\partial}{\partial x_i} (\rho u_{\text{vbr},is} v_i) &= \rho \frac{(u_{\text{vbr},is})_{\text{eq}} - u_{\text{vbr},is}}{\tau_{V-T,is}}, \quad is = 1, \dots, N_s; \\ \frac{\partial}{\partial t} \rho_{is} + \frac{\partial}{\partial x_i} (\rho_{is} v_i) + \frac{\partial}{\partial x_i} (\rho_{is} w_i) &= \Omega_{is}^{\text{ch}}, \quad is = 1, \dots, N_s. \end{aligned}$$

Since multi-component reacting gas is considered, new boundary conditions should be added to the system of equation. Usually a solid wall has a *no-slip* velocity boundary condition. Always on the wall, a temperature condition should be specified (value or flux) and, eventually, a catalytic specification, which describes how chemical reaction rates behave near the wall (e.g. a fully catalytic wall specification recombine dissociated species).

Chapter 2

Air models

This chapter presents the most relevant Earth's air models, which consist in specifying the species that should take into account in chemical reactions that occur in hypersonic flow, since the temperature commonly reaches high values. The behaviour of these models were analysed in terms of temperature-pressure variations using a basic self-developed non-linear system of equations solver which has been used in order to solve chemical equilibrium for each air model considered.

Atoms	χ	c	N_{ie}/N_N
Two atomic elements ($\mathcal{M} \approx 28.9 \text{ kg kmol}^{-1}$)			
N ₂	0.790	0.767	1
O ₂	0.210	0.233	42/158 \approx 0.266
Three atomic elements ($\mathcal{M} \approx 29.0 \text{ kg kmol}^{-1}$)			
N ₂	0.780	0.754	1
O ₂	0.210	0.232	42/156 \approx 0.269
Ar	0.010	0.014	1/156 \approx 6.41 \times 10 ⁻³

Table 2.1: initial composition of air models at 298.15 K.

2.1 Classification

It is clear that this models are designed to suit the Earth's inner atmospheric environment (appendix A, table A.1) and, obviously, others should be used in order to provide accurate calculations in different contexts (e.g. Mars' atmosphere it is composed almost exclusively by carbon dioxide, as the Venus' one, while Titan's atmosphere is essentially made of molecular nitrogen). First of all, it should be specified the number of atomic constituents of all the chemical species involved in the model. From table A.1 it is clear that for dry air, the most relevant atomic elements are Nitrogen and Oxygen. Argon may be included in case of gas ionization, since it does not react with other elements: its concentration is about 1% in terms of molar fraction at standard temperature, therefore its role still marginal. Initial composition and atomic ratio are reported in table 2.1.

2.1.1 Five species air model

This model has been designed for low temperature ranges and it includes only neutral species. Table 2.2 is the *formation matrix*, in other words how the single elements contribute to each species formation in terms of stoichiometric numbers.

Elem./Spec.	N ₂	N	O ₂	O	NO
N	2	1	0	0	1
O	0	0	2	1	1

Table 2.2: five species air model, formation matrix.

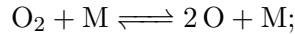
Reaction mechanisms

Reaction mechanisms of the five species model are the following (M is the third body of the chemical reaction):

- molecular nitrogen dissociation



- molecular oxygen dissociation



- nitrogen monoxide dissociation



- exchange mechanism (Zeldovich mechanism)



The third body, M, could be any species involved by this model (N₂, N, O₂, O, NO), therefore the total amount of chemical reaction is seventeen.

Chemical equilibrium system

In order to write, and hopefully solve, the system of equation for chemical equilibrium, the reaction process does not necessary involves the reaction mechanisms presented in the previous paragraph, which hold in a generic non-equilibrium situation. Since the model involves five species, the system should be composed by five independent equations:

- N_e independent equation on element conservation;
- N_s – N_e independent equation involving chemical reactions.

Element conservation equations are provided fixing initially the number of element particles and directly impose that

$$\sum_{is} a_{ie, is} N_{is} = \sum_{is} a_{ie, is} (N_{is})_0$$

for each element in table 2.2; $a_{ie, is}$ a generic entry of the formation matrix and the subscript 0 stands for the original/initial number of particles of the i -th element. Another way of writing element conservation is the use of Dalton's law (section 1.1.2) with $N_e - 1$ equations which constrain the element-ratios. This second solution is proposed by Anderson [1] and allows to directly specify the pressure of the mixture inside the system of equation. The remaining equations involve equilibrium constants, which depend on temperature; the specific chemical reactions still indifferent as long as the reaction processes are independent and involve all the chemical species of the model. The system of equations used in order to evaluate equilibrium condition at given temperature T_* and pressure p_* is the following:

$$\begin{cases} p_{N_2} + p_N + p_{O_2} + p_O + p_{NO} - p_* = 0; \\ 2p_{O_2} + p_O + p_{NO} - N_O/N_N (2p_{N_2} + p_N + p_{NO}) = 0; \\ p_N^2 - K_{p, N_2 \rightleftharpoons 2N}(T_*) p_{N_2} = 0; \\ p_O^2 - K_{p, O_2 \rightleftharpoons 2O}(T_*) p_{O_2} = 0; \\ p_{NO} - K_{p, N+O \rightleftharpoons NO}(T_*) p_N p_O = 0. \end{cases} \quad (2.1)$$

The solution of this non-linear system of equations is given in terms of partial pressure, the transformations seen in chapter 1 allow to obtain other quantities (molar fractions, concentration, mass ratios, ...).

2.1.2 Seven species air model

This model includes ionized species (NO^+ , e^-) and it is designed for higher temperature range. The formation matrix is reported in table 2.3.

Elem./Spec.	N ₂	N	O ₂	O	NO	NO ⁺	e ⁻
N	2	1	0	0	1	1	0
O	0	0	2	1	1	1	0
e ⁻	0	0	0	0	0	-1	1

Table 2.3: seven species air model, formation matrix.

Reaction mechanisms

Reaction mechanisms of the seven species model are the following:

- molecular nitrogen dissociation



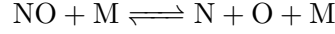
with M equal to N₂, N, O₂, O, NO, NO⁺, e⁻;

- molecular oxygen dissociation



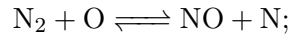
with M equal to $\text{N}_2, \text{N}, \text{O}_2, \text{O}, \text{NO}, \text{NO}^+$;

- nitrogen monoxide dissociation

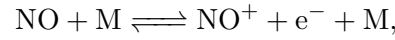


with M equal to $\text{N}_2, \text{N}, \text{O}_2, \text{O}, \text{NO}$;

- exchange mechanism (Zeldovich mechanism)



- NO ionization



with M equal to N_2, O_2 .

Chemical equilibrium system

Compared with the previous model, now it is necessary to add another conservation equation, since the total charge of the mixture must be constant:

$$p_{\text{NO}^+} - p_{\text{e}^-} = 0.$$

Therefore the full system of equations is the following:

$$\left\{ \begin{array}{l} p_{\text{N}_2} + p_{\text{N}} + p_{\text{O}_2} + p_{\text{O}} + p_{\text{NO}} + p_{\text{NO}^+} + p_{\text{e}^-} - p_* = 0; \\ 2p_{\text{O}_2} + p_{\text{O}} + p_{\text{NO}} + p_{\text{NO}^+} - N_{\text{O}}/N_{\text{N}} (2p_{\text{N}_2} + p_{\text{N}} + p_{\text{NO}} + p_{\text{NO}^+}) = 0; \\ p_{\text{NO}^+} - p_{\text{e}^-} = 0; \\ p_{\text{N}}^2 - K_{p, \text{N}_2 \rightleftharpoons 2\text{N}}(T_*) p_{\text{N}_2} = 0; \\ p_{\text{O}}^2 - K_{p, \text{O}_2 \rightleftharpoons 2\text{O}}(T_*) p_{\text{O}_2} = 0; \\ p_{\text{NO}} - K_{p, \text{N} + \text{O} \rightleftharpoons \text{NO}}(T_*) p_{\text{N}} p_{\text{O}} = 0; \\ p_{\text{NO}^+} p_{\text{e}^-} - K_{p, \text{NO} \rightleftharpoons \text{NO}^+ + \text{e}^-}(T_*) p_{\text{NO}} = 0. \end{array} \right. \quad (2.2)$$

2.1.3 Nine species air model

This model involves other two greater ions, N^+, O^+ . As before the formation matrix is in table 2.4.

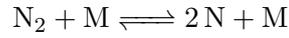
Elem./Spec.	N ₂	N	N ⁺	O ₂	O	O ⁺	NO	NO ⁺	e ⁻
N	2	1	1	0	0	0	1	1	0
O	0	0	0	2	1	1	1	1	0
e ⁻	0	0	-1	0	0	-1	0	-1	1

Table 2.4: nine species air model, formation matrix.

Reaction mechanisms

Reaction mechanisms of the seven species model are the following:

- molecular nitrogen dissociation



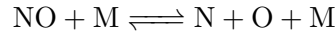
with M equal to N₂, N, N⁺, O₂, O, O⁺, NO, NO⁺, e⁻;

- molecular oxygen dissociation



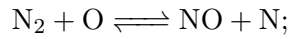
with M equal to N₂, N, N⁺, O₂, O, O⁺, NO, NO⁺;

- nitrogen monoxide dissociation

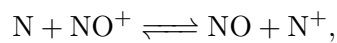
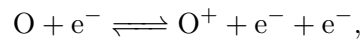


with M equal to N₂, N, O₂, O, NO;

- exchange mechanism (Zeldovich mechanism)



- ionization



with M equal to N₂, O₂.

Chemical equilibrium system

The full system of equations is the following:

$$\left\{ \begin{array}{l}
 p_{N_2} + p_N + p_{N^+} + p_{O_2} + p_O + p_{O^+} + \\
 \quad + p_{NO} + p_{NO^+} + p_{e^-} - p_* = 0; \\
 2p_{O_2} + p_O + p_{O^+} + p_{NO} + p_{NO^+} + \\
 \quad - N_O/N_N (2p_{N_2} + p_N + p_{N^+} + p_{NO} + p_{NO^+}) = 0; \\
 p_{N^+} + p_{O^+} + p_{NO^+} - p_{e^-} = 0; \\
 p_N^2 - K_{p, N_2 \rightleftharpoons 2N} (T_*) p_{N_2} = 0; \\
 p_O^2 - K_{p, O_2 \rightleftharpoons 2O} (T_*) p_{O_2} = 0; \\
 p_{NO} - K_{p, N+O \rightleftharpoons NO} (T_*) p_N p_O = 0; \\
 p_{NO} p_{e^-} - K_{p, NO \rightleftharpoons NO^+ + e^-} (T_*) p_{NO} = 0; \\
 p_{N^+} p_{e^-} - K_{p, N \rightleftharpoons N^+ + e^-} (T_*) p_N = 0; \\
 p_{O^+} p_{e^-} - K_{p, O \rightleftharpoons O^+ + e^-} (T_*) p_O = 0.
 \end{array} \right. \quad (2.3)$$

2.1.4 Eleven species air model

This model includes minor ions (N_2^+ , O_2^+). The formation matrix is reported in table 2.5.

Elem./Spec.	N_2	N	N^+	N_2^+	O_2	O	O^+	O_2^+	NO	NO^+	e^-
N	2	1	1	2	0	0	0	0	1	1	0
O	0	0	0	0	2	1	1	2	1	1	0
e^-	0	0	-1	-1	0	0	-1	-1	0	-1	1

Table 2.5: eleven species air model, formation matrix.

Reaction mechanisms

Reaction mechanisms of the seven species model are the following:

- molecular nitrogen dissociation



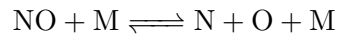
with M equal to $N_2, N, N^+, N_2^+, O_2, O, O^+, O_2^+, NO, NO^+, e^-$;

- molecular oxygen dissociation



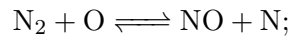
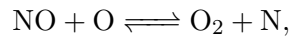
with M equal to $N_2, N, N^+, N_2^+, O_2, O, O^+, O_2^+, NO, NO^+$;

- nitrogen monoxide dissociation

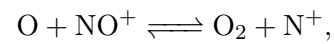
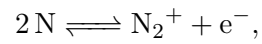
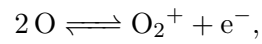
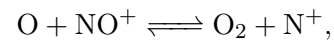
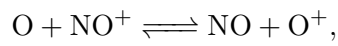
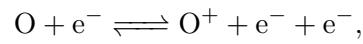
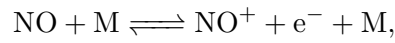


with M equal to $\text{N}_2, \text{N}, \text{O}_2, \text{O}, \text{NO}$;

- exchange mechanism (Zeldovich mechanism)



- ionization



with M equal to N_2, O_2 .

Chemical equilibrium system

The full system of equations is the following:

$$\left\{ \begin{array}{l}
 p_{N_2} + p_N + p_{N^+} + p_{N_2^+} + p_{O_2} + p_O + p_{O^+} + p_{O_2^+} + \\
 \quad + p_{NO} + p_{NO^+} + p_{e^-} - p_* = 0; \\
 2p_{O_2} + p_O + p_{O^+} + 2p_{O_2^+} + p_{NO} + p_{NO^+} + \\
 \quad - N_O/N_N \left(2p_{N_2} + p_N + p_{N^+} + 2p_{N_2^+} + p_{NO} + p_{NO^+} \right) = 0; \\
 p_{N^+} + p_{N_2^+} + p_{O^+} + p_{O_2^+} + p_{NO^+} - p_{e^-} = 0; \\
 p_N^2 - K_{p, N_2 \rightleftharpoons 2N} (T_*) p_{N_2} = 0; \\
 p_O^2 - K_{p, O_2 \rightleftharpoons 2O} (T_*) p_{O_2} = 0; \\
 p_{NO} - K_{p, N+O \rightleftharpoons NO} (T_*) p_N p_O = 0; \\
 p_{NO} p_{e^-} - K_{p, NO \rightleftharpoons NO^+ + e^-} (T_*) p_{NO} = 0; \\
 p_N p_{e^-} - K_{p, N \rightleftharpoons N^+ + e^-} (T_*) p_N = 0; \\
 p_O p_{e^-} - K_{p, O \rightleftharpoons O^+ + e^-} (T_*) p_O = 0; \\
 p_{N_2} p_{e^-} - K_{p, N_2 \rightleftharpoons N_2^+ + e^-} (T_*) p_{N_2} = 0; \\
 p_{O_2} p_{e^-} - K_{p, O_2 \rightleftharpoons O_2^+ + e^-} (T_*) p_{O_2} = 0.
 \end{array} \right. \quad (2.4)$$

2.1.5 Thirteen species air model

Argon gas and its ion (Ar, Ar^+) are added to the species model, as viewable in table 2.6.

Elem./Spec.	N_2	N	N^+	N_2^+	O_2	O	O^+	O_2^+	NO	NO^+	Ar	Ar^+	e^-
N	2	1	1	2	0	0	0	0	1	1	0	0	0
O	0	0	0	0	2	1	1	2	1	1	0	0	0
Ar	0	0	0	0	0	0	0	0	0	0	1	1	0
e^-	0	0	-1	-1	0	0	-1	-1	0	-1	0	-1	1

Table 2.6: thirteen species air model, formation matrix.

Reaction mechanism

In both [11, 19] are not mentioned reaction which involve Argon gas. It is conceivable that a ionization mechanism should be involved:



Chemical equilibrium system

The full system of equations is the following:

$$\left\{ \begin{array}{l}
 p_{\text{N}_2} + p_{\text{N}} + p_{\text{N}^+} + p_{\text{N}_2^+} + p_{\text{O}_2} + p_{\text{O}} + p_{\text{O}^+} + p_{\text{O}_2^+} + \\
 \quad + p_{\text{NO}} + p_{\text{NO}^+} + p_{\text{Ar}} + p_{\text{Ar}^+} + p_{\text{e}^-} - p_* = 0; \\
 2p_{\text{O}_2} + p_{\text{O}} + p_{\text{O}^+} + 2p_{\text{O}_2^+} + p_{\text{NO}} + p_{\text{NO}^+} + \\
 \quad - N_{\text{O}}/N_{\text{N}} \left(2p_{\text{N}_2} + p_{\text{N}} + p_{\text{N}^+} + 2p_{\text{N}_2^+} + p_{\text{NO}} + p_{\text{NO}^+} \right) = 0; \\
 p_{\text{Ar}} + p_{\text{Ar}^+} - N_{\text{Ar}}/N_{\text{N}} \left(2p_{\text{N}_2} + p_{\text{N}} + p_{\text{N}^+} + 2p_{\text{N}_2^+} + p_{\text{NO}} + p_{\text{NO}^+} \right) = 0; \\
 p_{\text{N}^+} + p_{\text{N}_2^+} + p_{\text{O}^+} + p_{\text{O}_2^+} + p_{\text{NO}^+} - p_{\text{e}^-} = 0; \\
 p_{\text{N}}^2 - K_{p, \text{N}_2 \rightleftharpoons 2\text{N}}(T_*) p_{\text{N}_2} = 0; \\
 p_{\text{O}}^2 - K_{p, \text{O}_2 \rightleftharpoons 2\text{O}}(T_*) p_{\text{O}_2} = 0; \\
 p_{\text{NO}} - K_{p, \text{N} + \text{O} \rightleftharpoons \text{NO}}(T_*) p_{\text{N}} p_{\text{O}} = 0; \\
 p_{\text{NO}^+} p_{\text{e}^-} - K_{p, \text{NO} \rightleftharpoons \text{NO}^+ + \text{e}^-}(T_*) p_{\text{NO}} = 0; \\
 p_{\text{N}^+} p_{\text{e}^-} - K_{p, \text{N} \rightleftharpoons \text{N}^+ + \text{e}^-}(T_*) p_{\text{N}} = 0; \\
 p_{\text{O}^+} p_{\text{e}^-} - K_{p, \text{O} \rightleftharpoons \text{O}^+ + \text{e}^-}(T_*) p_{\text{O}} = 0; \\
 p_{\text{N}_2^+} p_{\text{e}^-} - K_{p, \text{N}_2 \rightleftharpoons \text{N}_2^+ + \text{e}^-}(T_*) p_{\text{N}_2} = 0; \\
 p_{\text{O}_2^+} p_{\text{e}^-} - K_{p, \text{O}_2 \rightleftharpoons \text{O}_2^+ + \text{e}^-}(T_*) p_{\text{O}_2} = 0; \\
 p_{\text{Ar}^+} p_{\text{e}^-} - K_{p, \text{Ar} \rightleftharpoons \text{Ar}^+ + \text{e}^-}(T_*) p_{\text{Ar}} = 0.
 \end{array} \right. \quad (2.5)$$

Compared with equation (2.4), equation (2.5) has two more equations: another conservation equation referred to Argon atoms and Argon dissociation equation.

2.1.6 Numerical method

Since all the system of equations are clearly non-linear, iterative numerical approaches were the immediate choice in order to solve chemical equilibrium. Firstly, *SciPy* routines (e.g. `scipy.optimize.fsolve()`, `scipy.optimize.minimize()` [14]) were used; unfortunately, the convergence of the solution was hard to achieve with the increase of system dimension and defining solution boundaries not always was possible. Therefore, a basic self-made program, written with the C programming language, were designed, including a minimal, non-optimized, BLAS (Basic Linear Algebra Subprograms) library in order to support vector and matrix operations.

Newton-Raphson method

The numerical algorithm implemented is the Newton-Raphson method [22]. Basically, defining \mathbf{x} as the vector of the true solution of the system, $\tilde{\mathbf{x}}_i$ as the vector approximated solution, \mathbf{f}_i as the vector of the system in its implicit form and $\mathbf{J}_{\mathbf{f}_i}$ as the Jacobian matrix of \mathbf{f}_i at the i -th iteration, this method elementary step consists in

$$\tilde{\mathbf{x}}_{i+1} = \tilde{\mathbf{x}}_i - \mathbf{J}_{\mathbf{f}_i}^{-1} \mathbf{f}_i, \quad (2.6)$$

which ultimately involves the resolution of the following linear system

$$\mathbf{J}_{\mathbf{f}_i} \tilde{\mathbf{y}}_i = \mathbf{f}_i,$$

with $\tilde{\mathbf{y}}_i = \tilde{\mathbf{x}}_i - \tilde{\mathbf{x}}_{i+1}$. Since pressures are positive numbers, a boundary limit over $\tilde{\mathbf{x}}_i$ should be imposed. A possible approach, proposed in [20], is to take the absolute value of the solution of the linear system at each iteration. After some testing, this path has lead to overflow errors, probably due to the initial value $\tilde{\mathbf{x}}_0$. The issue has been fixed by limiting the pressure to the nearest boundary values, which are the lowest and the highest absolute double precision numbers (zero excluded). Jacobian evaluation is explicit, since its entries can be evaluated whit few functions. Initially it has been approximated using a second order finite difference scheme, unfortunately this approach has lead to numerical instability and bad convergence issues for higher order matrices: this obstacles have been resolved with an exact formulation of the Jacobian matrix.

Convergence and accuracy

If \mathbf{x} is known, the convergence of a method can be defined as follows:

$$\tilde{\mathbf{x}}_n \rightarrow \mathbf{x}, \quad \text{as } n \rightarrow +\infty,$$

where n is the iteration number. Newton-Raphson method convergence is strongly dependent on the initial value $\tilde{\mathbf{x}}_0$, which is initialized as pseudo-random vector. For this reason, a double convergence check has been implemented. Firstly, two iteration constraints are defined:

- `maximum_iter` = 50000, maximum iteration allowed for equation (2.6);
- `abs_tol` = 1×10^{-12} , maximum desired tolerance that the residual $\|\mathbf{f}_i\|_\infty$ must satisfy.

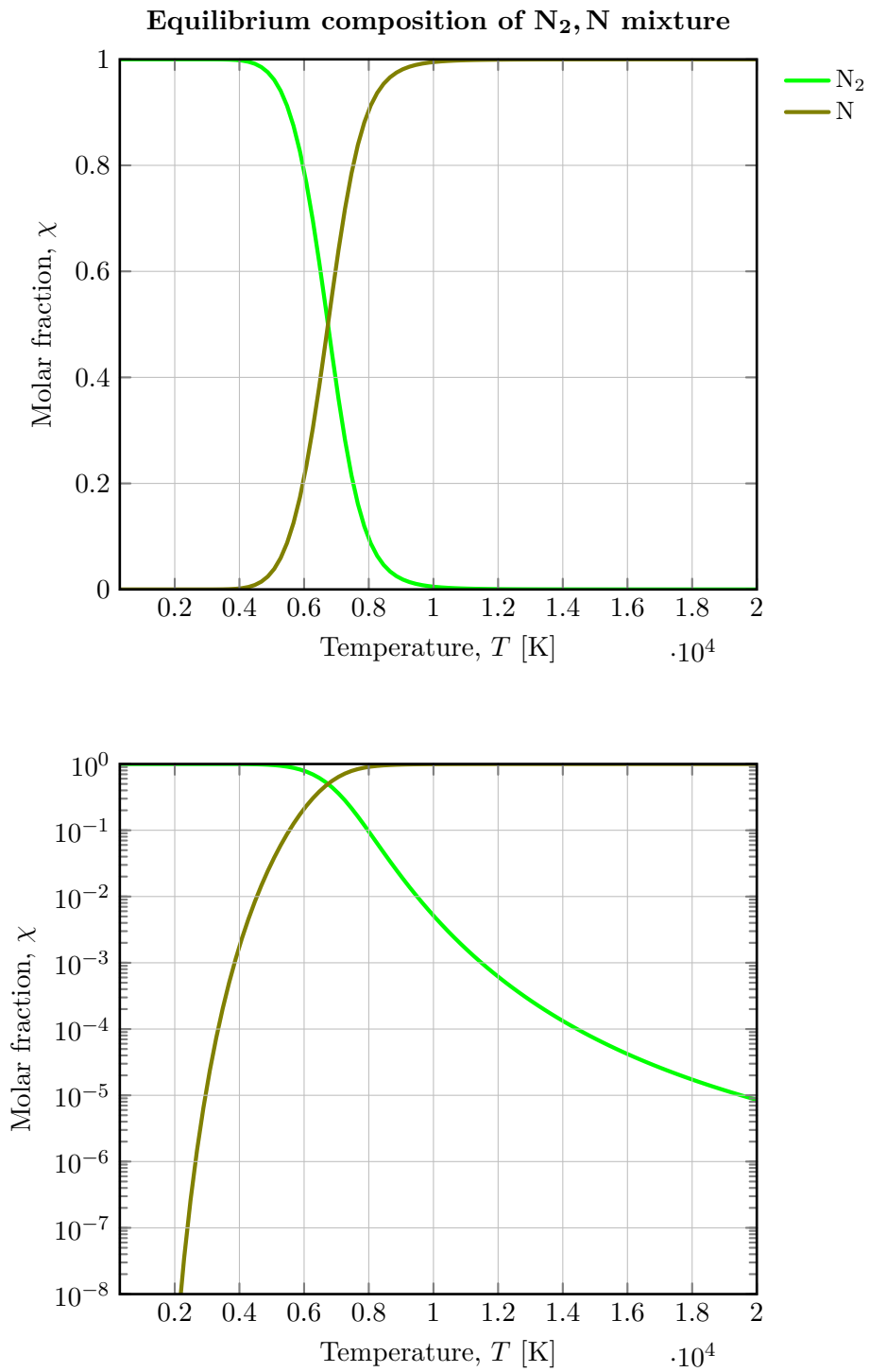
If, at the i -th iteration, the tolerance constrain is satisfied before the maximum iteration number is reached the solution $\tilde{\mathbf{x}}_i$ is considered valid and convergence achieved; conversely, a new initialization of $\tilde{\mathbf{x}}_0$ is performed and this iteration process continues until convergence is reached. It is possible to improve the solution accuracy applying the natural logarithm to chemical equilibrium equations, as pointed out in [3]. However, during code testing, it happened that this formulation still more sensible to initial solution estimation $\tilde{\mathbf{x}}_0$.

2.2 Single element-made species equilibrium behaviour

In this section are printed the chemical equilibrium results at pressure of 1 bar for homogeneous gaseous mixtures composed only by species made of only one element, excepted ions (e.g. N_2 , N , N_2^+ , N^+). Equilibrium constant were computed using thermochemical property polynomials of [16].

Observations

Nitrogen dissociation occurs over 4000 K while Oxygen begins this process at lower temperatures, 2000 K. Over 8000 K Oxygen is substantially completely dissociated and, for temperature higher than 10 000 K, also Nitrogen. Ionization processes begins at 8000 K and over 20 000 K all mixtures are fully ionized. Both N_2^+ and O_2^+ do not heavily participate in ionization process. It is noticeable that N_2^+ and O_2^+ are the first species to

Figure 2.1: chemical equilibrium at $p = 1$ bar for N₂, N mixture.

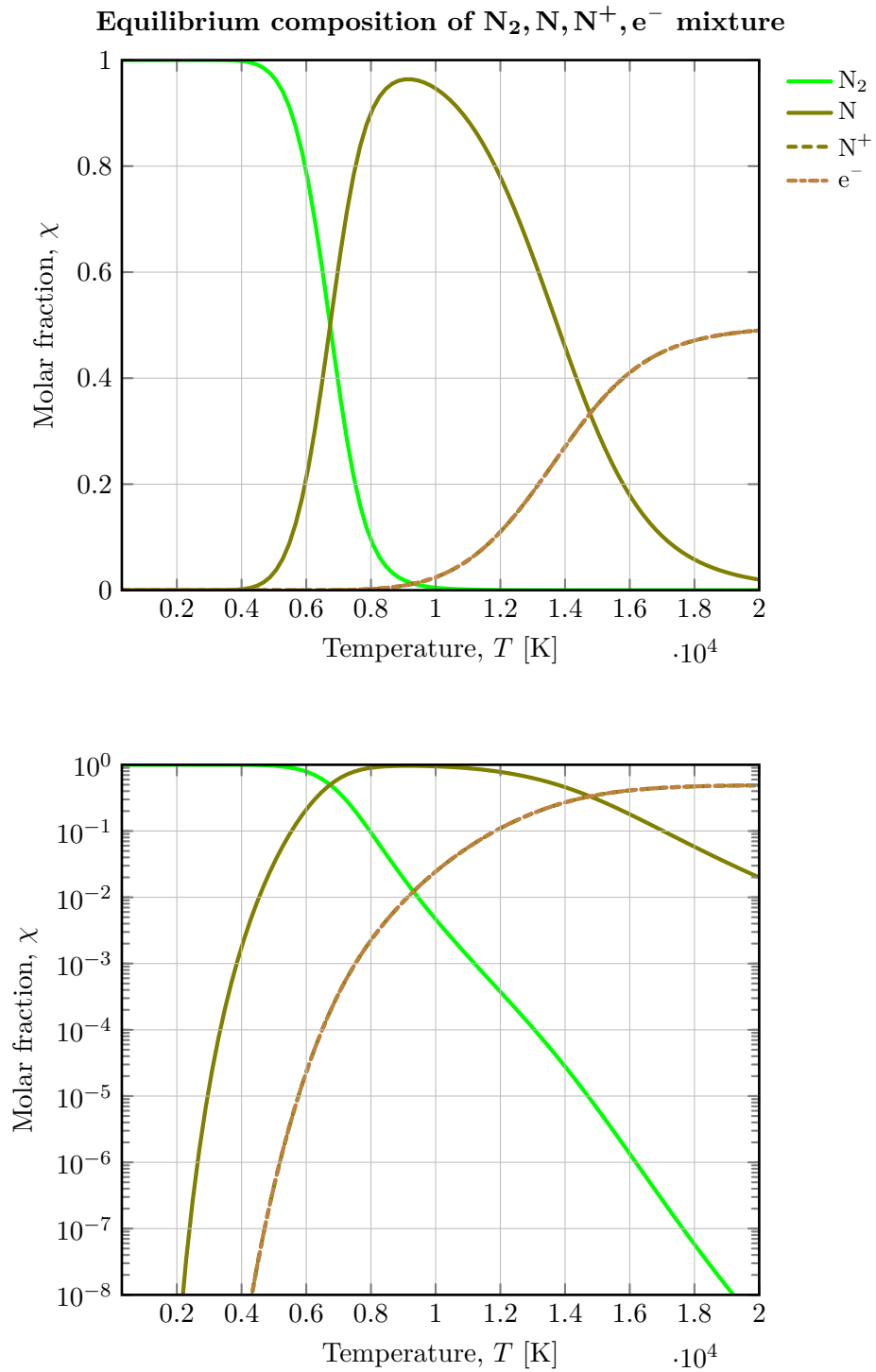


Figure 2.2: chemical equilibrium at $p = 1$ bar for N_2, N, N^+, e^- mixture.

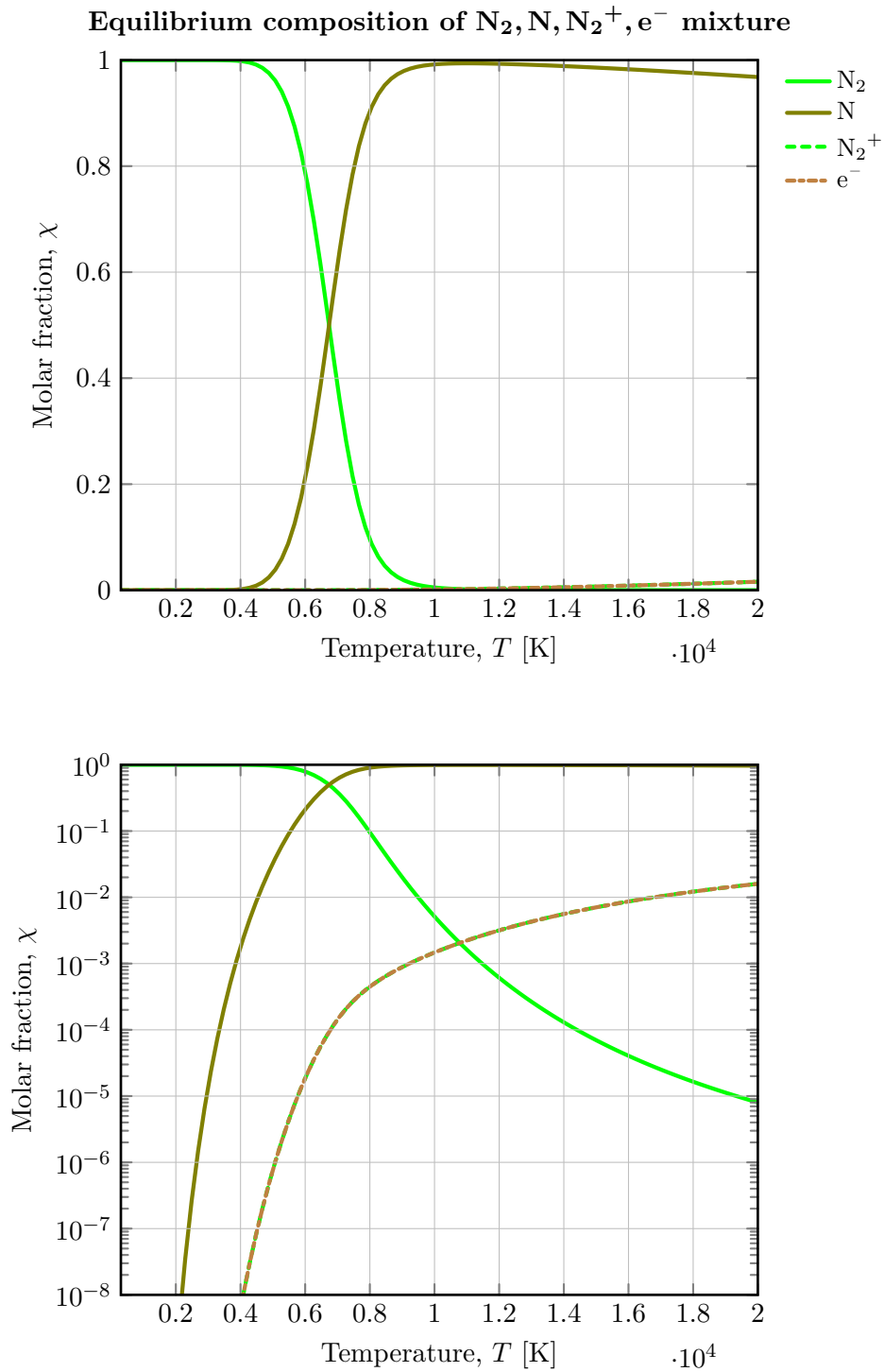


Figure 2.3: chemical equilibrium at $p = 1$ bar for N_2, N, N_2^+, e^- mixture.

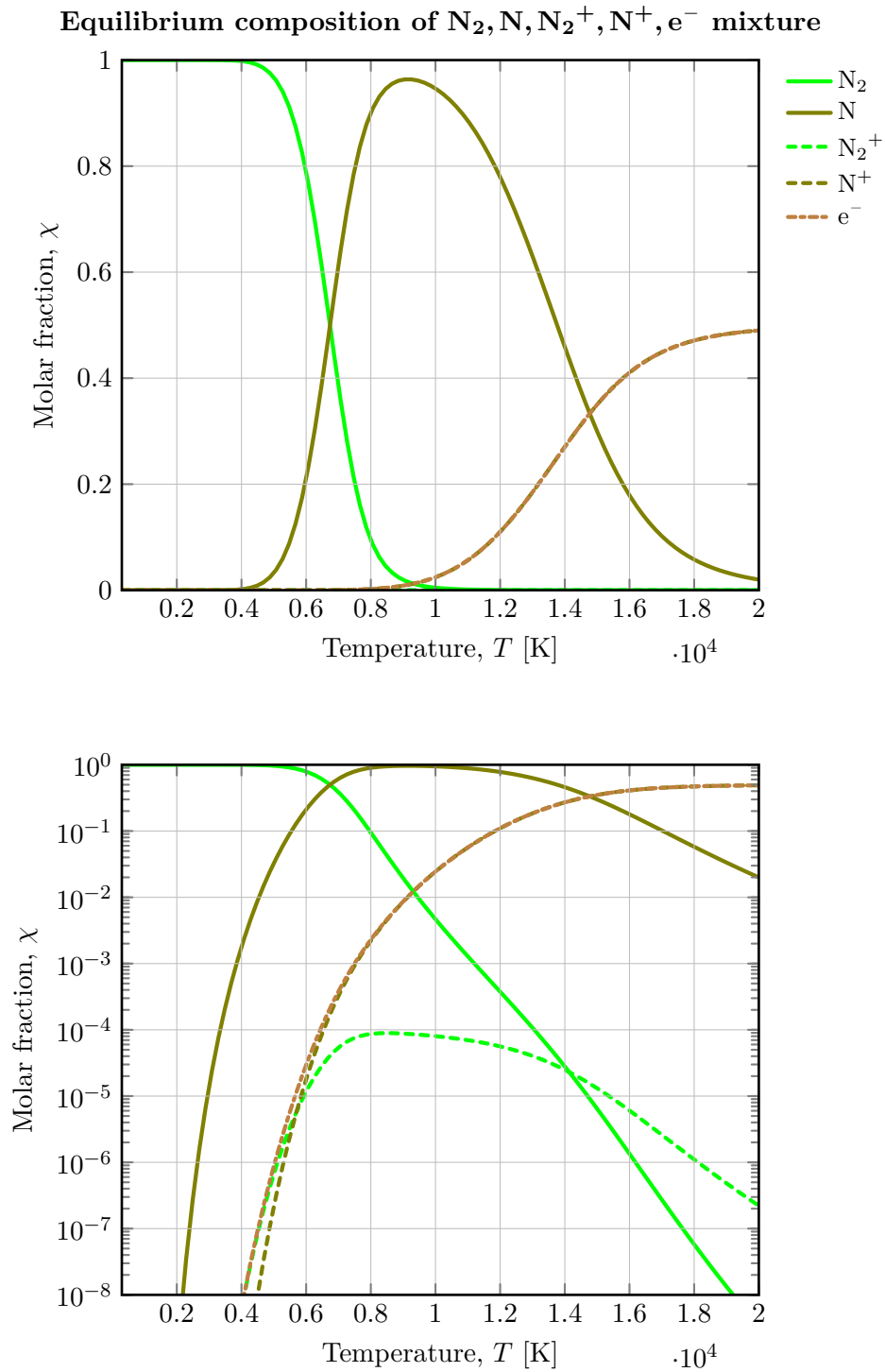
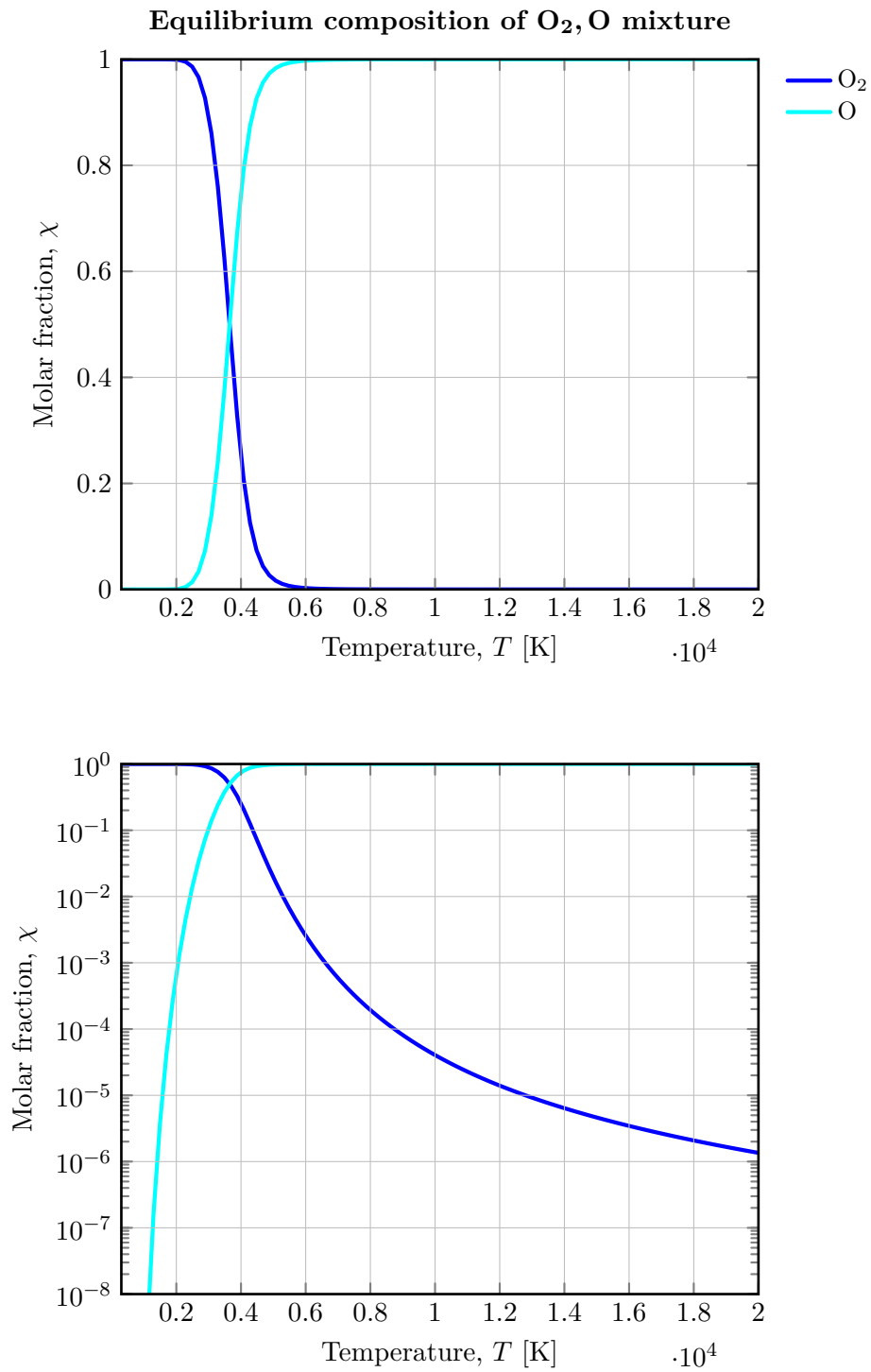


Figure 2.4: chemical equilibrium at $p = 1$ bar for N_2, N, N_2^+, N^+ mixture.

Figure 2.5: chemical equilibrium at $p = 1$ bar for O₂, O mixture.

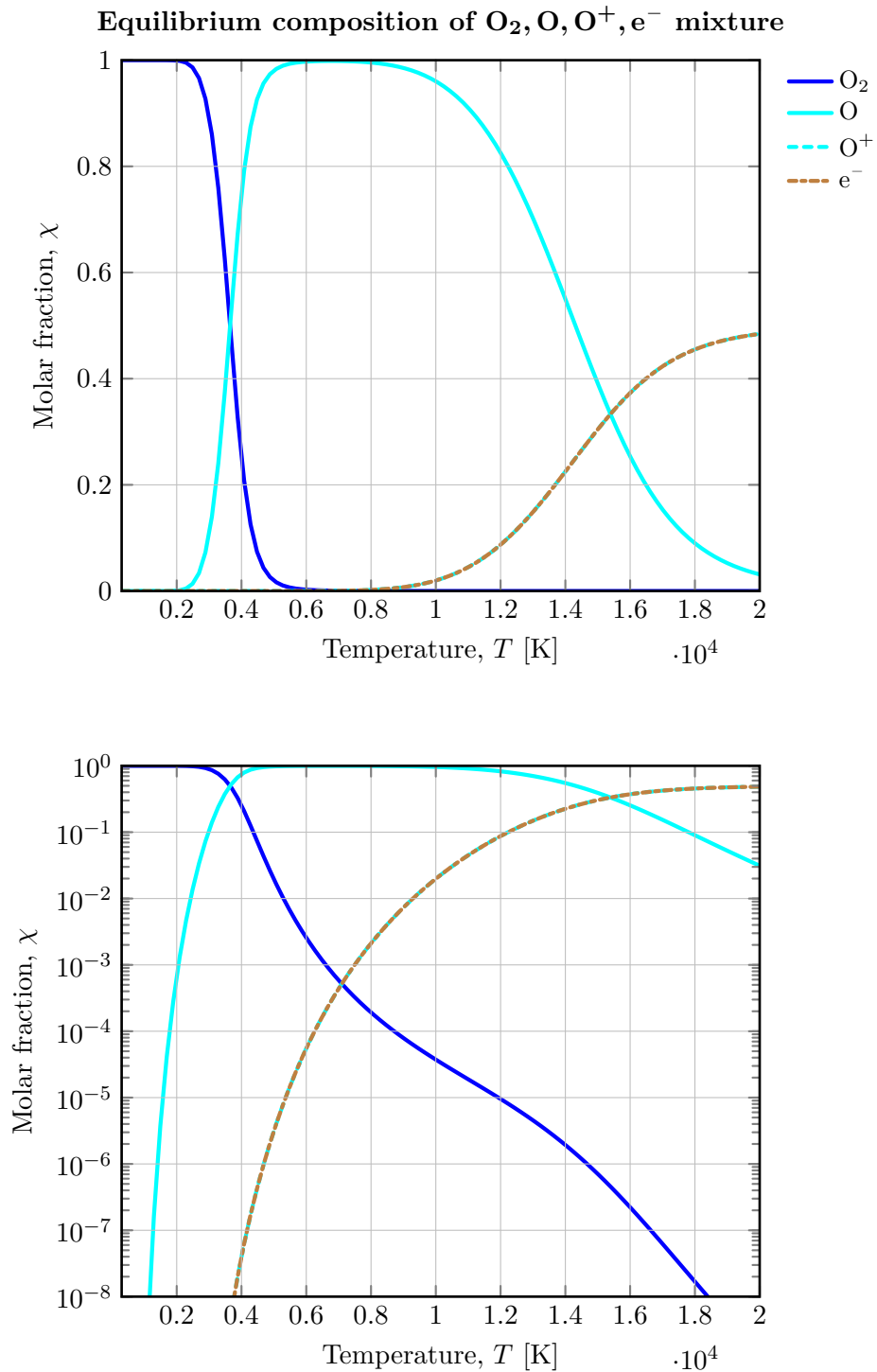


Figure 2.6: chemical equilibrium at $p = 1$ bar for $\text{O}_2, \text{O}, \text{O}^+, \text{e}^-$ mixture.

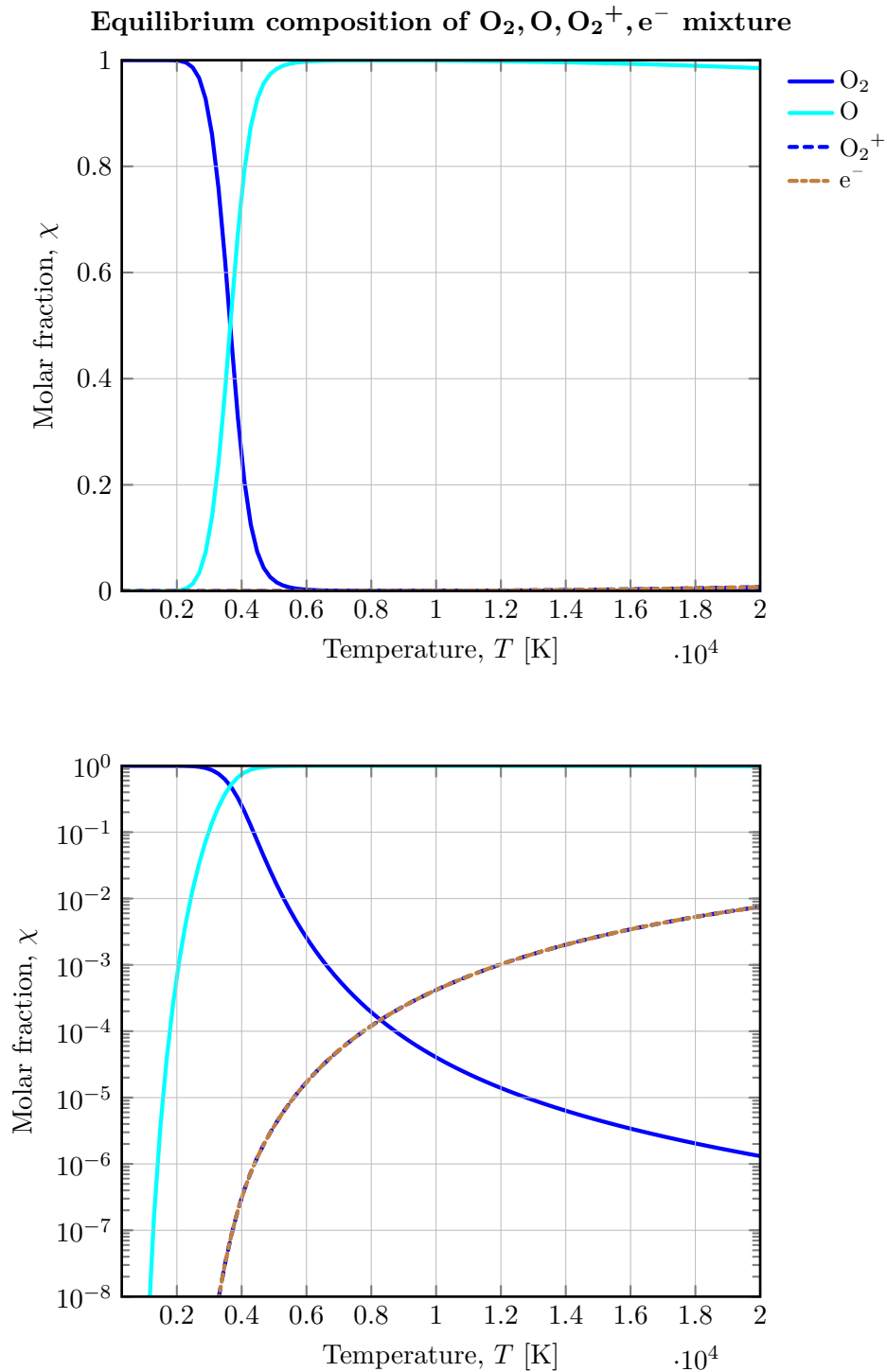


Figure 2.7: chemical equilibrium at $p = 1$ bar for O_2, O, O_2^+, e^- mixture.

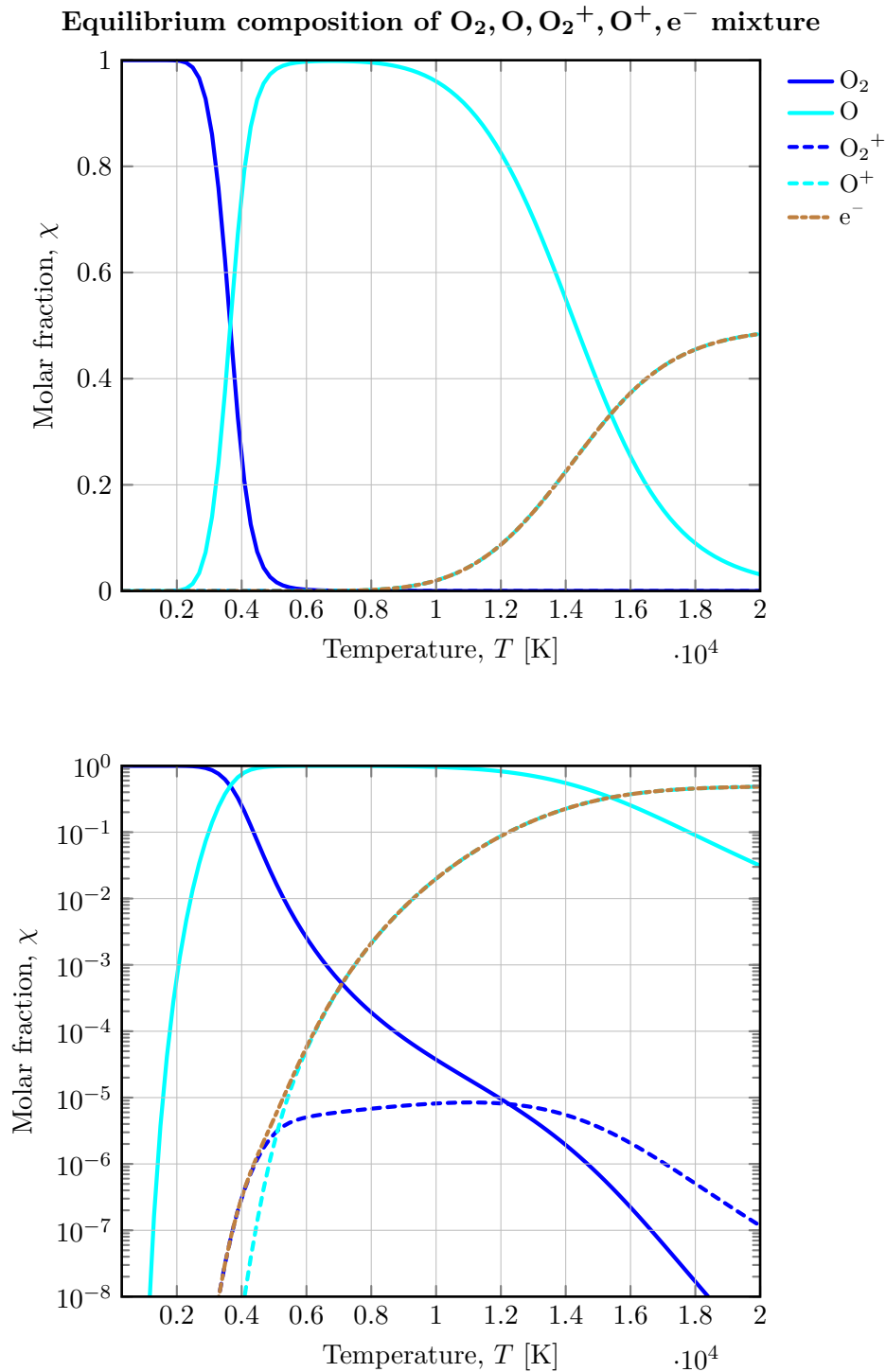


Figure 2.8: chemical equilibrium at $p = 1$ bar for $\text{O}_2, \text{O}, \text{O}_2^+, \text{O}^+, \text{e}^-$ mixture.

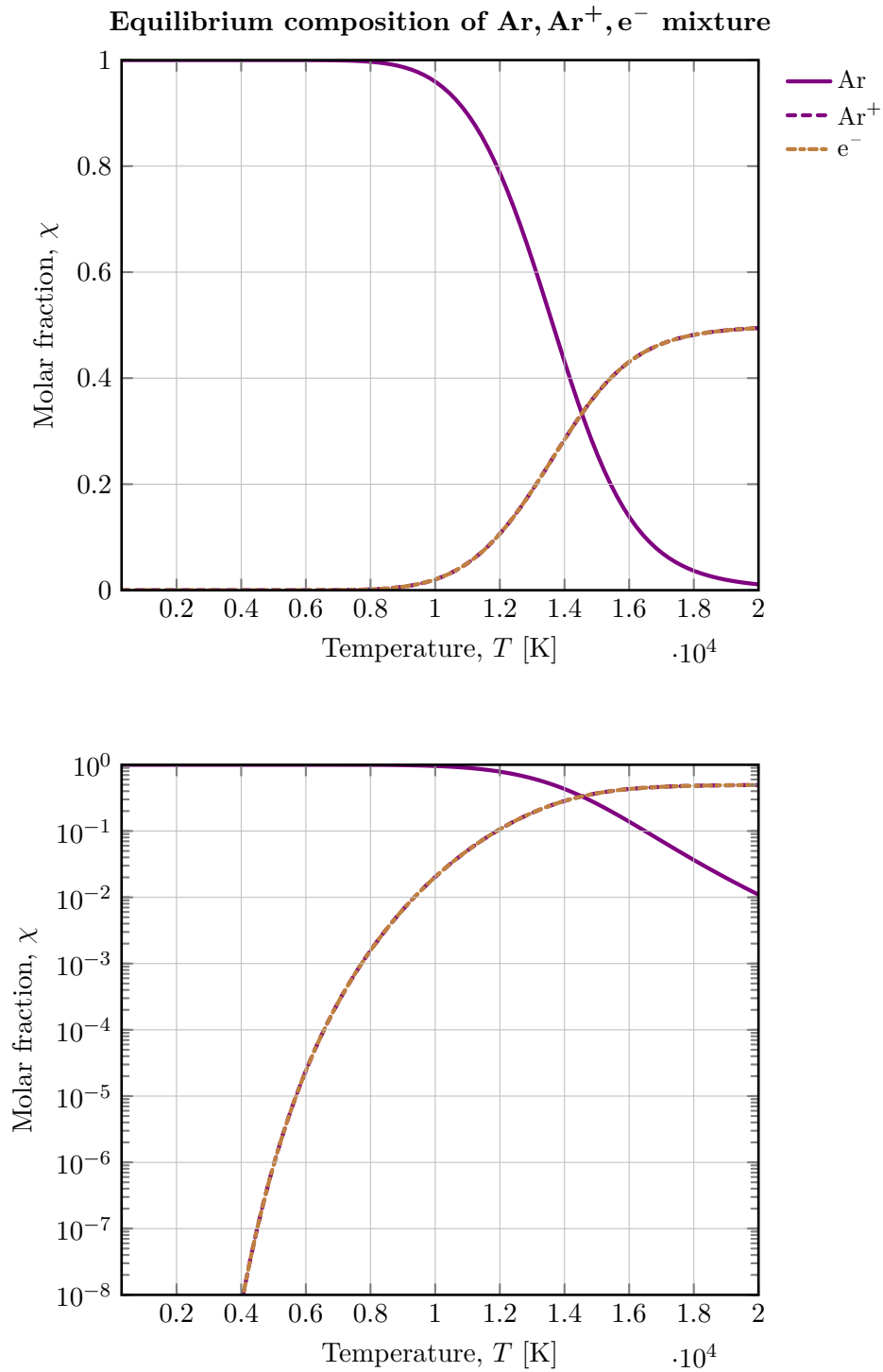


Figure 2.9: chemical equilibrium at $p = 1$ bar for Ar, Ar⁺, e⁻ mixture.

ionize, although at extremely low concentration. Argon gas can only ionize, as shown in figure 2.9, its ionization starts around 8000 K.

2.3 Air models chemical equilibrium analysis

As it has been done for single-element species mixtures, now it will be analysed how air models behaves when their chemical equilibrium is reached. The five species model does not include ionized species and, seems to be valid up to 4000 K. Between 3000 K and 6000 K ionized gas is primarily made of NO^+ , therefore up to this last temperature a seven species air model should be enough accurate. At temperature higher than 8000 K ionized gas is mainly composed by N^+ and O^+ . Nine and eleven species air models are substantially equivalent since minor ions (N_2^+ , O_2^+) dissociate at high temperatures. Argon contribution to plasma formation still limited to few thousandths of molar fraction for temperature higher than 16 000 K. These considerations hold as long as the pressure of the gas is 1 bar. Since Earth's atmosphere covers a wide range of pressures in its vertical distribution (appendix A.3.3), a deeper analysis was made, involving both temperature and pressure variations.

2.3.1 Temperature-Pressure analysis

Equilibrium condition of the thirteen species air model were analysed varying both temperature and pressure. The ranges are the following:

- temperature from 300 K to 20 000 K;
- pressure from 1 Pa to 1×10^7 Pa.

2.3.2 Results and observations

The influence that pressure has on chemical equilibrium composition using the thirteen species air model has been investigated. The first clear result is that dissociation, ionization and nitric oxide formation processes are shifted as the pressure level varies. In fact, low pressure levels start these chemical reactions at lower temperature, respect to the reference pressure of 1 bar. This observation is extremely obvious for dissociation reactions (figure 2.15). The second effect regards molar fractions: at high pressure levels, concentration of products related NO and NO^+ reactions are higher then of those at low pressure levels. Conversely the other reaction process have higher concentrations at low pressures. This last remark is noteworthy: figure 2.18 shows the overall plasma formation at equilibrium. At the lowest involved pressure, the gas is essentially fully ionized at 8000 K while at the highest considered pressure level should be doubled the temperature. It is reasonable that in hypersonic regime gas ionization is easy to reach at higher altitudes.

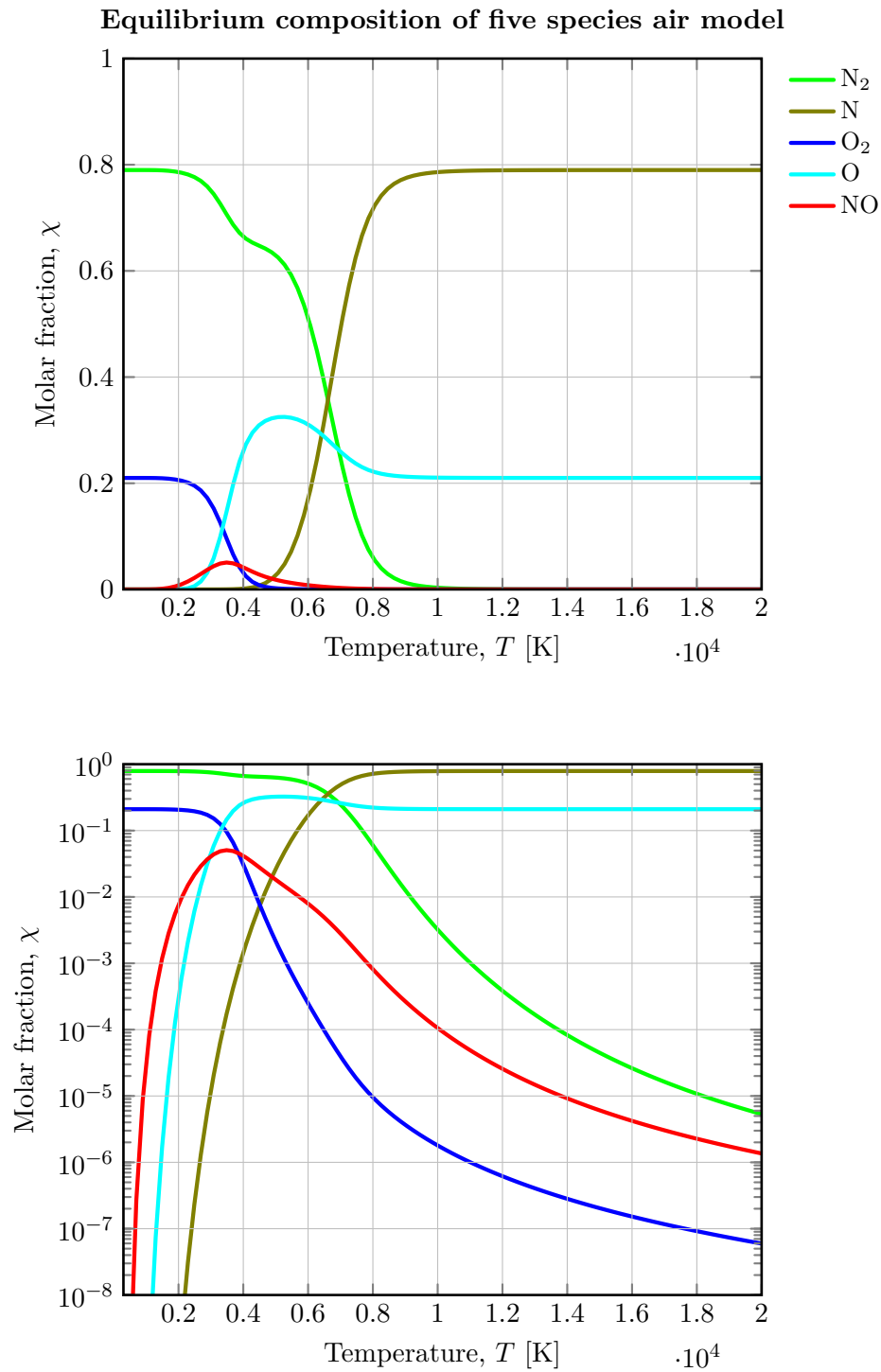


Figure 2.10: chemical equilibrium at $p = 1$ bar for five species air model, initial molar fraction, $\chi_{N_2} = 0.79$, $\chi_{O_2} = 0.21$.

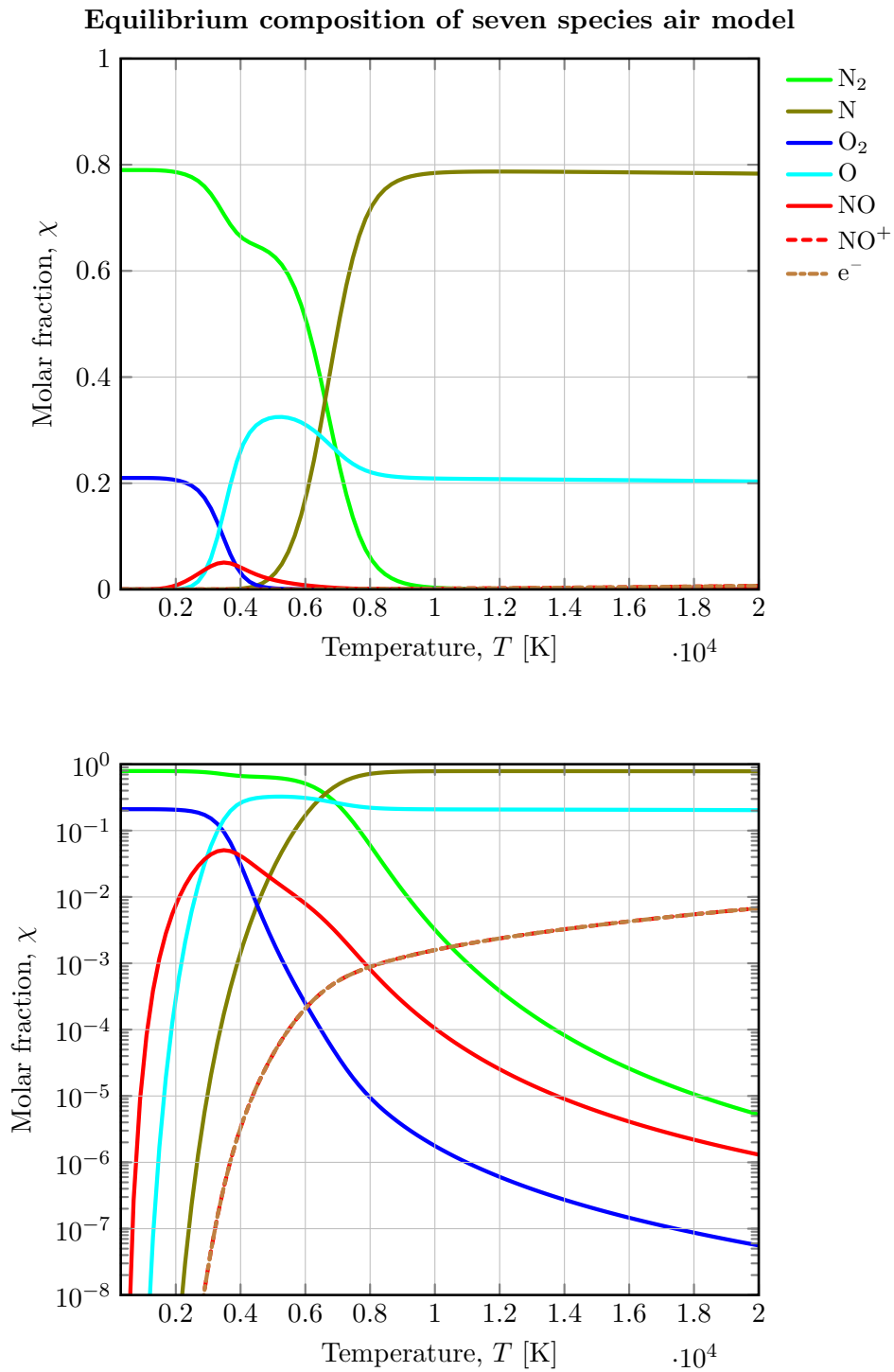


Figure 2.11: chemical equilibrium at $p = 1$ bar for seven species air model, initial molar fraction, $\chi_{N_2} = 0.79$, $\chi_{O_2} = 0.21$.

Equilibrium composition of nine species air model

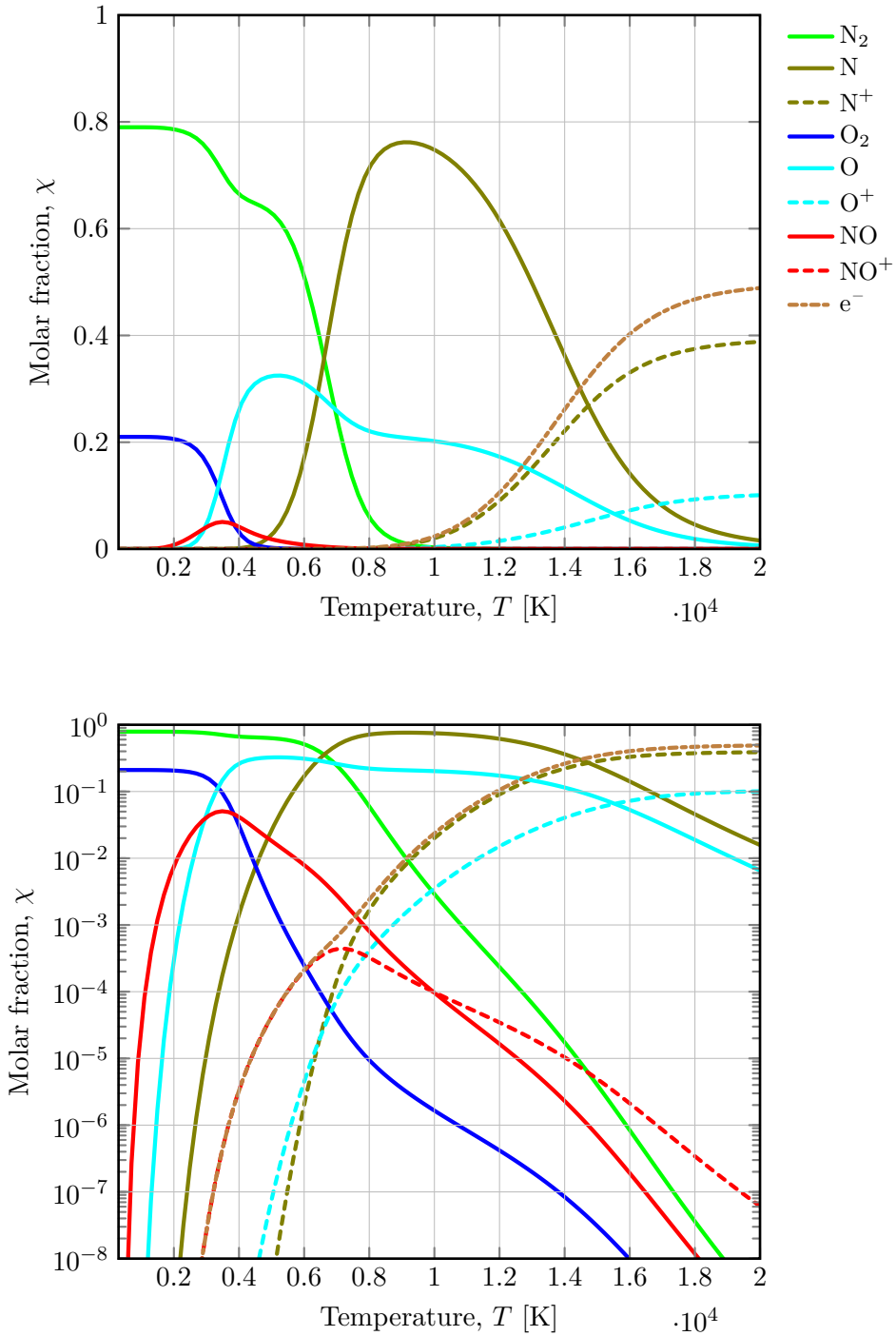


Figure 2.12: chemical equilibrium at $p = 1$ bar for nine species air model, initial molar fraction, $\chi_{N_2} = 0.79$, $\chi_{O_2} = 0.21$.

Equilibrium composition of eleven species air model

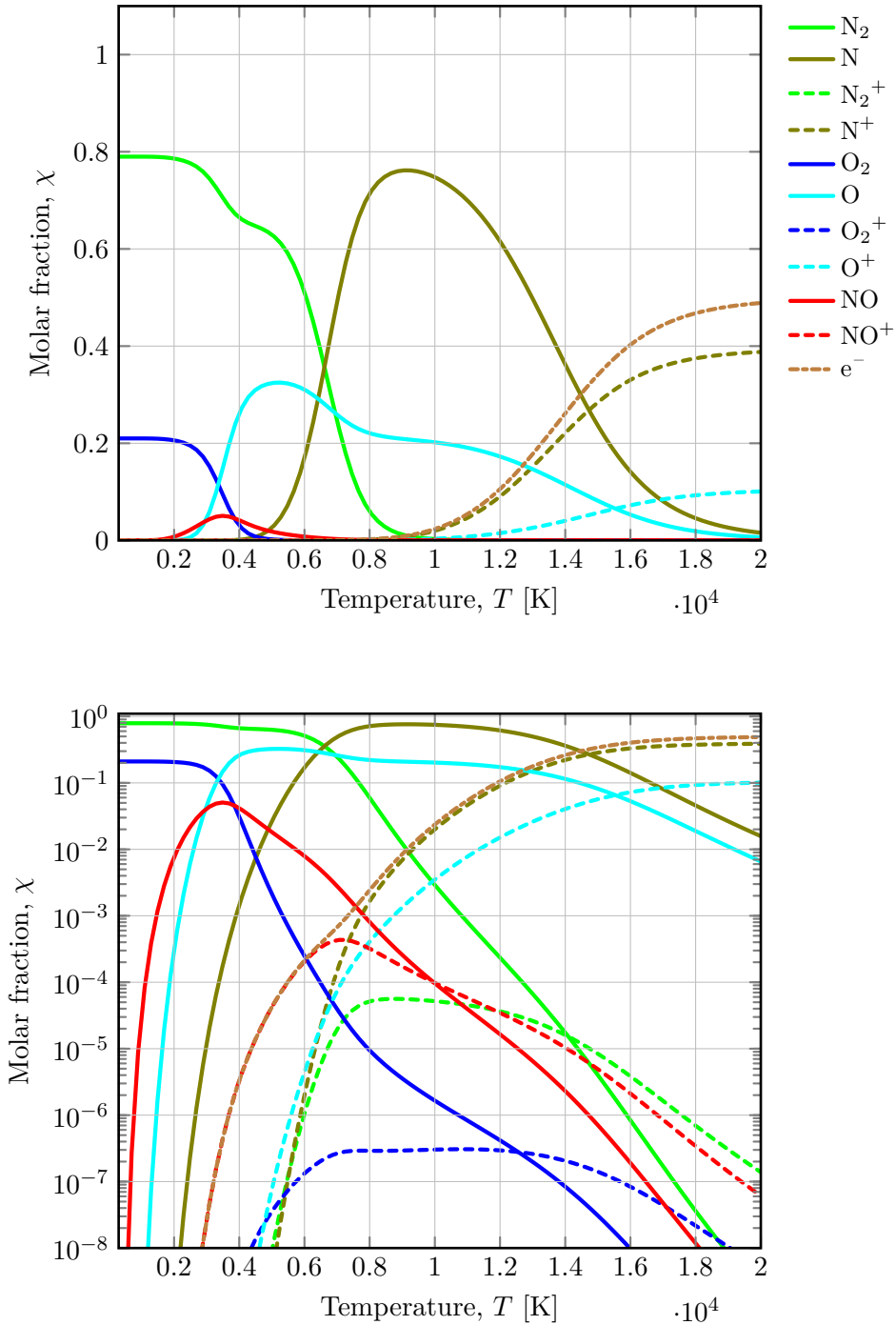


Figure 2.13: chemical equilibrium at $p = 1$ bar for eleven species air model, initial molar fraction, $\chi_{N_2} = 0.79$, $\chi_{O_2} = 0.21$.

Equilibrium composition of thiteen species air model

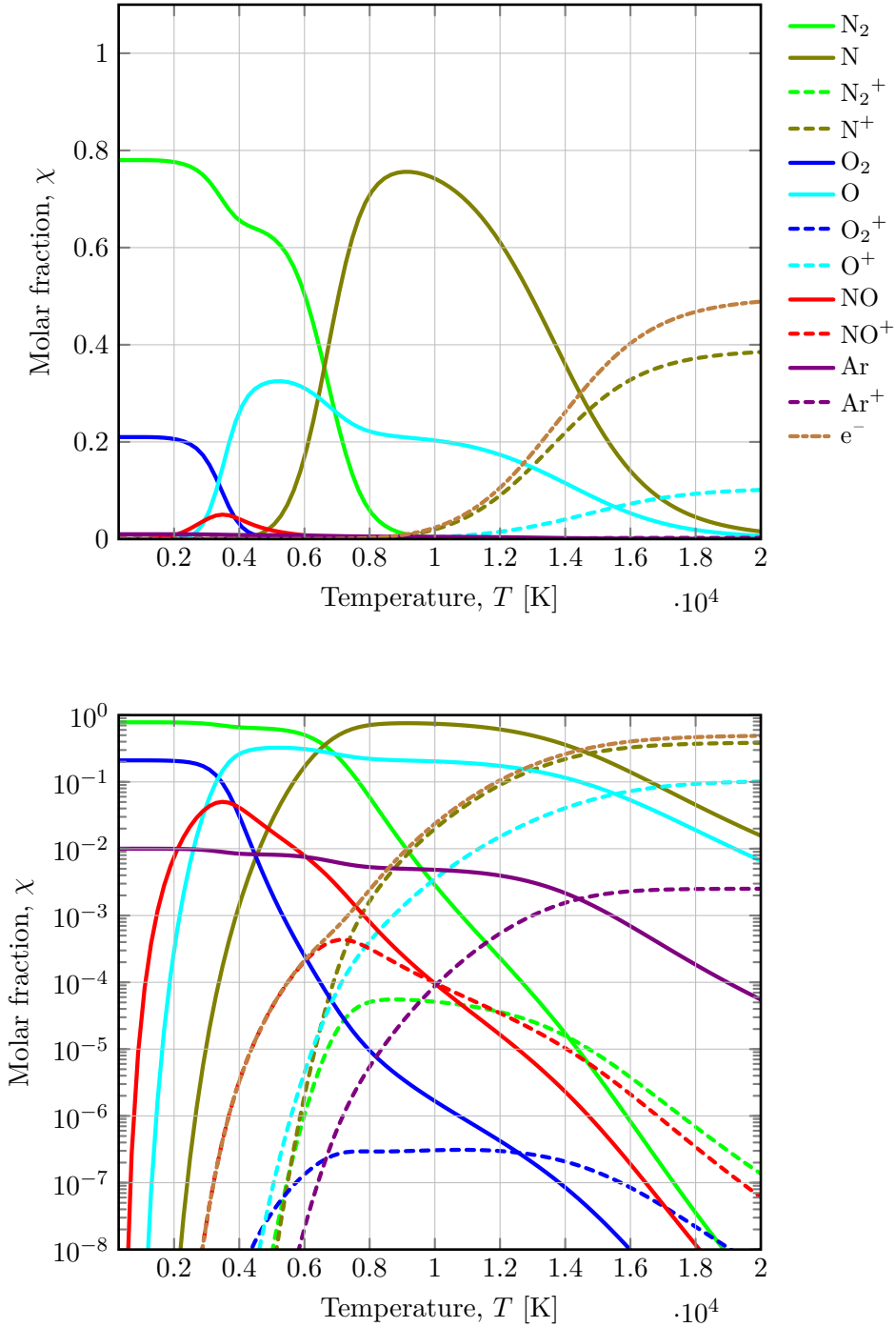


Figure 2.14: chemical equilibrium at $p = 1$ bar for thirteen species air model, initial molar fraction, $\chi_{N_2} = 0.78$, $\chi_{O_2} = 0.21$, $\chi_{Ar} = 0.01$.

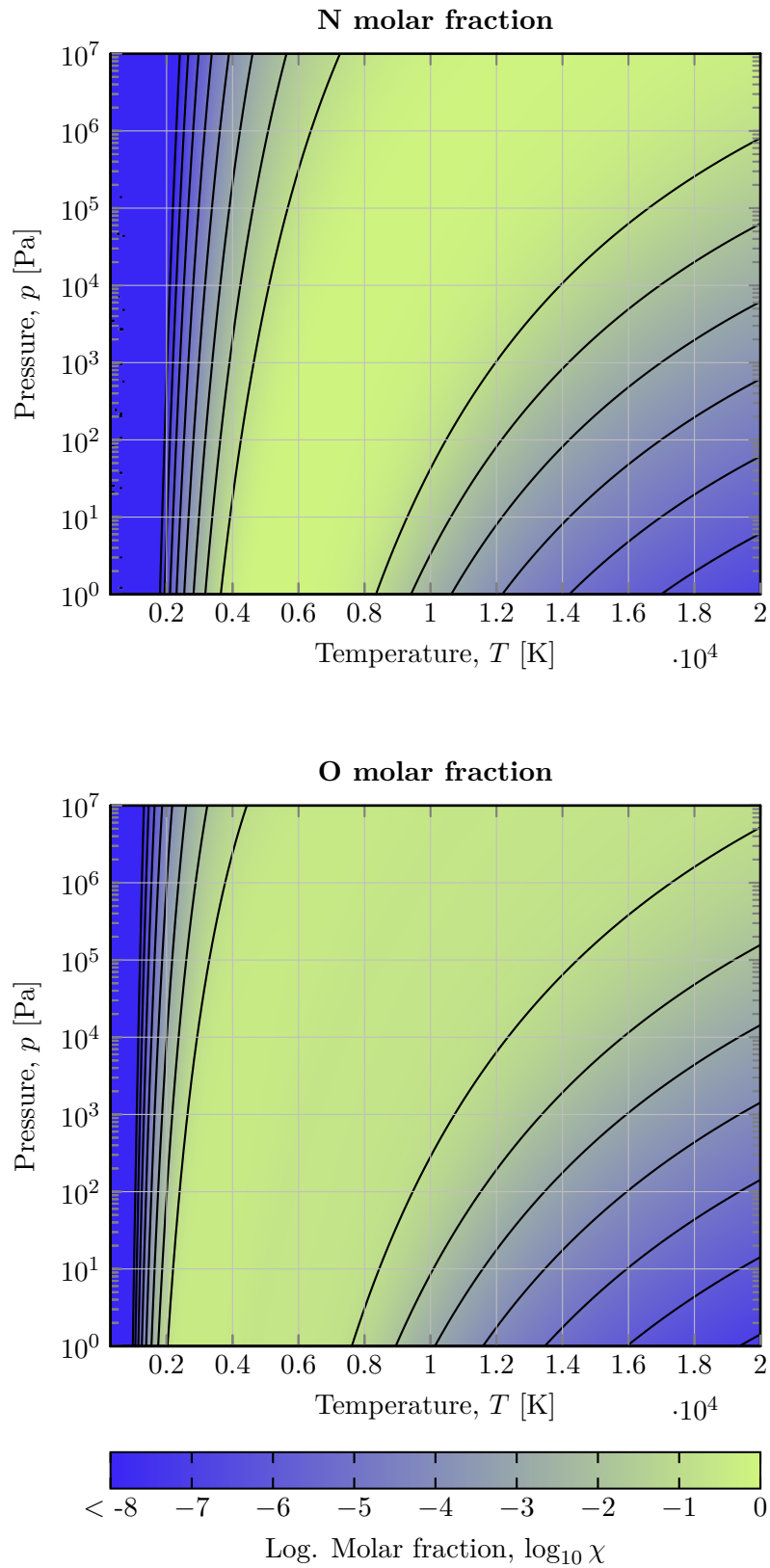


Figure 2.15: dissociated species at equilibrium condition for the thirteen species air model.

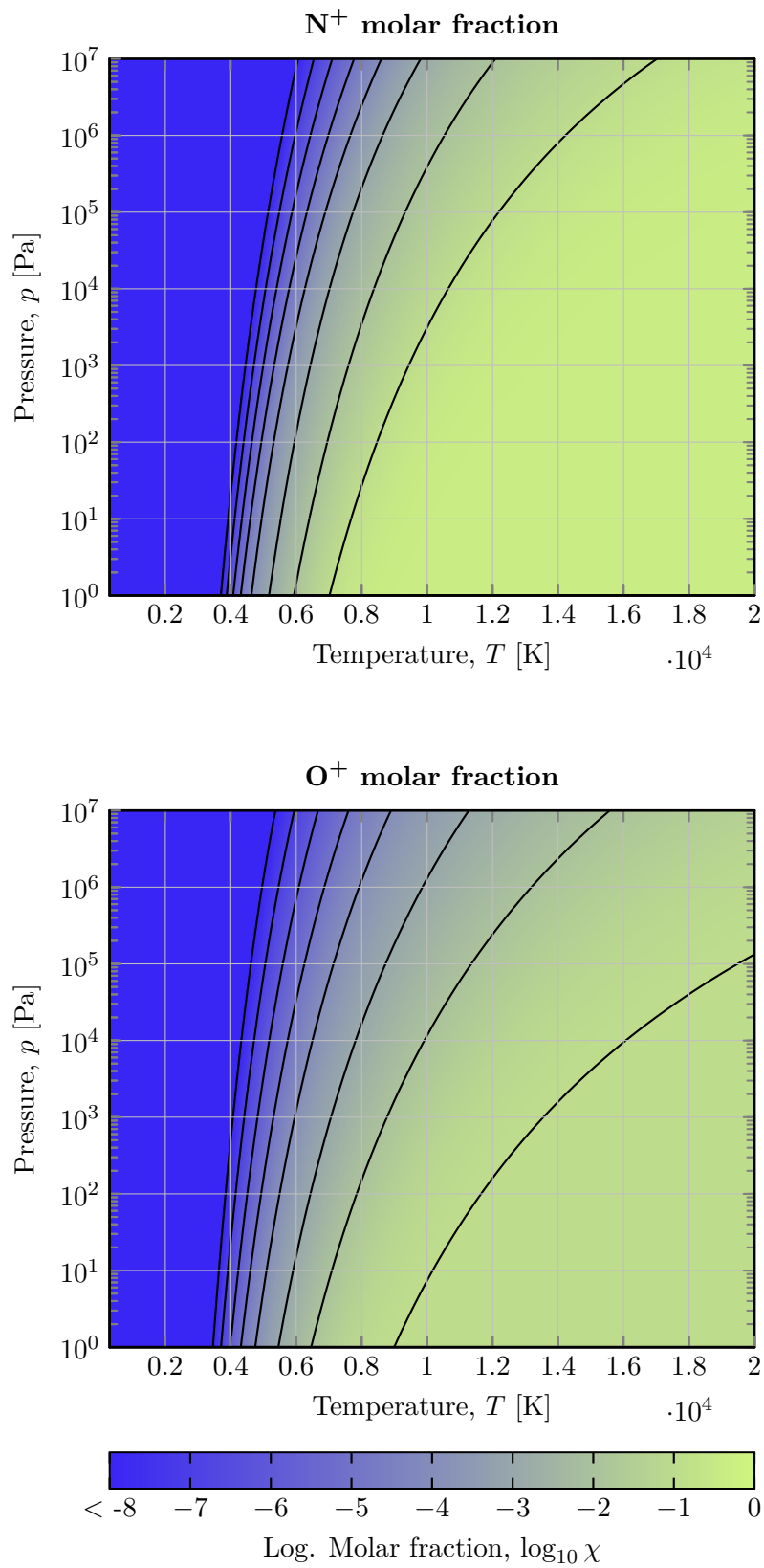


Figure 2.16: main ionized species at equilibrium condition for the thirteen species air model.

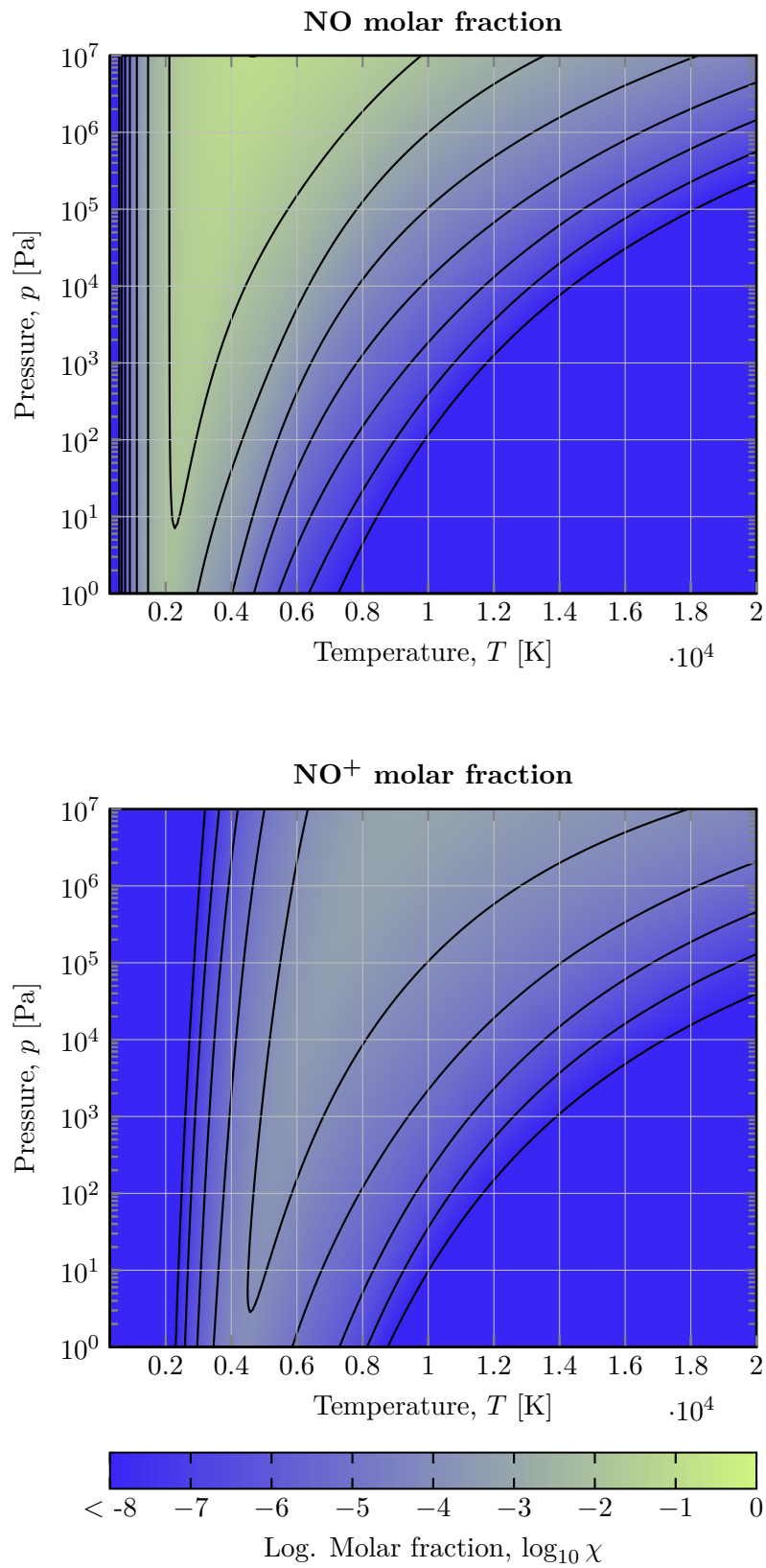


Figure 2.17: NO and NO⁺ at equilibrium condition for the thirteen species air model.

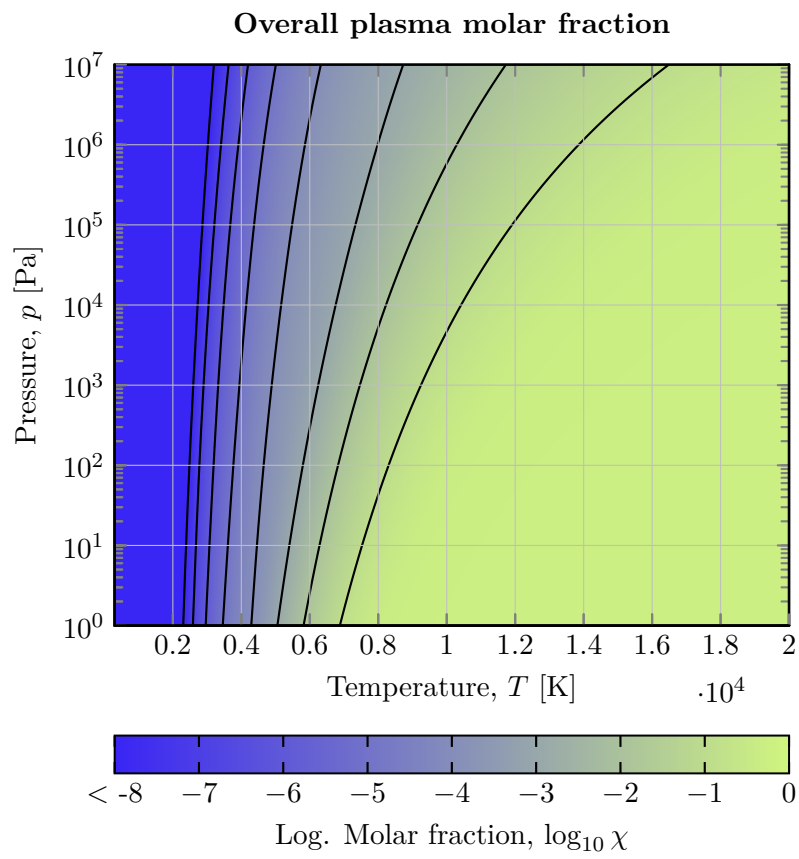


Figure 2.18: plasma at equilibrium condition for the thirteen species air model.

Chapter 3

Computational fluid dynamic simulation

This chapter focusses on modelling hypersonic flows in a numerical context using a commercial CFD software. Firstly, the geometry of the test case will be presented; after that mesh characteristics and refinement method will shown and finally, physical model implementation and boundary conditions will be illustrated.

3.1 Geometry

The geometry used in this case study is taken from [21] and it is illustrated in figure 3.1. It is basically a cone with a blunted nose (blunt shapes are extremely common in hypersonic designs since the wall heat flux is proportional to the inverse square root of the local wall radius). The numerical analyses were performed at null angle of attack, therefore the generated CAD geometry is a simple extrusion of the bidimensional drawing. In addition, since the case is symmetric with respect to the longitudinal axis, the 2D sketch traces only one half of the full side view. The sketch is made by three part:

- elliptic nose (semi-minor axis: 2.5 cm, semi-major axis: 5.5 cm);
- horizontal line (length: 2.5 cm);
- rest of the cone projection, which closes at the horizontal axis.

The computing domain is obtained subtracting the cone-like geometry from a larger one delimited by a curve designed to roughly fit the shock-wave. Finally, the geometry obtained is reported in figure 3.2.

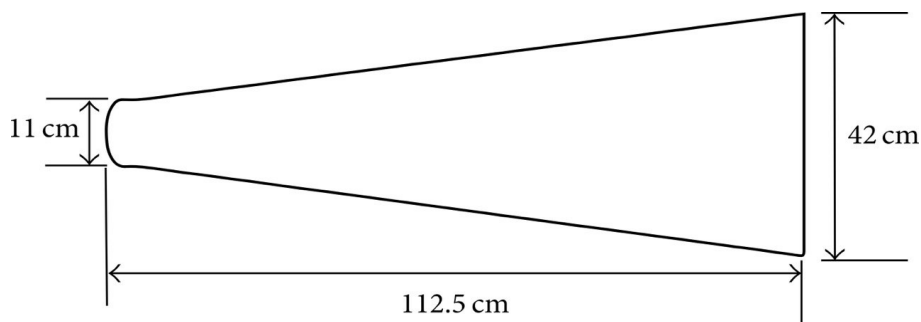


Figure 3.1: side view of the cone-like geometry [21].

Simcenter STAR-CCM+



Figure 3.2: CAD geometry.

3.1.1 Meshing operations

The meshing operation consist in generating a discrete computational grid, which is necessary to numerically solve the system of equations. Since simulations are axisymmetric, the mesh is bidimensional. The mesh used is unstructured and polygonal with a dedicated prism layer at wall boundaries. The customized properties used by the mesh routines are the following:

Polygonal mesher

- target surface size: 0.5 mm;
- minimum surface size: 0.1 mm;

Prism layer mesher

- stretching function: geometric progression;
- number of prism layers: 12;
- prism layer near wall thickness: 1×10^{-5} m;
- prism layer total thickness: 0.2 mm;

The prism layer is near wall mesh type which is characterized by regular prismatic cell.

3.1.2 Mesh refinement

Flow discontinuities are numerically resolved in few cells; in order to properly capture shock-waves it is crucial to locally reduce the mesh cell size. The technique consists in defining a *field function* (customizable tool that allows the user to define and read data from the computational domain [23]) defined as follows:

$$\log (|\nabla M|) \quad (3.1)$$

Simcenter STAR-CCM+

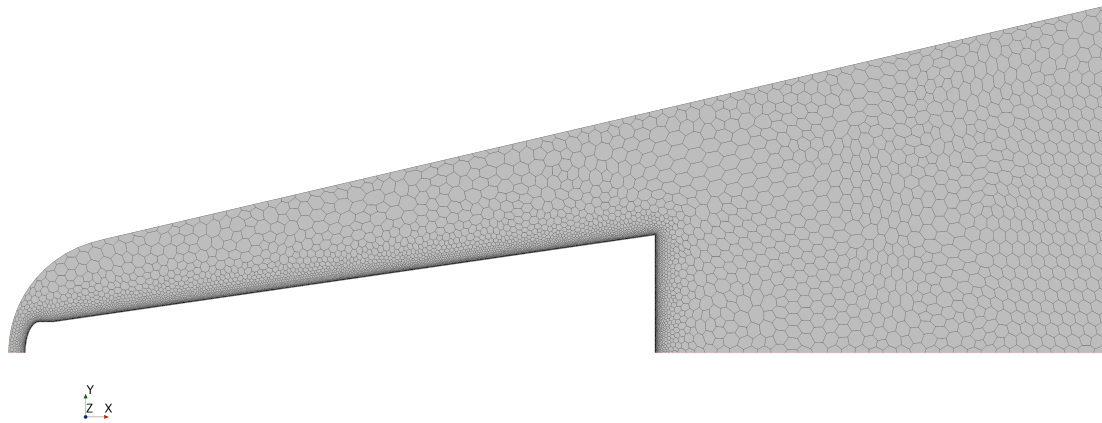
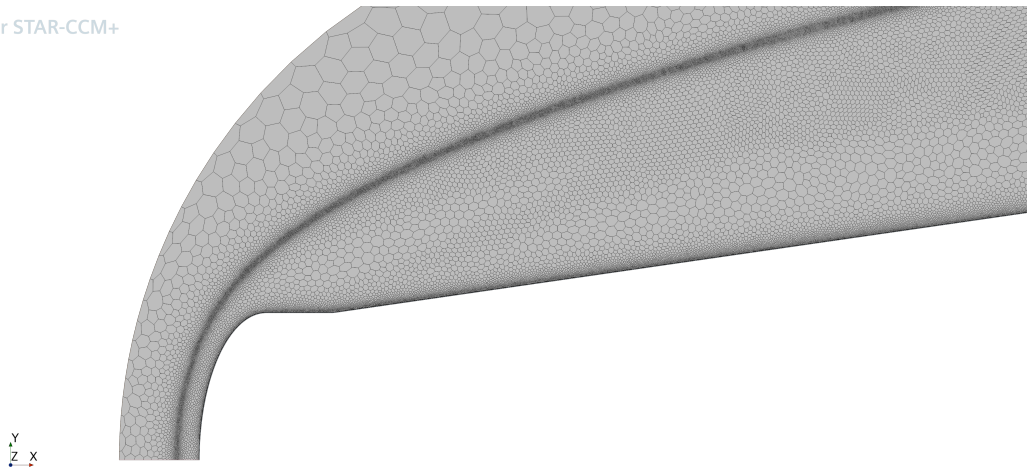


Figure 3.3: full domain starting mesh.

Simcenter STAR-CCM+

Figure 3.4: mesh refined at nose ($M_\infty = 14$, $Z_a = 30$ km).

where the Mach number M is referred to the Mach number field function of STAR-CCM+. Another user defined field function allows to specify the cell size based on equation (3.1) and its naive implementation is presented down below.

The undeclared parameters are defined as follows:

- `threshold = 3;`
- `delta = 0.4;`
- `cell_size_0 = 0.25 mm.`

The mesh refinement process is implemented by a macro script that rebuild a new mesh every 1500 solver iterations, decreasing the cell size where the Mach gradient is large enough. The choice of these values was made based on the experience of prof. D. D'Ambrosio and S. Esposito. An example of how this mesh refinement technique performs is shown in figures 3.4 to 3.7; the lower the mesh refinement level, the denser the mesh will be. All full domain simulations start with the same mesh (figure 3.3).

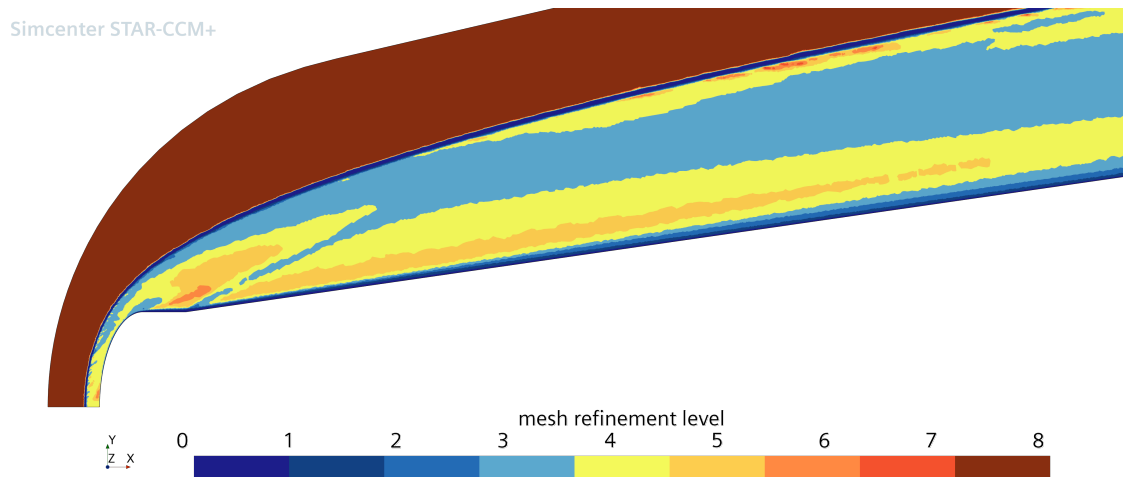


Figure 3.5: mesh refinement level at nose ($M_\infty = 14$, $Z_a = 30$ km).

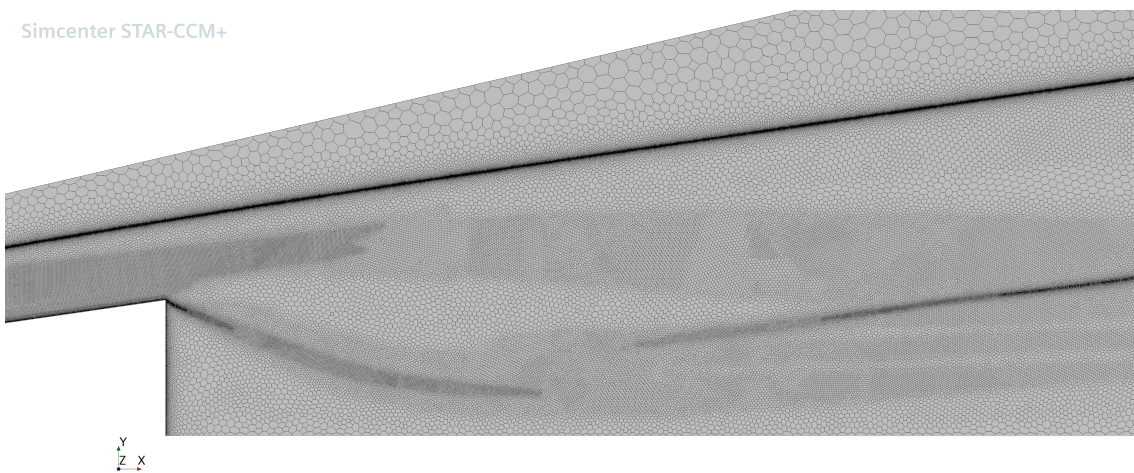


Figure 3.6: mesh refined in the cone wake ($M_\infty = 14$, $Z_a = 30$ km).

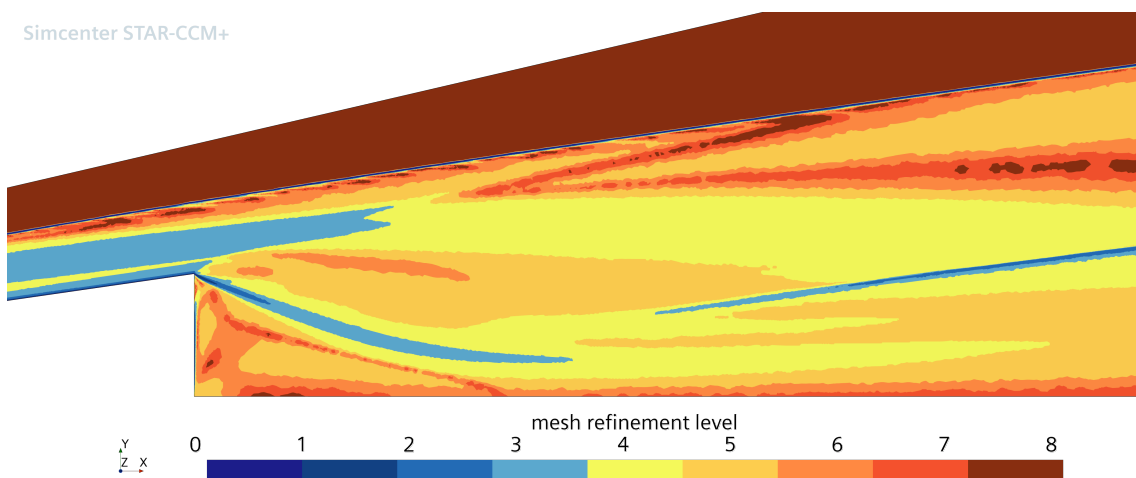


Figure 3.7: mesh refinement level in the cone wake ($M_\infty = 14$, $Z_a = 30$ km).

Algorithm 1: mesh refinement function pseudocode.

```

1 let log_mag_grad_mach = log (||∇M||)
2 for i ← 0 to 8 do
3   if threshold - (i - 1) delta < log_mag_grad_mach and
4     threshold - i delta > log_mag_grad_mach then
5     | cell_size = cell_size_0 2i
6   end
7 end

```

3.2 Physical model selection

In the physics model selection section of STAR-CCM+ it is possible to chose different physical models and formulations that will be used in simulations. For the purpose of this, the following settings were selected:

- steady;
- bidimensional;
- axisymmetric;
- ideal gas;
- coupled flow;
- coupled energy;
- multi-component gas;
- reacting;
- complex chemistry;
- reacting species transport;
- coupled species;
- laminar flame concept;
- turbulent (SST $k - \omega$).

3.2.1 Complex chemistry, multi-component gas, chemical reactions and transport properties

The air model used in the simulation is given by writing it in a *CHEMKIN* file format (see appendix B). More specifically, a seven species air model has been used for all the simulations. For dynamic viscosity and thermal conductivity the Mathur-Saxena average has been implemented in two separated field functions. Individual species follows this curve fits [11]:

$$\mu_{is} = e^{C_{\mu_{is}}} T^{A_{\mu_{is}}} \ln T + B_{\mu_{is}}$$

$$k_{t, is} = e^{E_{k_{t, is}}} T^{A_{k_{t, is}}} \ln(T)^3 + B_{k_{t, is}} \ln(T)^2 + C_{k_{t, is}} \ln T + D_{k_{t, is}}$$

Simcenter STAR-CCM+

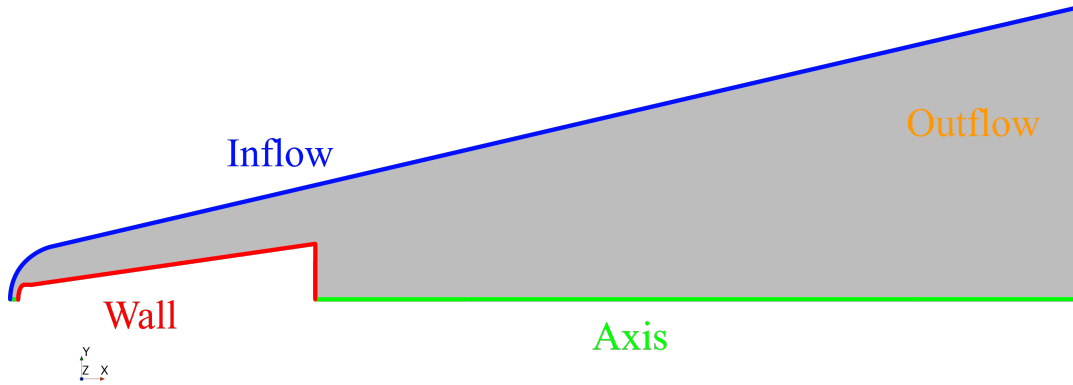


Figure 3.8: full domain with boundary conditions.

Simcenter STAR-CCM+

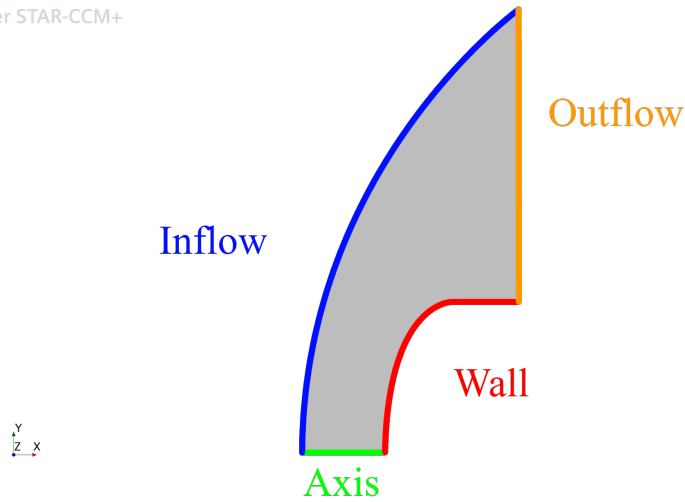


Figure 3.9: nose domain with boundary conditions.

Also the binary diffusion coefficients are given as a curve fit [11]:

$$D_{is,js} = \frac{1}{p} e^{D_{D_{is,js}} T^{A_{D_{is,js}}} \ln(T)^2 + B_{D_{is,js}} \ln T + C_{D_{is,js}}}$$

Thermodynamic properties of individual species are specified at internal thermal equilibrium by polynomial fits [11, 4, 16] (see appendix B). Further informations about this aspect are provided in the next paragraphs.

3.2.2 Boundary conditions

Four boundaries have been defined (see figures 3.8 and 3.9):

Inflow: it involves the circular arc and the contiguous oblique upper line;

Axis: it includes the two horizontal lines;

Outflow: the vertical segment at the left;

Wall: it involves all the segments of the cone-like geometry.

Inflow and Outflow

A *free stream* boundary condition type has been applied to both the patches. Specifically the parameters setted are the following:

- Mach number and horizontal flow direction;
- static pressure and temperature;
- species mass fractions ($c_{\text{N}_2} = 0.767$, $c_{\text{O}_2} = 0.233$, see table 2.1);
- turbulence intensity coefficient, 0.01;
- turbulent viscosity ratio, 10.

Turbulence model settings were left as the default ones. Free stream Mach number, static pressure and temperature were changed from case to case.

Axis

The boundary condition imposes axisymmetric constrain.

Wall

All the wall of the cone-like body are solid wall which are impermeable to the flow. Furthermore it has no catalytic function in reacting flow. The *no-slip* condition imposes that the flow velocity at the wall has the same velocity of the wall: since the body is considered motionless the velocity is zero. In the thermal specifications the heat flux is defined in order to model an adiabatic-radiative wall:

$$\Phi_{\text{gw}} - \underbrace{\varepsilon_w \sigma T^4}_{\Phi_{\text{rad}}} = 0,$$

where Φ_{gw} is the convective heat flux due to the fluid and Φ_{rad} is the radiative heat flux of the heated wall surface. The emissivity ε_w is defined using a field function and assumes multiple values; at the nose $\varepsilon_w = 0.8$.

3.2.3 Initial condition

The initial conditions are assigned to each computing domain cell before starting the simulation routine. Temperature, pressure and turbulence parameters are equal to free stream values. The initialized velocity field is for most of the domain the same as the free stream, in the wake is defined a linear velocity ramp from 0 at the bottom of the cone to the free stream value (see figure 3.10). This initialization prevents to reach low pressure at the bottom of the cone during the non-physical transition to the steady solution.

3.3 Simulation cases

The aim of all simulations conducted is to observe how the seven species air model worked in multiple free-stream conditions. Properly speaking, the boundary constrains of the inlet patch were modified in order to match multiple altitudes and Mach numbers. Some simulation cases were performed considering only the high-temperature nose (the outlet

Simcenter STAR-CCM+

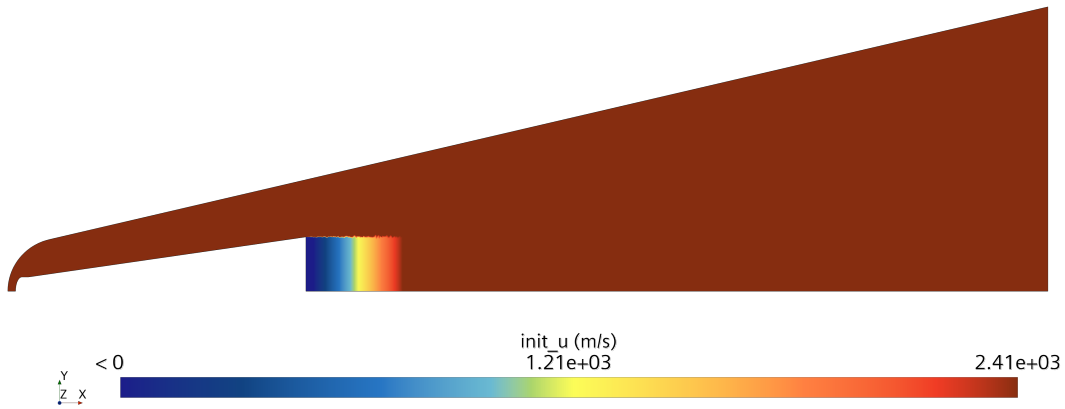


Figure 3.10: initial velocity field ($M_\infty = 8$, $Z_a = 30$ km).

patch was moved at the slope change between the horizontal nose wall and the oblique cone surface, figure 3.9) in order to compare different thermodynamic property polynomial fits, specifically Burcat polynomials [4], which cover temperatures up to 6000 K, and Gupta [11] and McBride [16] ones (up to 30 000 K and 20 000 K respectively). To ensure the convergence of the simulation some key parameters were monitored:

- maximum NO^+ number density;
- maximum wall temperature.

The n_{NO^+} , and its associated plasma frequency, were monitored not only across the entire computing domain but also considering its maximum value at the outlet: this procedure allowed to ensure that the chemical species of the air model could reach the wake of the cone and the end of the domain. A comprehensive representation of all conducted simulation is reported in table 3.1.

		Geo-potential altitude, Z_a			
		20 km	30 km	50 km	70 km
Free stream Mach number, M_∞	8	FD(BR)	FD(BR) ND(BR, GP)	FD(BR)	—
	9	FD(BR)	FD(BR) ND(BR, GP)	FD(BR)	FD(BR)
	10	FD(BR)	FD(BR) ND(BR, MB)	FD(BR)	FD(BR)
	12	FD(BR)	FD(BR) ND(BR, MB)	FD(BR)	FD(BR)
	14	FD(BR)	FD(BR) ND(BR, MB)	FD(BR) ND(BR, MB)	FD(BR)
	16	FD(BR)	ND(BR, MB)	FD(BR) ND(BR, MB)	FD(BR)

FD: full domain
ND: nose domain
BR: Burcat polynomials [4]
GP: Gupta polynomials [11]
MB: McBride polynomials [16]

Table 3.1: simulation cases.

		Pressure, p [Pa]	Temperature, T [K]	Density, ρ [kg m^{-3}]
Geo-potential altitude, Z_a [km]	20	5.47×10^3	216.65	8.80×10^{-2}
	30	1.17×10^3	226.65	1.80×10^{-2}
	50	7.59×10^1	270.65	9.78×10^{-4}
	70	4.63	217.45	7.42×10^{-5}

Table 3.2: standard atmosphere free-stream boundary conditions.

Chapter 4

Simulation results

This chapter summarizes some relevant results obtained from the numerical simulations that have been described in chapter 3. Particular attention was given to the analysis of thermodynamic properties and species concentrations referred to the stagnation streamline; furthermore, the production of ionized species, NO^+ specifically, has been monitored.

4.1 Global parameters

This section considers global quantities that affect the whole flow field and that, in a certain way, can be taken into account during the design process of hypersonic technologies (e.g. re-entry modules, missiles and weapons, . . .):

- maximum and post-shock temperature, pressure and density;
- wall temperature and pressure distributions;
- drag coefficient;
- stand-off distance.

4.1.1 Post-shock conditions

After a shock-wave, the flow undergoes compression and its temperature, pressure and density rise. Numerical results relative to the stagnation streamline were compared to the 1D inviscid normal shock theory [1] (basically the theory considers a calorically perfect gas, which has constant thermodynamic properties, chapter 1) and the results are reported in figures 4.1 to 4.3. Starting with the pressure ratio, the theory, using $\gamma = 1.4$, slightly underestimates the simulation results by about 10%. In figure 4.2 the ratio between post-shock and free stream temperatures is compared with the theoretical prediction, which is well above the numerical values. Finally, the density ratio has a theoretical asymptotic value of 6 (always for $\gamma = 1.4$), however the simulation results easily exceed it; moreover there is no asymptote in numerical values. Summing up, all the discrepancies between simulations and theory can be explained taking into account that γ in a reacting flow is not constant. The normal shock relations used are based on a calorically perfect gas behaviour, which means that γ is constant. The predicted theoretical temperature ratios using $\gamma = 1.33$ are closer to the numerical results.

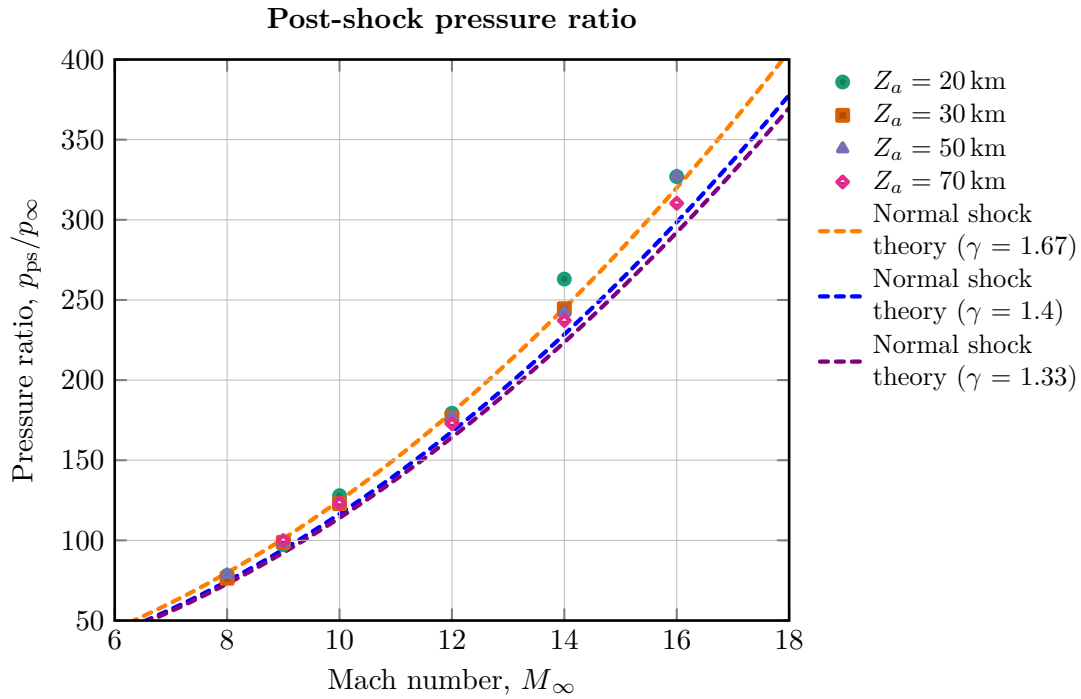


Figure 4.1: post-shock pressure ratio at different Mach numbers and altitudes.

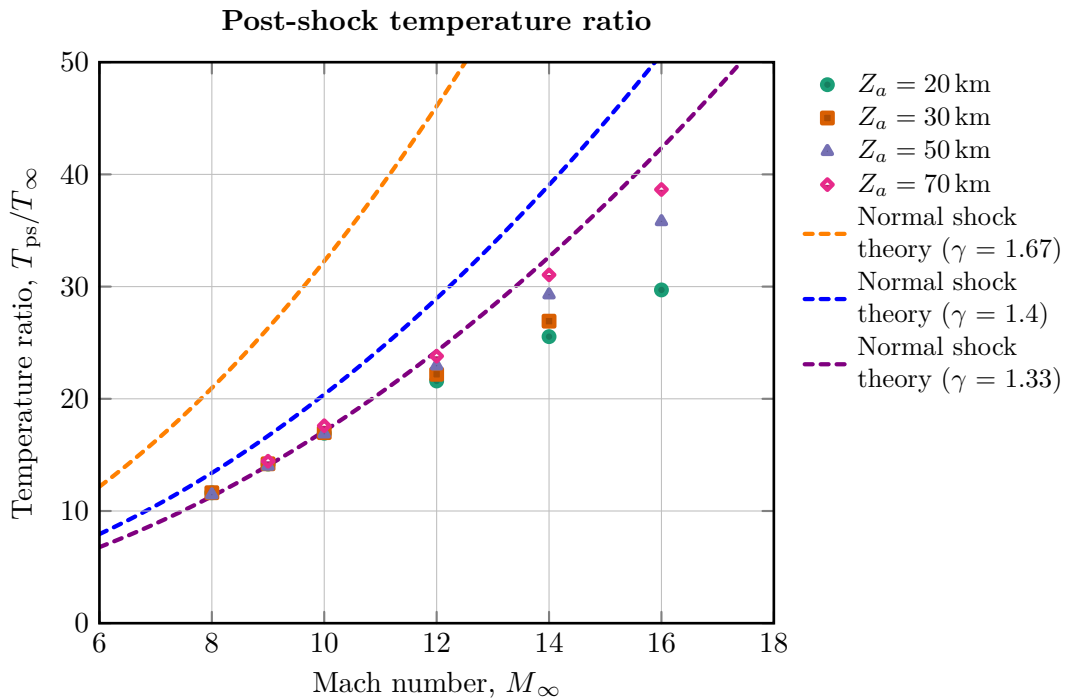


Figure 4.2: post-shock temperature ratio at different Mach numbers and altitudes.

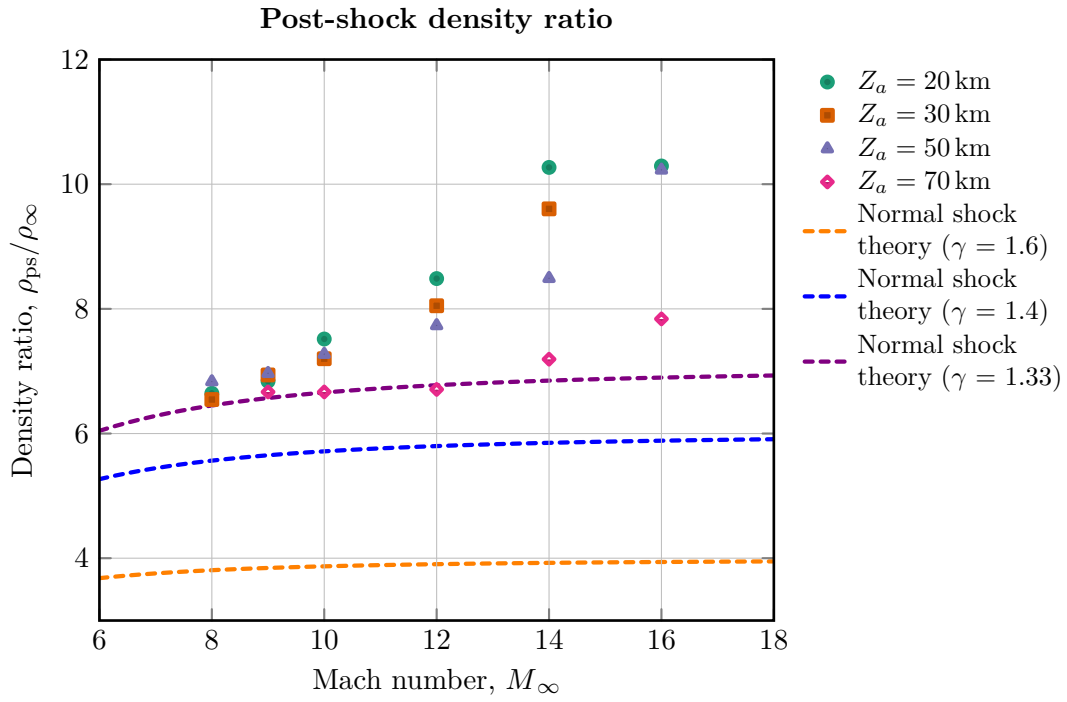


Figure 4.3: post-shock density ratio at different Mach numbers and altitudes.

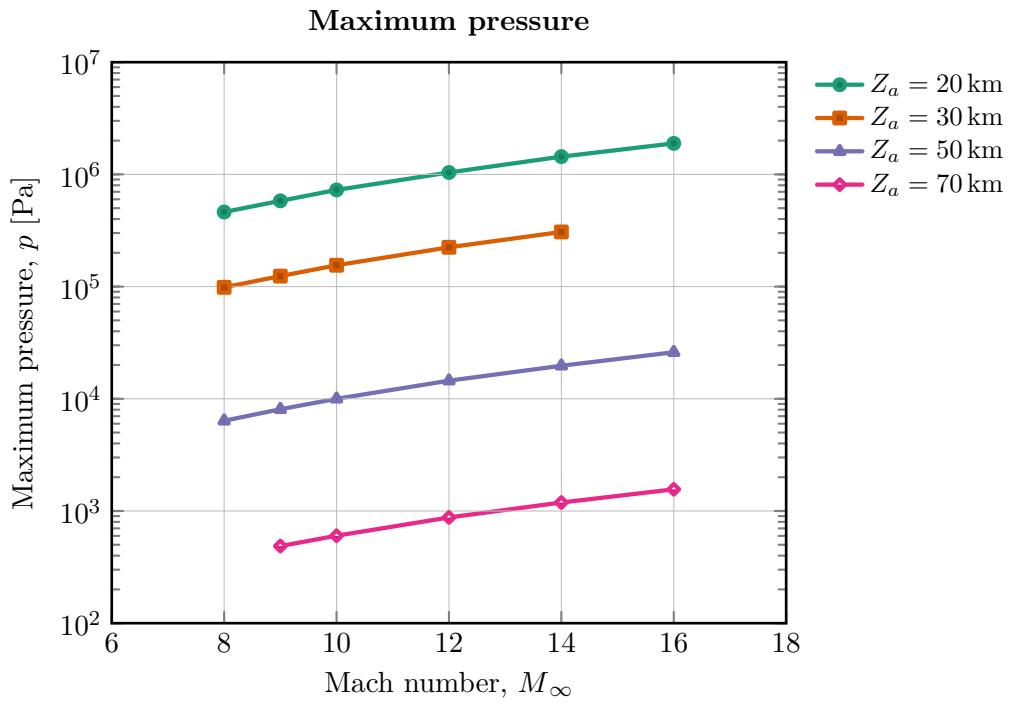


Figure 4.4: maximum pressure at different Mach numbers and altitudes.

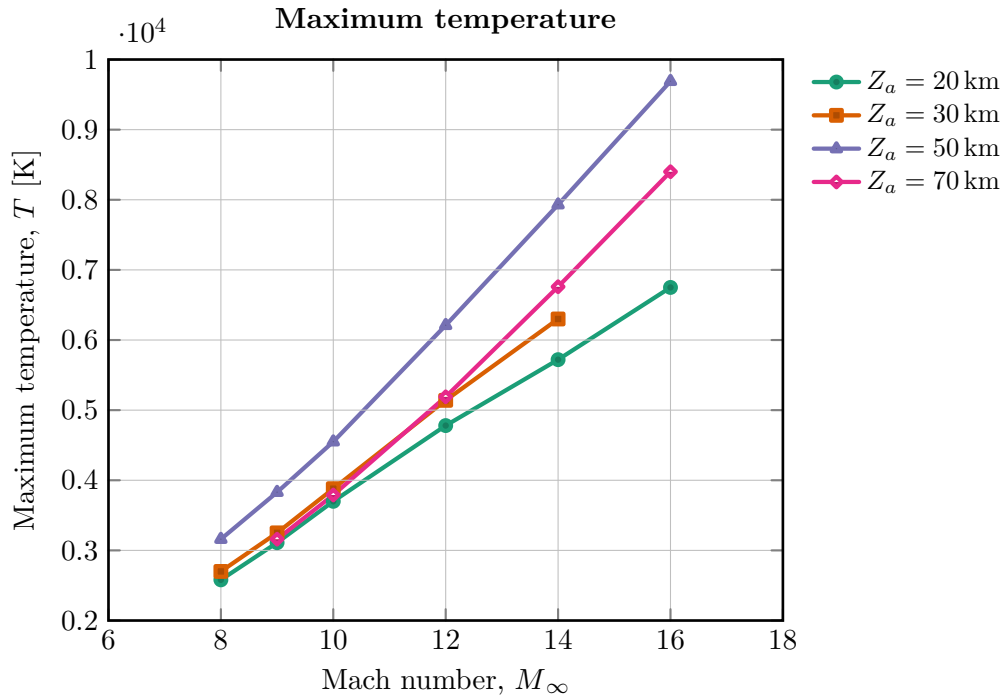


Figure 4.5: maximum temperature at different Mach numbers and altitudes.

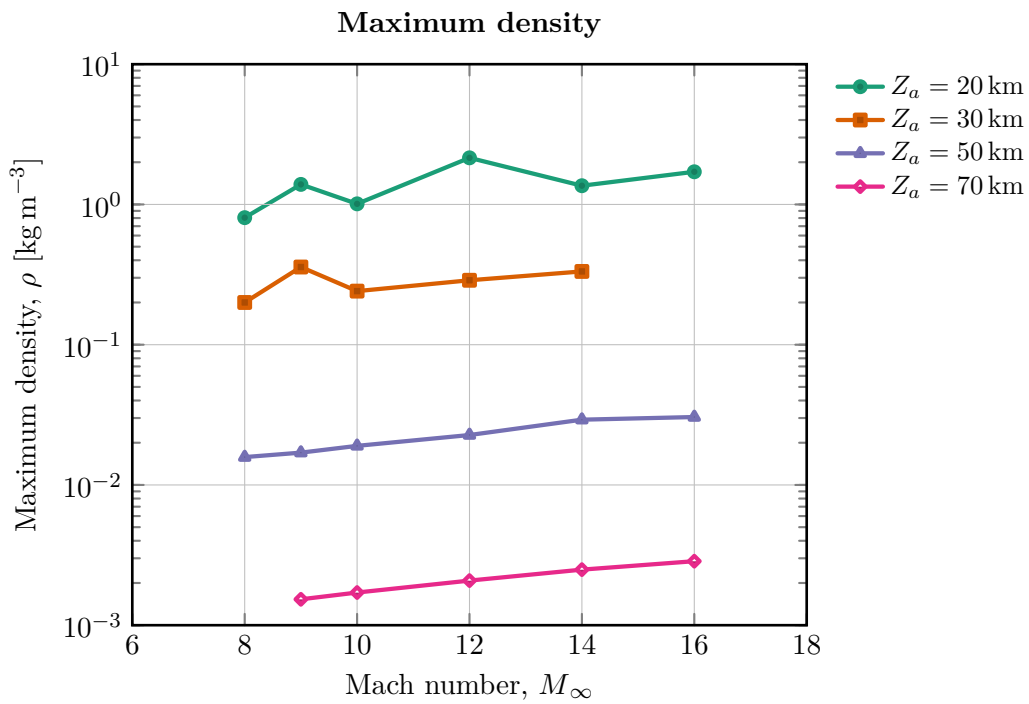


Figure 4.6: maximum density at different Mach numbers and altitudes.

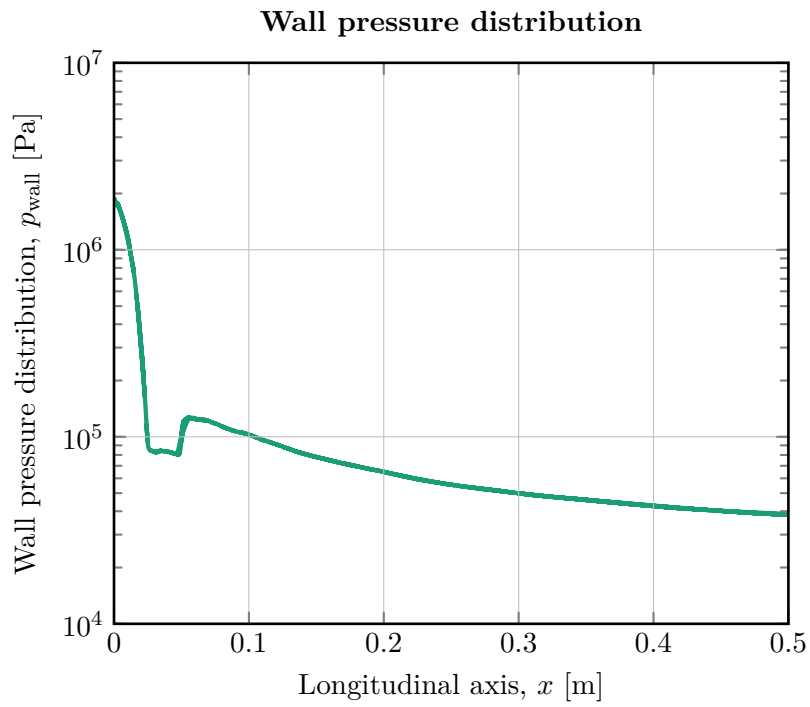


Figure 4.7: wall pressure distribution for $M = 16$ and $Z_a = 20$ km.

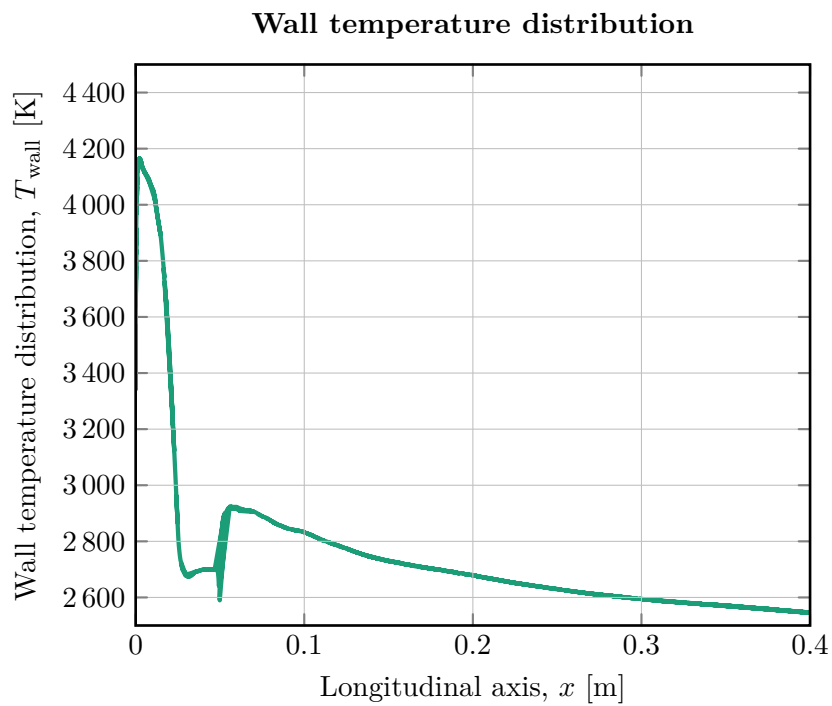


Figure 4.8: wall temperature distribution for $M = 16$ and $Z_a = 20$ km.

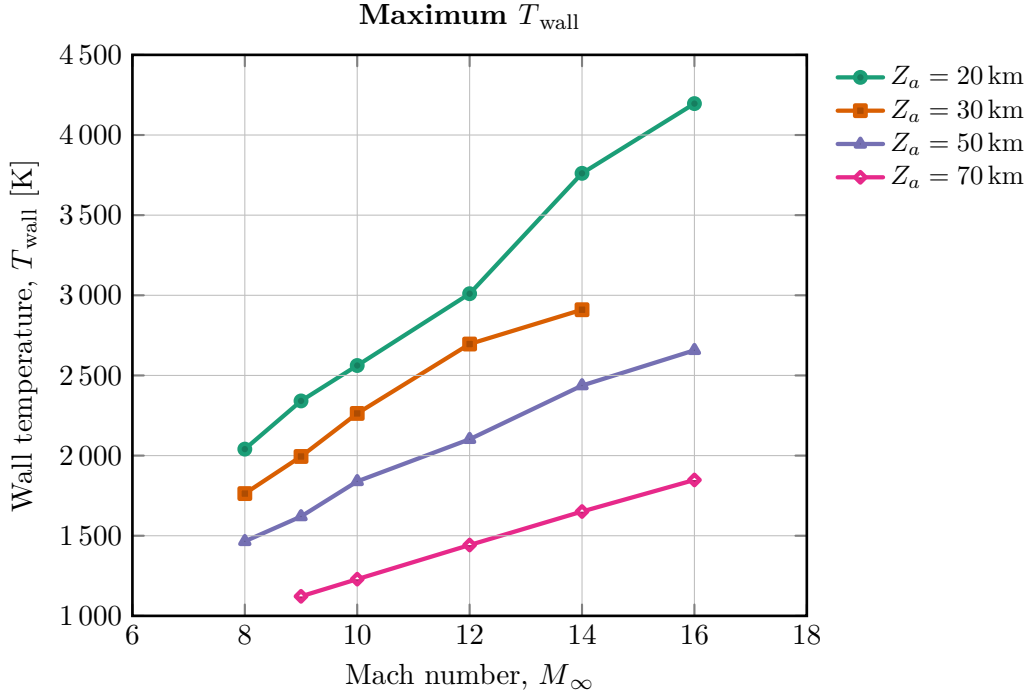


Figure 4.9: maximum wall temperature at different Mach numbers and altitudes.

4.1.2 Maximum pressure, temperature and density

Figures 4.4 to 4.6 show the maximum values of pressure, temperature and density reached in each simulated case. Both pressure and temperature monotonically rise with the Mach number, which is consistent with post-shock considerations made previously. Since pressure decays exponentially as the altitude increases (appendix A.3.3), maximum pressure values are found at lower altitudes. Conversely, the temperature has not a monotonic profile throughout the atmosphere and for this reason, at the same Mach number, all $Z_a = 50$ km cases reach higher maximum temperatures. Density largely depends on air chemical composition, anyway slightly rises as the Mach number increases. Wall pressure and temperature distributions can be shown in figures 4.7 and 4.8 in the two worst case scenarios. The peak values are located at the nose zone and the discontinuities in pressure and temperature distributions are positioned where the geometry rapidly changes. It is interesting to note that the peak wall temperature (figure 4.9) is higher for $Z_a = 20$ km cases than $Z_a = 50$ km ones, where the maximum temperature values are even higher than the $Z_a = 20$ km simulations.

4.1.3 Drag coefficient

STAR-CCM+ allows to measure some quantities by using *report* options. In order to evaluate the force exchanged between the flow and the cone-like body has been considered both the pressure and shear contributions. Since all the simulations are axisymmetric, the drag force evaluated by its report, D_r is computed by assuming that the mesh is swept through a one-radian angle [23]. The overall drag force, D , is obviously computed multiplying the report result by 2π [7]. In the end, drag coefficient, C_D , is evaluated as follows:

$$C_D := \frac{2D}{\rho_\infty \|\mathbf{v}_\infty\|^2 A_b} = 4\pi \frac{D_r}{\rho_\infty \|\mathbf{v}_\infty\|^2 A_b},$$

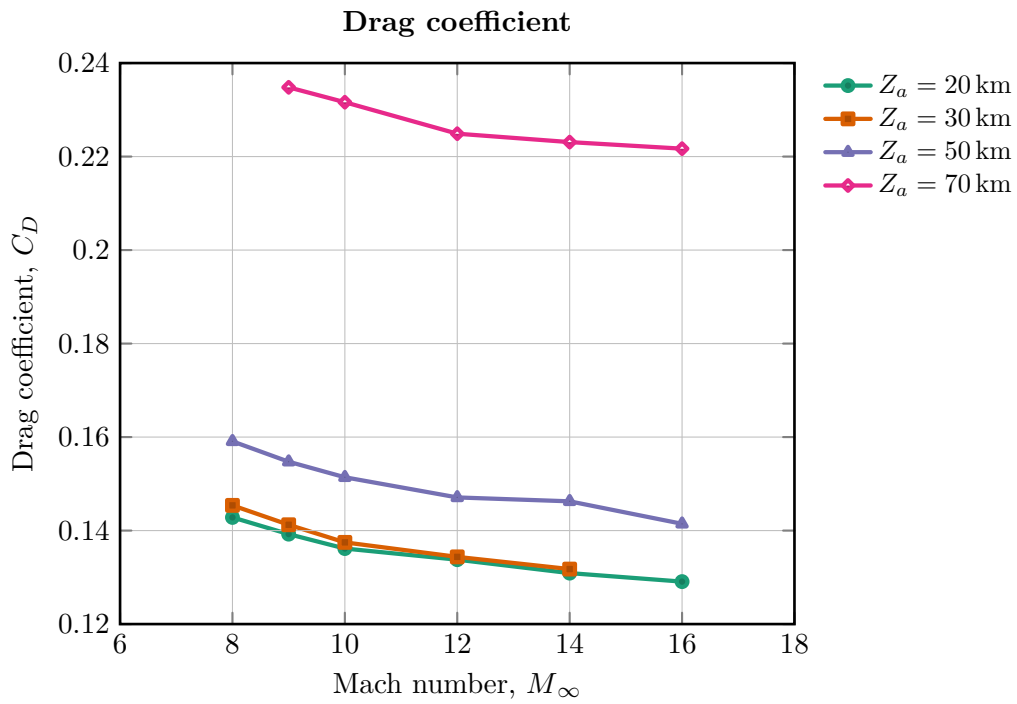


Figure 4.10: drag coefficient at different Mach numbers and altitudes.

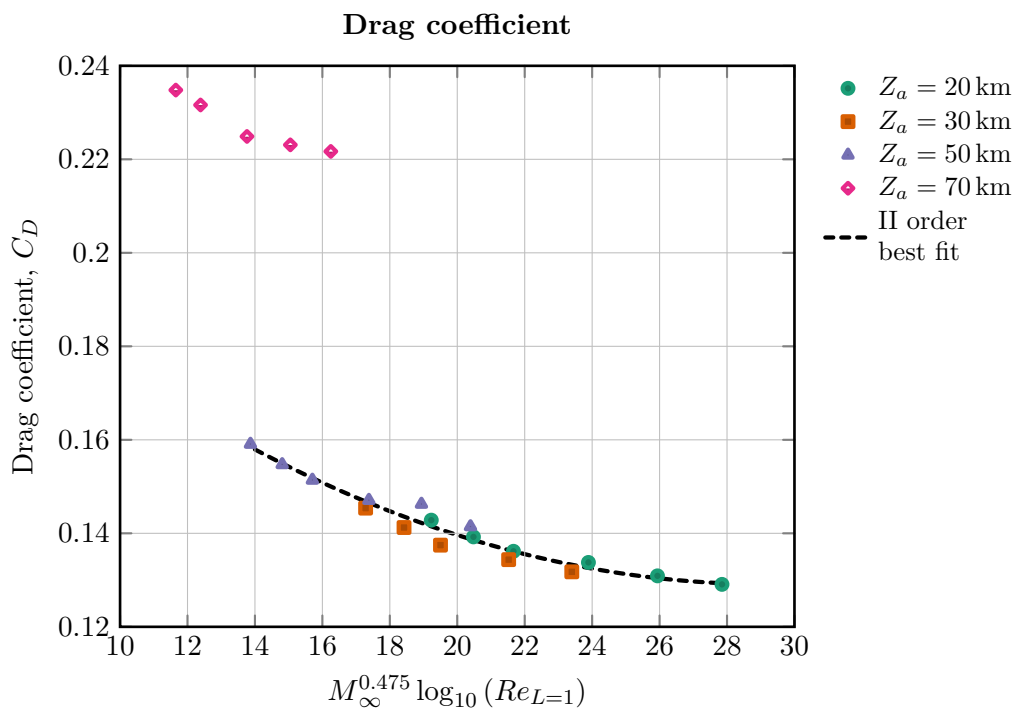


Figure 4.11: drag coefficient on modified scale.

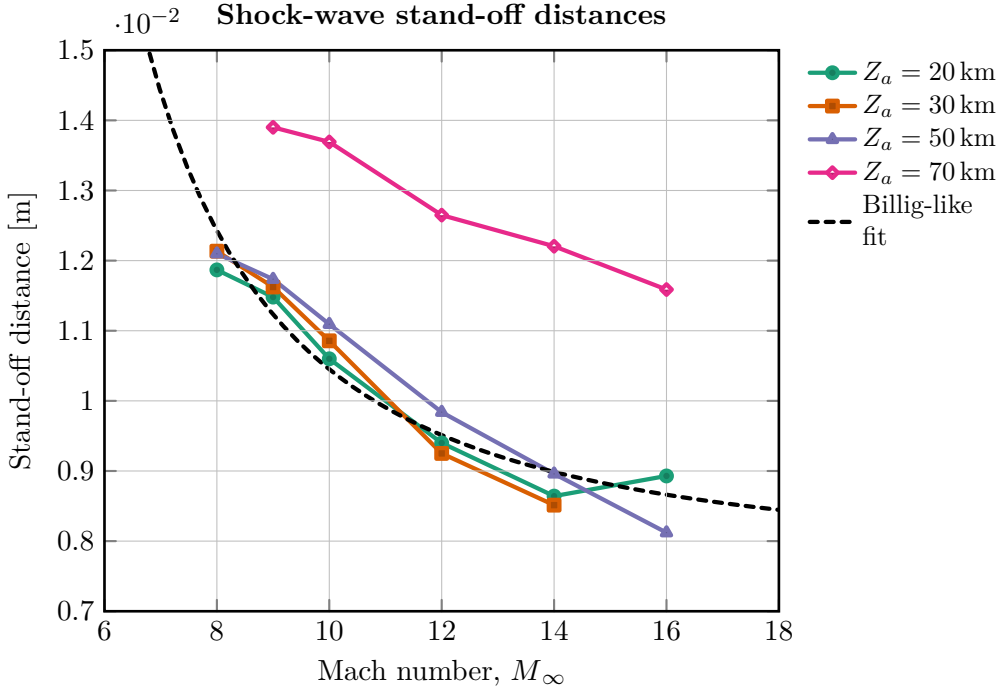


Figure 4.12: simulation shock stand-off distances at different Mach numbers and altitudes.

where A_b is the base area of the cone (see figure 3.1). The figure 4.10 shows drag coefficient as function of Mach number at different geo-potential altitudes. According to the *Oswatitsch Mach number independence principle* [5], the drag coefficient should reach an asymptotic value for large Mach numbers. Observing simulations at the same altitude it is clear that the drag coefficient does not change much. For altitudes of 20 km, 30 km, 50 km it is mostly limited between 0.13 and 0.16. Conversely, at 70 km the drag coefficient rises on average by a 50% respect to the other altitudes. After some attempts, the horizontal axis of figure 4.10 has been modified introducing the Reynolds number evaluated on a characteristic length L of 1 m, $Re_{L=1}$, so that the density variation (see appendix A.3.3) can be taken into consideration. For the first three data series (20 km, 30 km, 50 km) a good overlapping was found, which can be fitted by the following polynomial function:

$$C_D(x) = 1.25 \times 10^{-4} x^2 - 7.31 \times 10^{-3} x + 2.36 \times 10^{-1}.$$

with $x = M^{0.475} \log_{10}(Re_{L=1})$ for a compact writing. In figure 4.11 can be seen the rescaled drag coefficient plot, unfortunately the last data series (70 km) does not overlap to the others. The choice to adopt $M^{0.475} \log_{10}(Re_{L=1})$ as parameter is not really justified by any physical observation but it is an attempt to find a way to find a fitting function which properly represent 20 km, 30 km, 50 km cases.

4.1.4 Stand-off distance

It is the distance between the stagnation point located at the solid wall and the shock-wave. In these cases it can be measured by taking the Mach number along the stagnation streamline and evaluating the position of the discontinuity relative to the wall. On the practical side a second order finite difference scheme was used to evaluate Mach number gradient and then a weighed average (clearly the weight used were Mach number gradient discrete values) was used to determine the location of the shock-wave relatively to the

nose of the cone. The processed data are plotted in figure 4.12. The stand-off distances monotonically decrease in all cases (except for $M = 16, Z_a = 20$ km, probably due to numerical interpolation issues). This result is coherent with some literature results and correlations. For example, the *Billig correlation* [2] predicts the shape of a shock-wave based essentially on the free stream Mach number. The stand-off distance formula reported in [2] has the following form:

$$\Delta = A \exp(BM^{-2}) \quad (4.1)$$

where A and B depends on shape and local wall curvature and Δ is the stand-off distance. The parameters proposed by Billig does not really match the data of these simulation and, considering only 20 km, 30 km, 50 km cases, the parameters of equation (4.1) that match this case study are

$$A = 7.68 \times 10^{-3} \text{ m}$$

$$B = 3.08 \times 10^1.$$

From [2] the parameters should be the following:

$$A = 2.64 \times 10^{-2} \text{ m}$$

$$B = 3.24.$$

Again, the higher altitude simulations have produced results that does not correlate with others.

4.2 Reacting flow

This section reports data simulation related the reacting flow. Particularly to the NO and NO⁺ production.

4.2.1 Ions formation

Plasma formation is one relevant aspect of hypersonic technologies. Since ionized gas is electrically charged, it may interfere with radio-frequency system (radar, telecommunication systems, ...) and it should be taken into account. The number density on NO⁺, n_{NO^+} , has been monitored an the nose, where it is produced by the high temperature, and the NO⁺ plasma frequency, which is function of its number density (since the only two ionized species are NO⁺ and e⁻)

$$f_{\text{NO}^+} = \frac{1}{2\pi} \sqrt{\frac{n_{\text{NO}^+} q_{e^-}^2}{m_{e^-} \varepsilon_0}}$$

where q_{e^-} is the electron electric charge, m_{e^-} its mass and ε_0 the permittivity on free space. Form figure 4.13 it is clear that plasma formation better correlates with maximum wall temperature that maximum temperature (figure 4.5). The explanation is linked to the fact that chemical reactions are not instantaneous and, furthermore, dissociation and ionization are endothermic. Figure 4.15 shows NO, NO⁺ molar fractions and temperature along the stagnation streamline. In the subsonic region simultaneously to the production of NO⁺ the temperature is reduced. The transport of ionized species at the outlet boundary

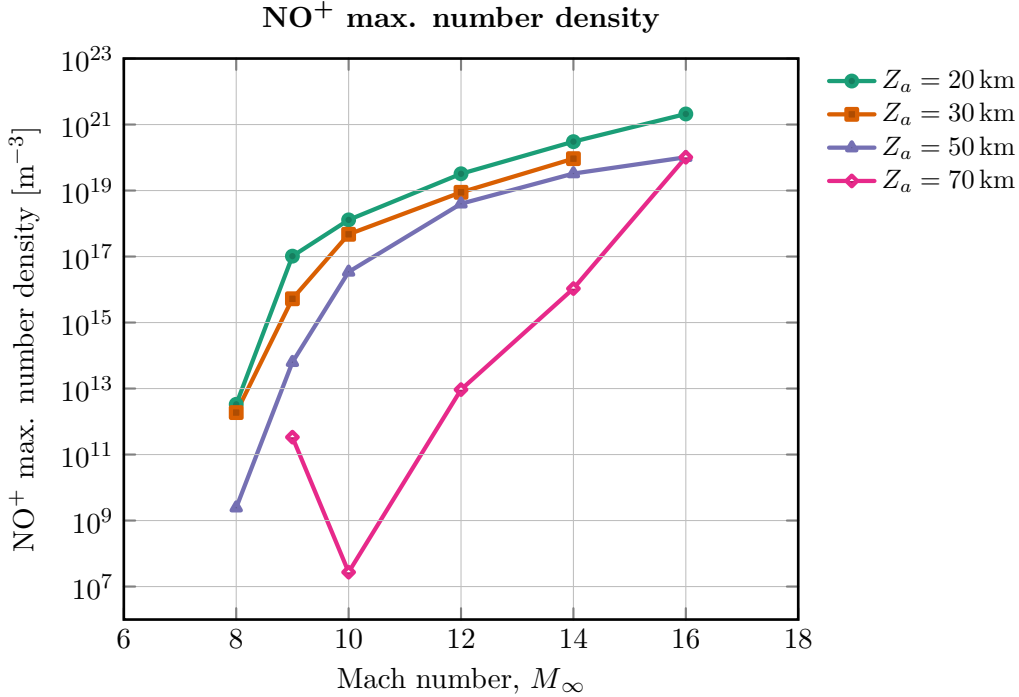


Figure 4.13: NO^+ maximum number density at different Mach numbers and altitudes.

is reported in figure 4.14. In both figures 4.13 and 4.14 the $Z_a = 70$ km simulation data series, again, does not follow a similar behaviour the the other simulation results. Now, it is possible to suppose that the convergence for $Z_a = 70$ km simulation cases has not been fully reached. Figures 4.16 to 4.19 show the NO and NO^+ production along the stagnation streamline. In the case tested, it seems that N plays a role as a limiting reactant in nitric oxide production (see figure 4.20): from the equilibrium study (see chapter 2) N_2 dissociates at higher temperature that O_2 .

4.2.2 Polynomial comparison

All full domain simulations (table 3.1) were performed using Burcat polynomials [4]. Considering only the nose region, a series of simulations were performed in order to compare different thermodynamic properties polynomials [11, 16]. The results reported in figure 4.21 shows that in the used temperature ranges the polynomials behaves in the tested cases almost the same. The maximum NO^+ number density computed in the nose-only simulations is consistent with the full domain simulated cases.

4.3 Limitations of numerical model

The physical model implemented in STAR-CCM+ assumes the gas in internal thermal equilibrium, which means that all the particle energy levels are in equilibrium. Therefore, no vibrational non-equilibrium modelling has been taken into consideration, and thermodynamic property polynomials were used instead: this choice was made because thermal non-equilibrium is not clearly documented in the software user guide. Furthermore, charged particles behaviour is not very accurate: electrons, especially at high altitudes, spread in the entire domain (figure 4.28), this because no *ambipolar diffusion* modelling is used and this causes an unrealistic electron diffusion phenomenon. Lastly, some numer-

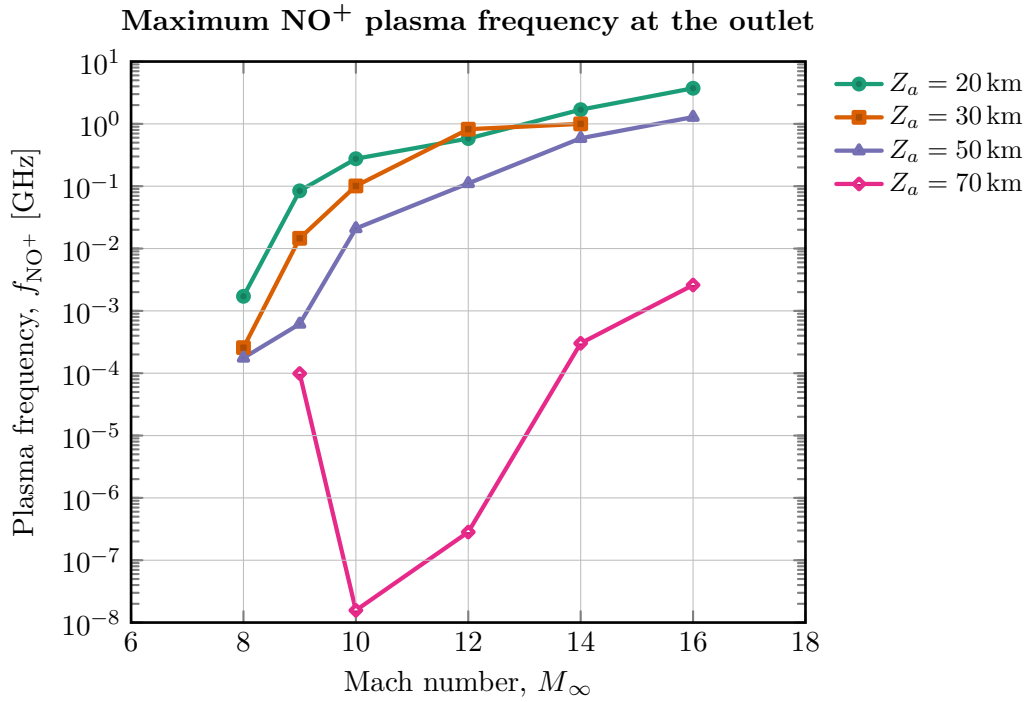


Figure 4.14: maximum NO⁺ plasma frequency at the outlet at different Mach numbers and altitudes.

ical instabilities have been encountered in some simulation cases: the cause is probably linked to chemical non-equilibrium numerical solver which causes the Algebraic Multigrid linear solver to fail. Apparently discontinuities in mesh cell quality trigger this numerical phenomenon.

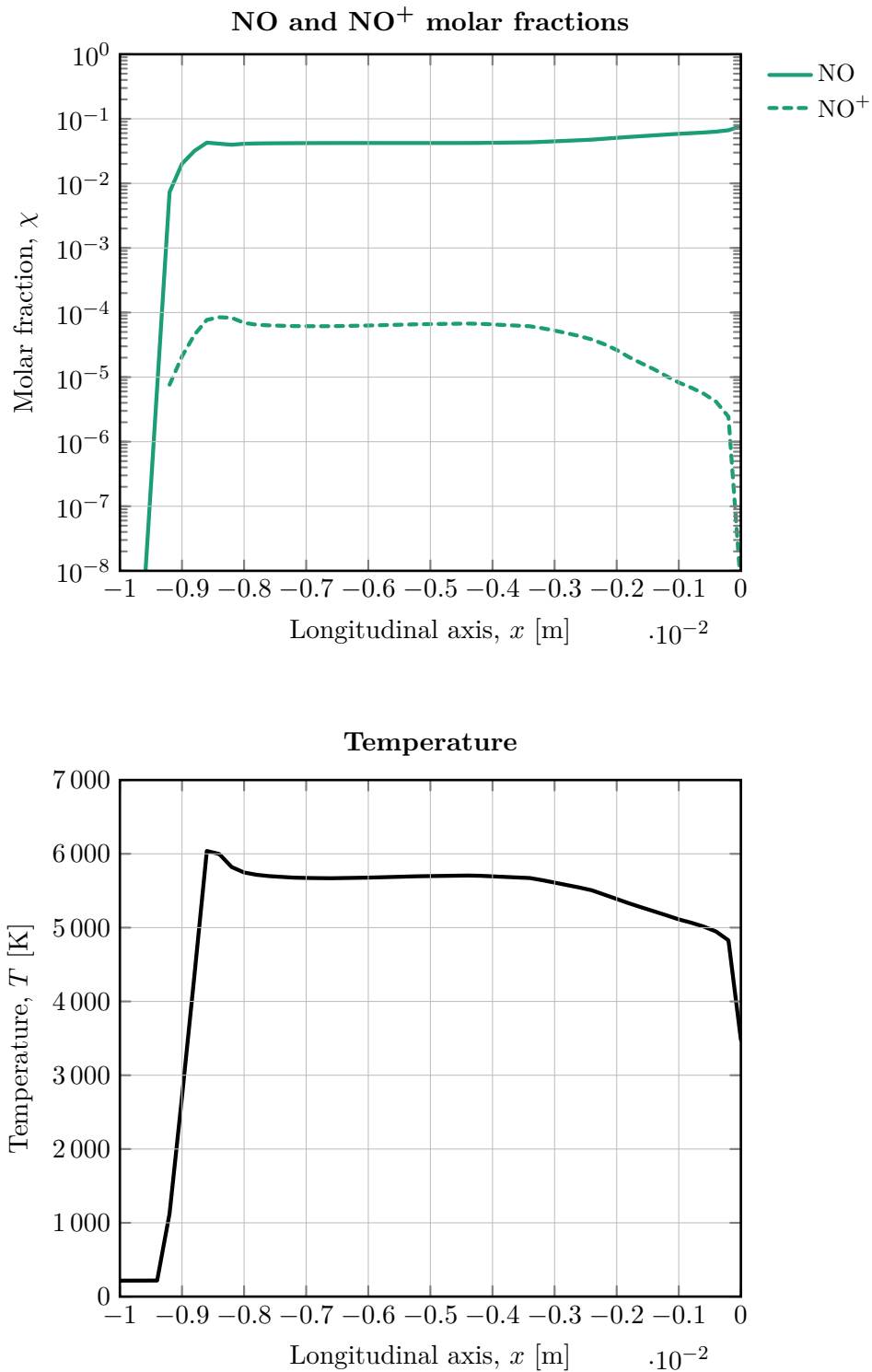


Figure 4.15: NO, NO⁺ molar fraction and temperature along stagnation streamline for simulation case $M_\infty = 16$ and $Z_a = 20$ km.

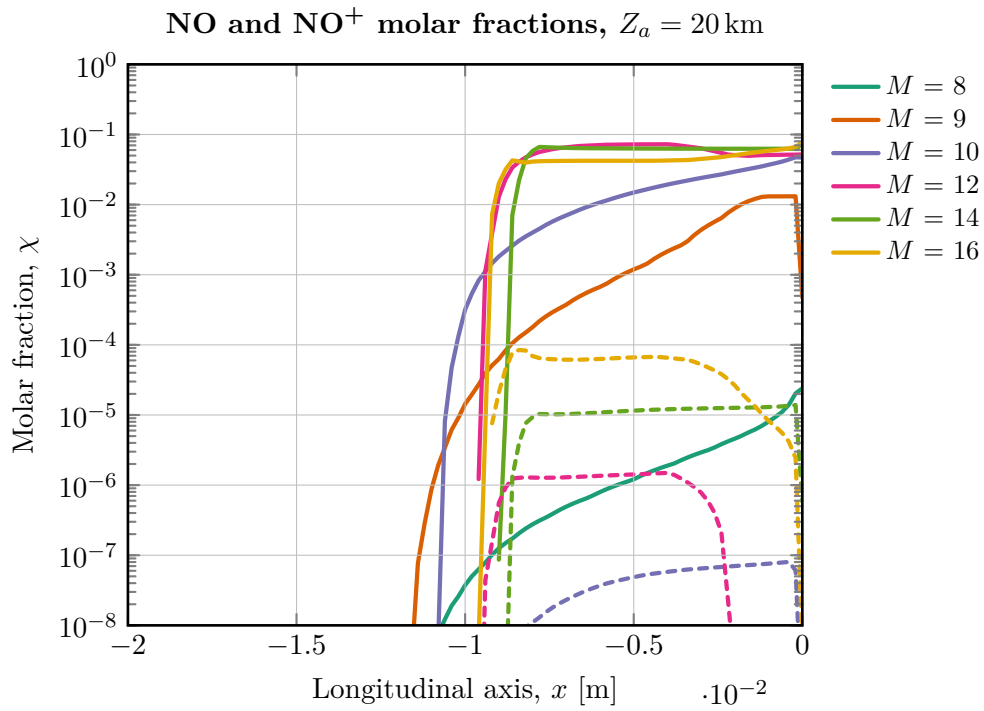


Figure 4.16: NO (solid) and NO⁺ (dashed) molar fractions at longitudinal symmetry axis at $Z_a = 20$ km and varying Mach number.

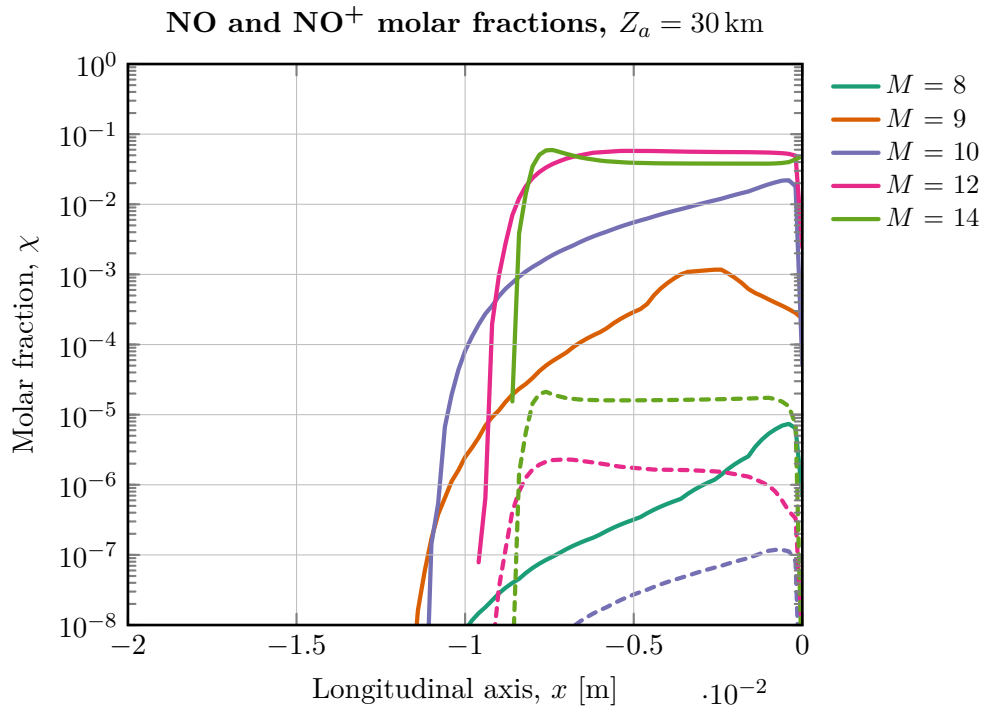


Figure 4.17: NO (solid) and NO⁺ (dashed) molar fractions at longitudinal symmetry axis at $Z_a = 30$ km and varying Mach number.

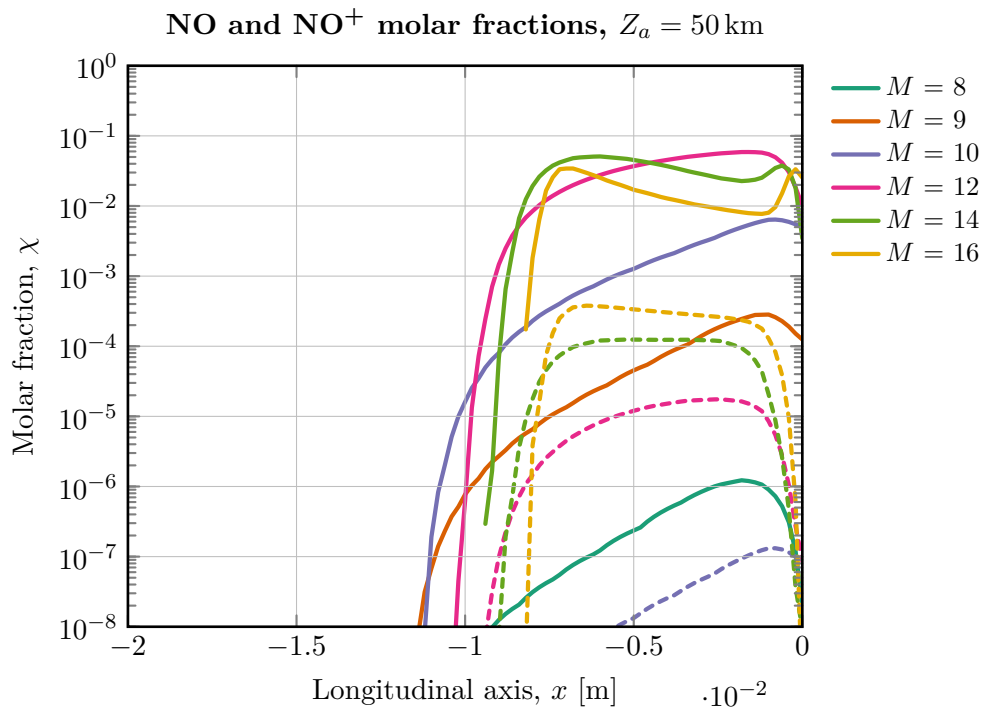


Figure 4.18: NO (solid) and NO⁺ (dashed) molar fractions at longitudinal symmetry axis at $Z_a = 50$ km and varying Mach number.

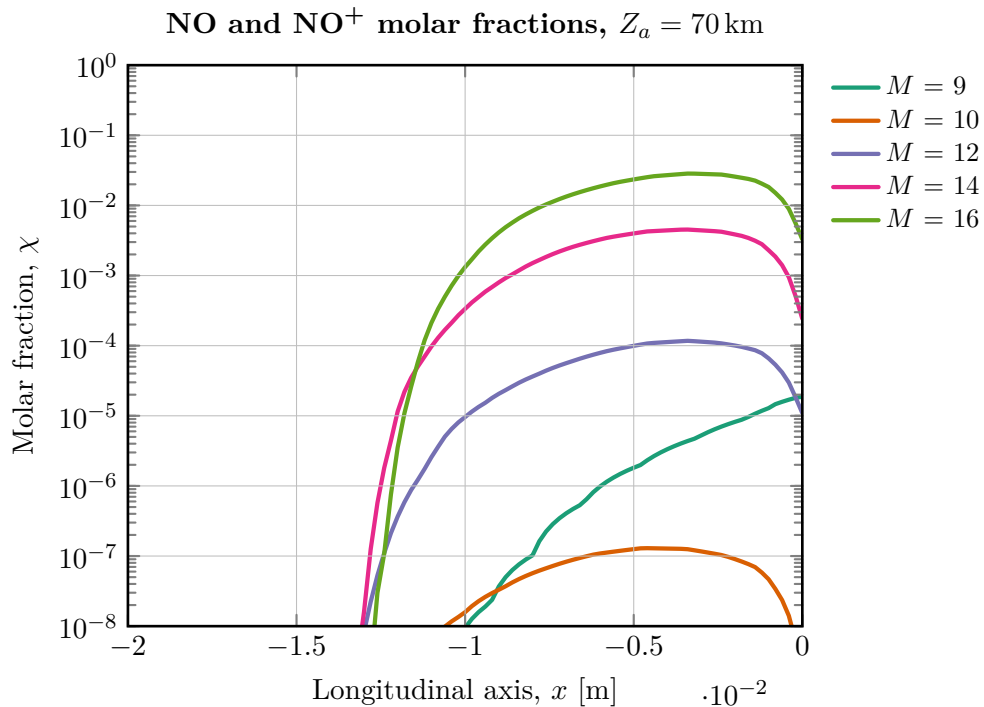


Figure 4.19: NO (solid) and NO⁺ (dashed, not displayed, molar fraction lower than 1×10^{-8}) molar fractions at longitudinal symmetry axis at $Z_a = 70$ km and varying Mach number.

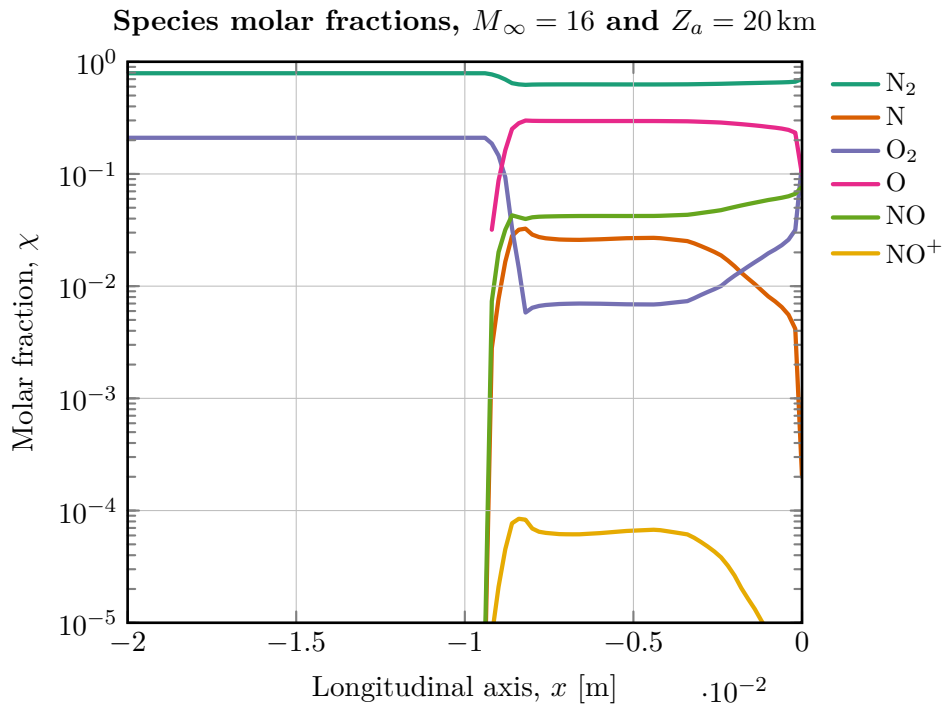


Figure 4.20: species molar fraction along stagnation streamline for $M_\infty = 16$ and $Z_a = 20$ km.

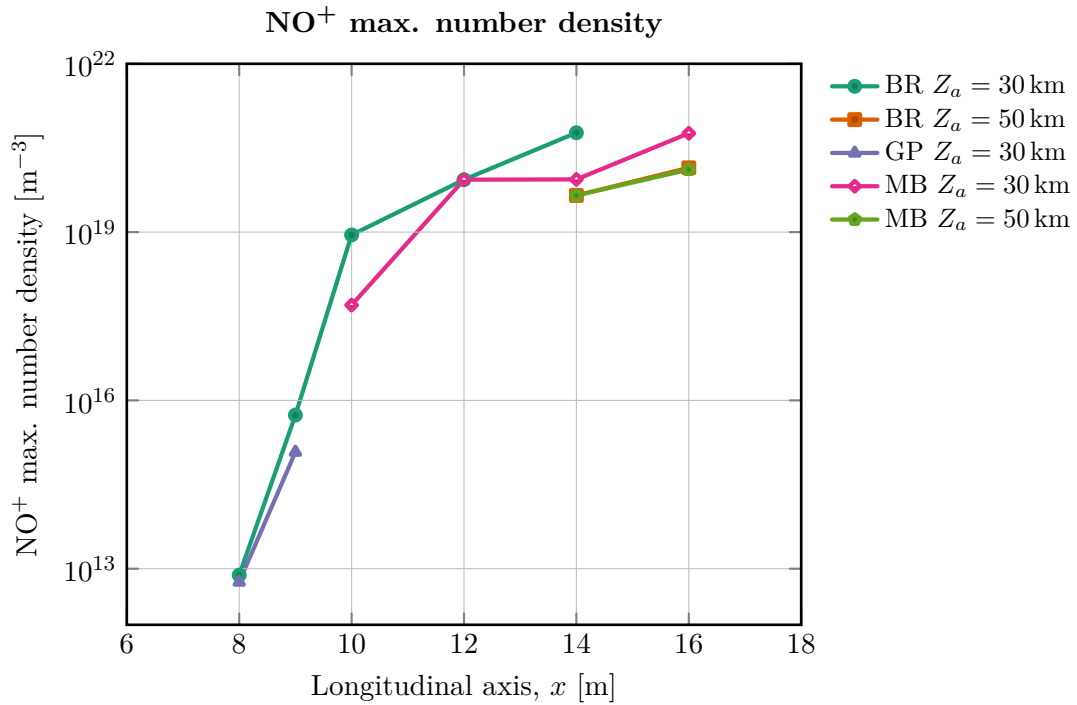


Figure 4.21: comparison of maximum NO⁺ number density using different thermodynamic properties polynomials $Z_a = 20$ km (BR - Burcat [4]; GP - Gupta [11]; MB - McBride [16]).

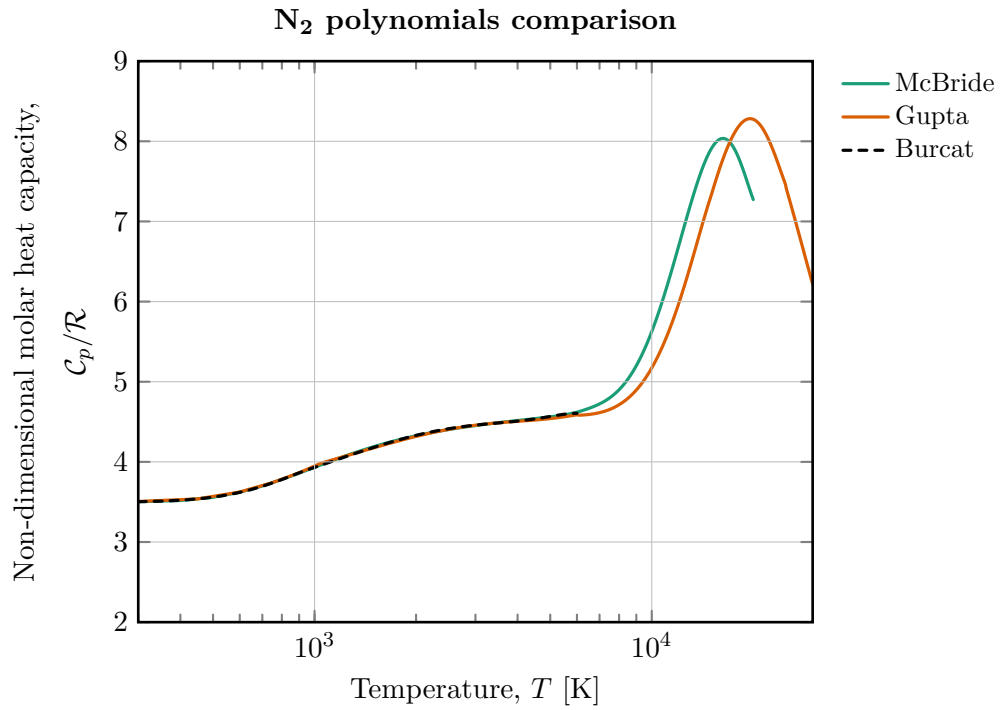


Figure 4.22: comparison between heat capacity polynomial fits of N₂ [16, 11, 4].

Simcenter STAR-CCM+

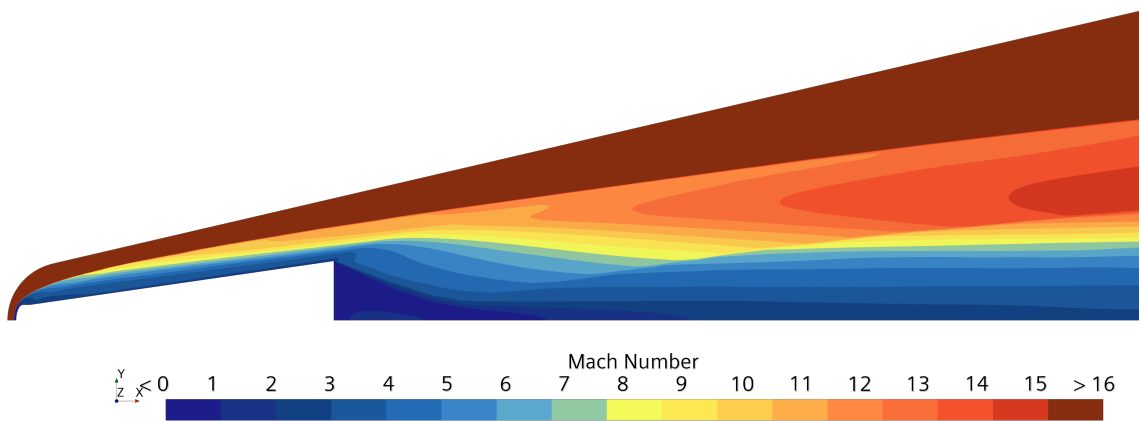


Figure 4.23: Mach number, $M_\infty = 16$ and $Z_a = 20$ km.

Simcenter STAR-CCM+

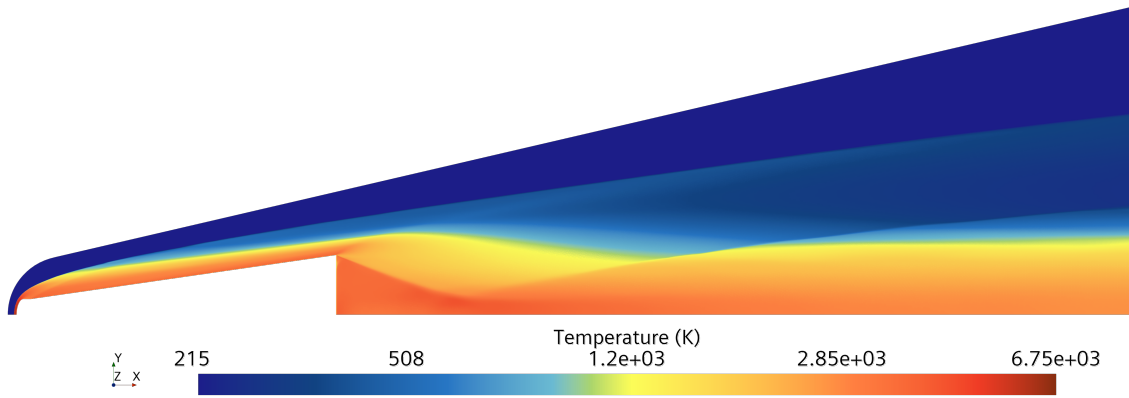


Figure 4.24: temperature, $M_\infty = 16$ and $Z_a = 20$ km.

Simcenter STAR-CCM+

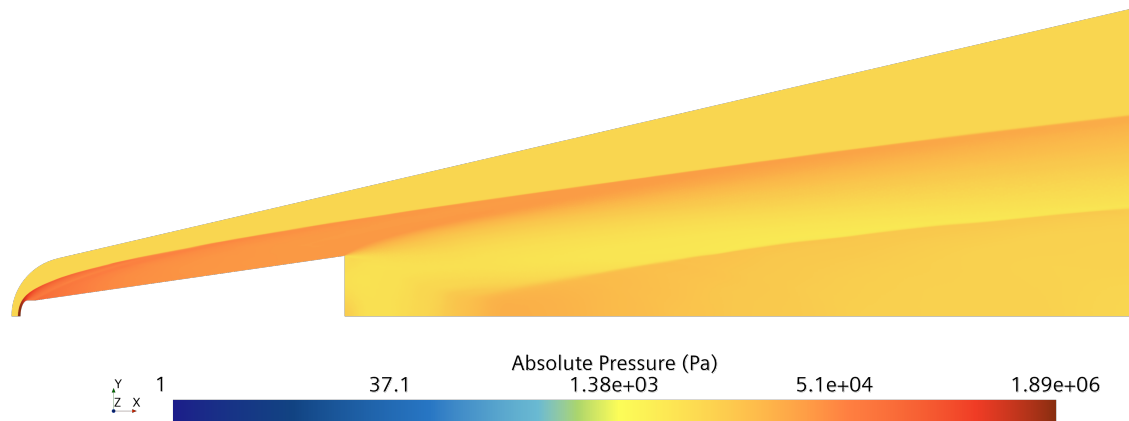


Figure 4.25: pressure, $M_\infty = 16$ and $Z_a = 20$ km.

Simcenter STAR-CCM+

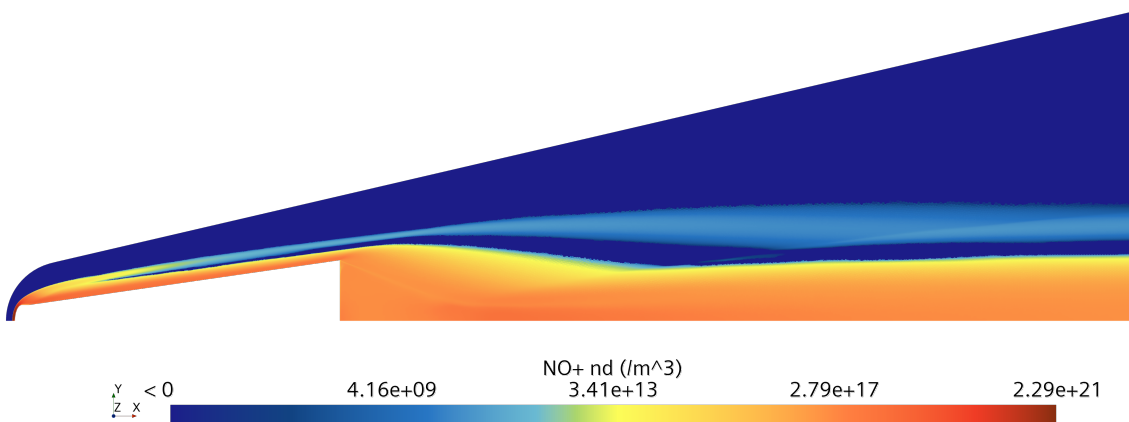
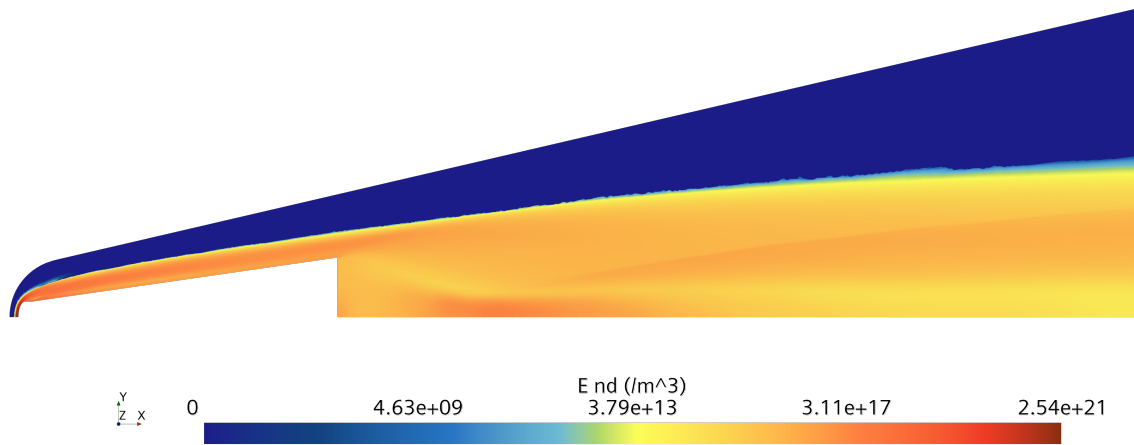
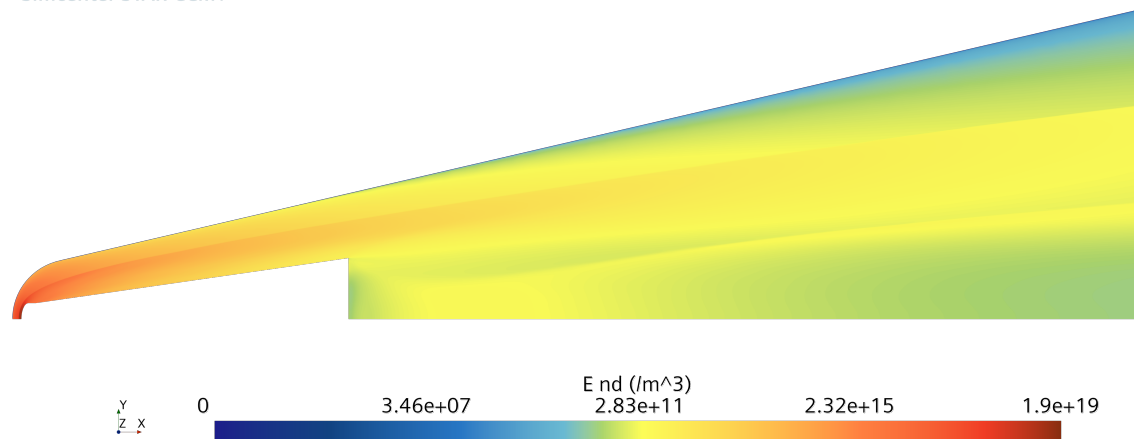


Figure 4.26: NO^+ number density, $M_\infty = 16$ and $Z_a = 20$ km.

Simcenter STAR-CCM+

Figure 4.27: electron number density, $M_\infty = 16$ and $Z_a = 20$ km.

Simcenter STAR-CCM+

Figure 4.28: electron number density, $M_\infty = 14$ and $Z_a = 50$ km.

Chapter 5

Conclusions

In this thesis work the chemical equilibrium in hypersonic flows has been widely investigated. For all the standard air models it has been analysed their chemical composition in a wide range of thermodynamic states. This study allowed to identify the most relevant species and to evaluate which temperature and pressure ranges trigger the formation of ionized species which contribute to the plasma production. The numerical simulations performed on a cone-like axisymmetric body were executed in order to monitor the plasma production over a blunt body and how ionized gas species spread in the wake region. Different free stream boundary conditions were applied and the parametric study of the numerical solutions has helped to describe the effects that Mach number and altitude have on plasma formation. Thermodynamic property polynomial fits were compared in a limited number of scenarios, however no discrepancies between the analysed models were highlighted: this aspect needs a deeper investigation study in order to assess how the differences in the curve fits affect the fluid dynamics, especially at temperature higher than 1×10^4 K. All the simulation used a seven species air model, which besides electrons, includes only NO^+ as ionized species. Since from the chemical equilibrium study has been highlighted that NO^+ is the first significant ionized species at relatively low temperature, it is conceivable that at higher free stream Mach number the seven species air model does not adequately model the hypersonic flow field. Using an improved air model that contains other ionized species (e.g. N^+ and O^+), besides the higher numerical cost, does not guarantee an improvement in the physical description since the charged particle modelling is not adequate in the physical model implemented in STAR-CCM+ (no ambipolar diffusion has been taken into consideration). Furthermore, the large discrepancies that can be recognized in drag coefficient, stand-off distance and ionized nitric oxide number density when $Z_a = 70$ km cases are compared with the lower altitudes numerical results, are probably linked to the different flow regime, due to the lower Reynolds number ($Re_{L=1} \approx 1 \times 10^4$). However, it would be necessary to evaluate a laminar modelling for $Z_a = 70$ km and eventually better understand and justify the flow behaviour in the range 50 to 70 km through other numerical simulation.

Appendix A

Standard Earth's atmosphere models

A so called standard atmosphere model is a rational way to describe how thermodynamic variables of air, such as temperature, pressure and density, change varying the altitude. What this model returns it is an approximation of the state of the Earth's atmosphere that - as anyone knows from his personal experience - changes continuously with time. For a series of obvious reasons, such as calibration of instrumentations and aircraft or rocket performance evaluations throughout their design, a first standard atmospheric model were published by the United States NACA in the 1922 [13], providing information up to 20 km above MSL [25]. Further historical informations about reference atmosphere models can be found in [13, 25]. At the moment both the COESA U. S. Standard Atmosphere (1976) [17] and the ICAO Standard Atmosphere (1993) [18] provide a consistent and pertinent description of the vertical distribution temperature, pressure and density inside the Earth's homosphere (see figure A.1).

A.1 Geo-potential and geometric altitudes

Introducing the gravity potential Φ_g , defined as

$$\Phi_g(z_a) := \int_0^{z_a} g_a(z_a) dz_a, \quad (\text{A.1})$$

the *geo-potential altitude*, which is a way to measure altitude based on gravitational equipotentials, is specified by the following expression:

$$Z_a := \frac{\Phi_g(z_a)}{g_0}. \quad (\text{A.2})$$

Since geo-potential and geometric altitudes are not equal, can be derived the relation between the two quantities. It is noted, for the purpose of this atmospheric models, that

$$g \propto r^{-2} \quad g_0 \propto r_0^{-2},$$

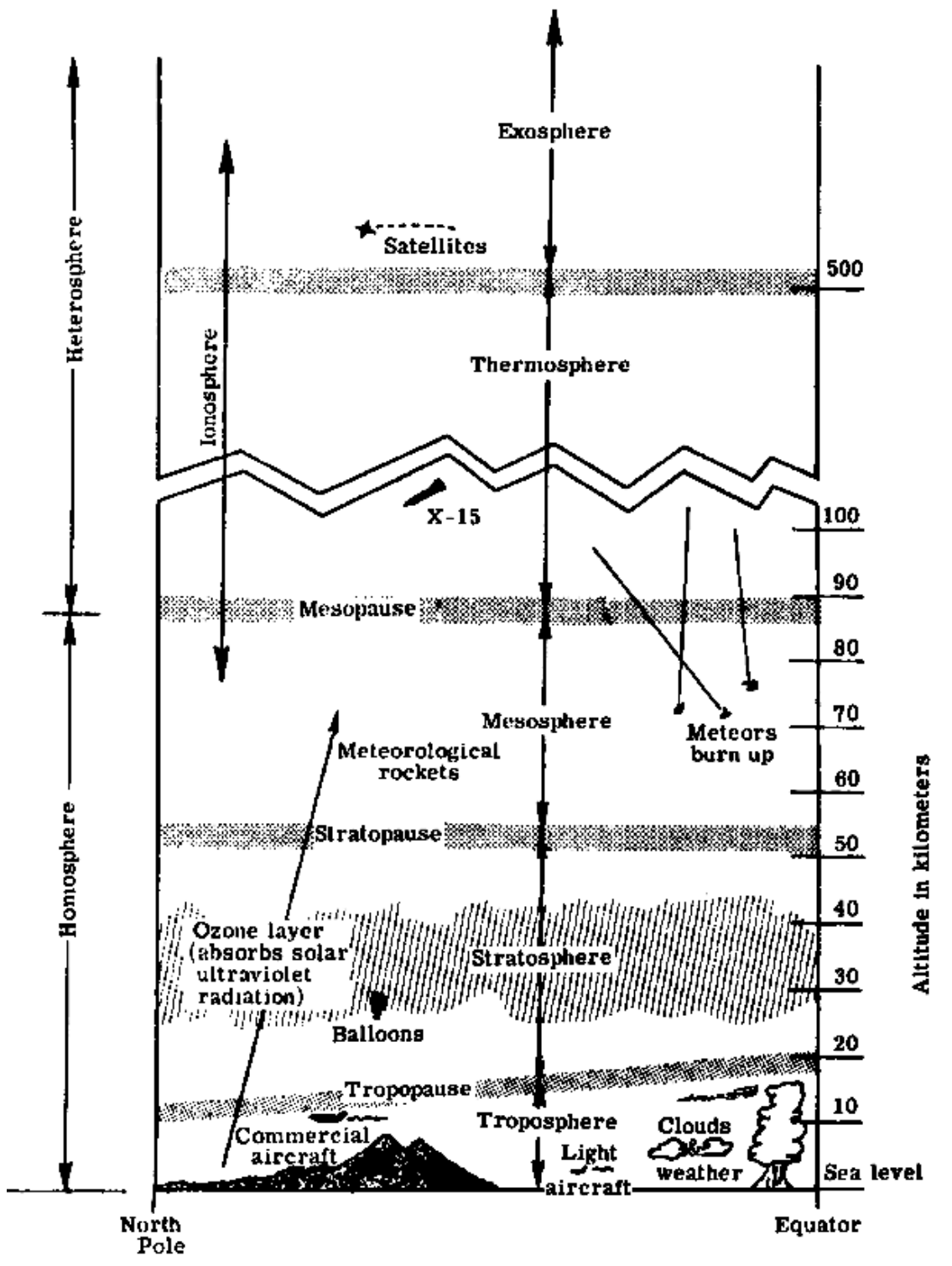


Figure A.1: Earth's atmospheric structure [25].

where $r < r_0$ is a geometric length correlated with the altitude. So the gravitational acceleration changes with the geometric altitude with the following law:

$$g(z_a) = g_0 \left(\frac{r_0}{r_0 + z_a} \right)^2. \quad (\text{A.3})$$

The integrand function of equation (A.1) has now an explicit form, so the integral can be calculated and the following relation can be found:

$$Z_a = \frac{r_0 z_a}{r_0 + z_a}, \quad z_a = \frac{r_0 Z_a}{r_0 - z_a}. \quad (\text{A.4})$$

A.2 Atmosphere composition

The standard atmosphere model taken in consideration [17] assume a constant composition and dry¹ gaseous mixture for $Z_a \lesssim 95$ km [18]. Further information about chemical composition of the Earth's atmosphere can be found in [17]: these information are not relevant for the purposes of this work. The composition of dry air in reported in table A.1.

A.3 Physical characterization of the Earth's atmosphere

The model assumes defined values of air pressure, temperature and density at MSL:

$$\begin{aligned} p_0 &= 1.01325 \times 10^5 \text{ Pa}, \\ T_0 &= 288.15 \text{ K}, \\ \rho_0 &= 1.225 \text{ kg m}^{-3}. \end{aligned}$$

The other characteristic quantities (speed of sound, mean free path, dynamic viscosity and so on) can be derived in a second place.

A.3.1 Vertical temperature gradient

The Earth's atmosphere can be represented as several layer stacked on top of each other (figure A.1). Each layer has its own vertical temperature gradient that can be well represented by the following law:

$$T = T_b + \beta (Z_a - Z_{a,b}), \quad (\text{A.5})$$

where T_b and $Z_{a,b}$ are respectively the temperature and the geo-potential altitude of the lower limit of the layer concerned and β is basically the vertical temperature gradient, which can be assumed constant for each individual layer. A comprehensive schematization summarizes the vertical gradient throughout the Earth's homosphere is reported in table A.2.

¹no gaseous water is considered.

Gas	Molar fraction (%)	Molar mass (kg kmol ⁻¹)
Nitrogen (N ₂)	78.084	28.0134
Oxygen (O ₂)	20.9476	31.9988
Argon (Ar)	0.934	39.948
Carbon dioxide (CO ₂)	0.0314*	44.00995
Neon (Ne)	1.828×10^{-3}	20.183
Helium (He)	5.240×10^{-4}	4.0026
Krypton (Kr)	1.140×10^{-4}	83.80
Xenon (Xe)	8.7×10^{-6}	131.30
Hydrogen(H ₂)	50.0×10^{-6}	2.01594
Nitrogen monoxide (N ₂ O)	50.0×10^{-6} *	44.0128
Methane (CH ₄)	2×10^{-4}	16.04303
Ozone (O ₃)	in summer up to 7.0×10^{-6} *	47.9982
	in winter up to 2.0×10^{-6} *	47.9982
Sulphur dioxide (SO ₂)	up to 1×10^{-4} *	64.0628
Nitrogen dioxide (NO ₂)	up to 2.0×10^{-6} *	46.0055
Iodine (I ₂)	up to 1.0×10^{-6} *	253.8088
Dry air	100	28.964420**

* The content of the gas may undergo significant variations from time to time or from place to place.

** This value is obtained from equation (A.6).

Table A.1: dry, clean air composition near sea level [18].

Geo-potential altitude (km)	Temperature (K)	Temperature gradient (K km ⁻¹)	Notes
-5.00	320.65	-6.50	Lower limit [18]
0.00	288.15	-6.50	
11.00	216.65	0.00	
20.00	216.65	+1.00	
32.00	228.65	+2.80	
47.00	270.65	0.00	
51.00	270.65	-2.80	
71.00	214.65	-2.00	
80.00	196.65	—	Upper limit [18]
84.8520	186.87	—	Upper limit*[17]

* COESA in [17] extends the upper limit of the entire standard model up to a geometric height of 1000 km. The outer layers of Earth's atmosphere still not so relevant in this thesis work.

Table A.2: temperatures and vertical temperature gradients [17, 18].

A.3.2 Pressure

The model treats the air as a perfect gas, so the perfect gas law still holds for altitudes sufficiently low. The molar mass of air can be calculated as follows:

$$\mathcal{M}_0 := \frac{\rho_0 \mathcal{R} T_0}{p_0}, \quad (\text{A.6})$$

such that

$$R_0 = \frac{\mathcal{R}}{\mathcal{M}_0}.$$

Since equilibrium is assumed, from hydrostatic balance

$$dp(z_a) = -g_a \rho dz_a,$$

which holds for altitudes below 86 km, with the perfect gas law the following expression can be obtained:

$$d(\ln p) = -\frac{g_a}{R_0 T} dz_a.$$

The integrand function can be rewritten in explicit form using equations (A.3) to (A.5). The following relation between pressure and geo-potential altitude can be obtained by

performing the integral:

$$p = p_b \left[1 + \frac{\beta}{T_b} (Z_a - Z_{a,b}) \right]^{-\frac{g_0}{\beta R_0}} \quad \text{for } \beta \neq 0,$$
$$p = p_b \exp \left[-\frac{g_0}{R_0 T_b} (Z_a - Z_{a,b}) \right] \quad \text{for } \beta = 0.$$

A.3.3 Density

Air density is calculated using perfect gas law, just knowing pressure and temperature:

$$\rho = \frac{p}{R_0 T}.$$

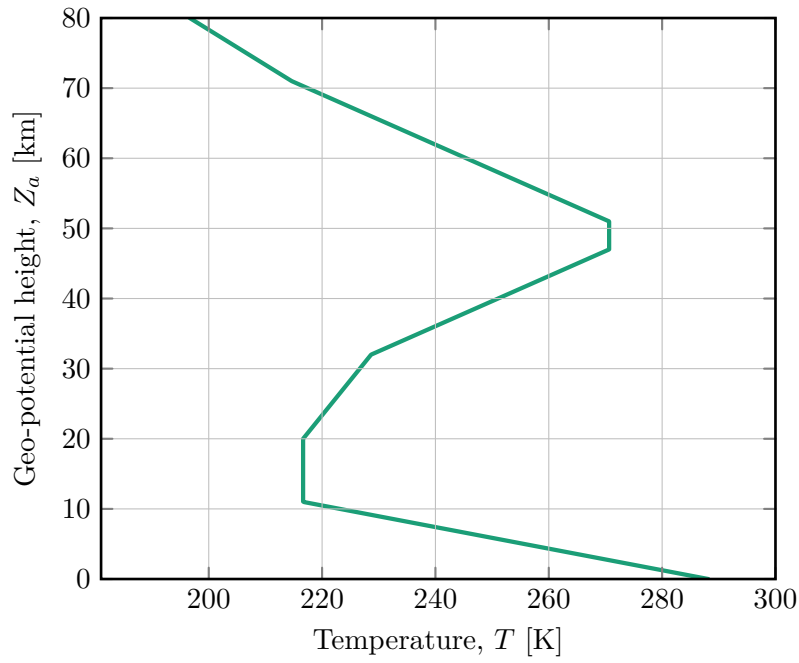


Figure A.2: temperature vertical distribution [18].

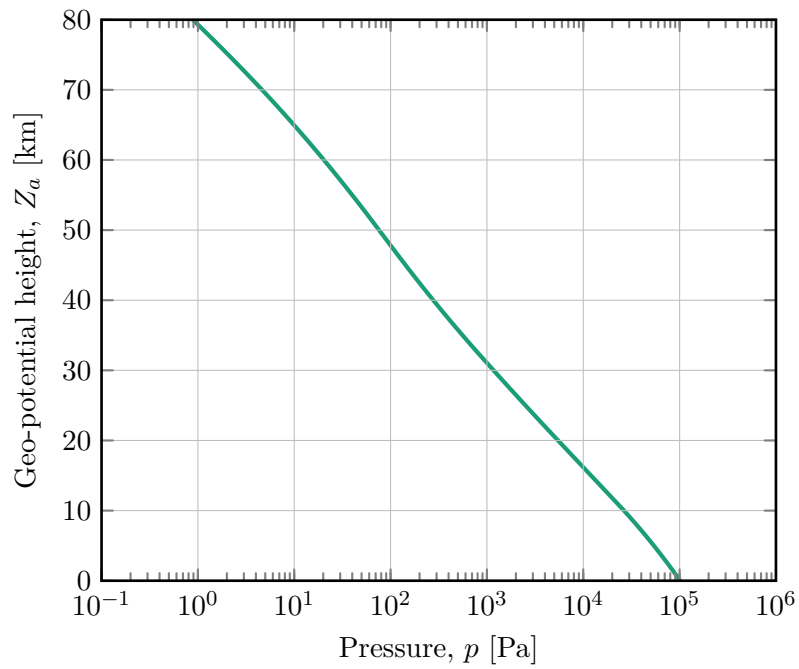


Figure A.3: pressure vertical distribution [18].

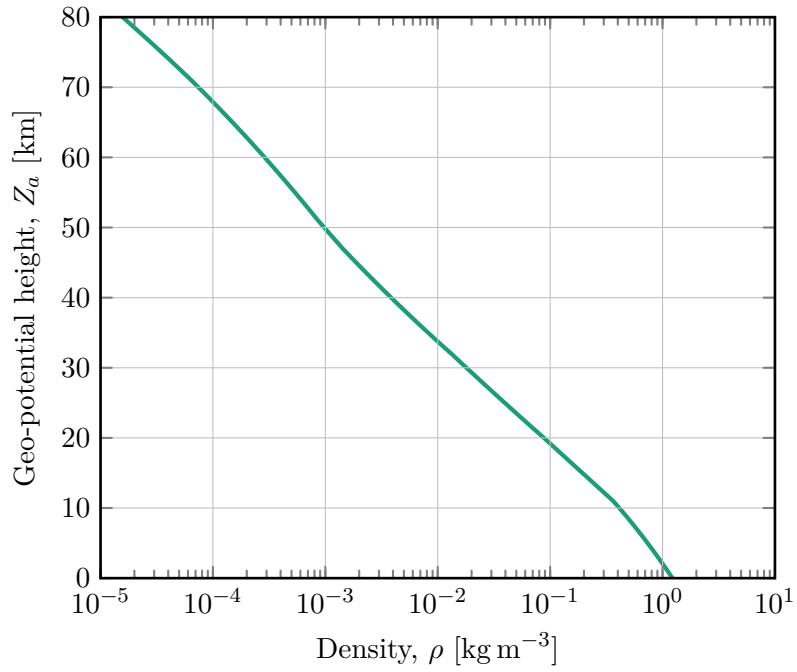


Figure A.4: density vertical distribution [18].

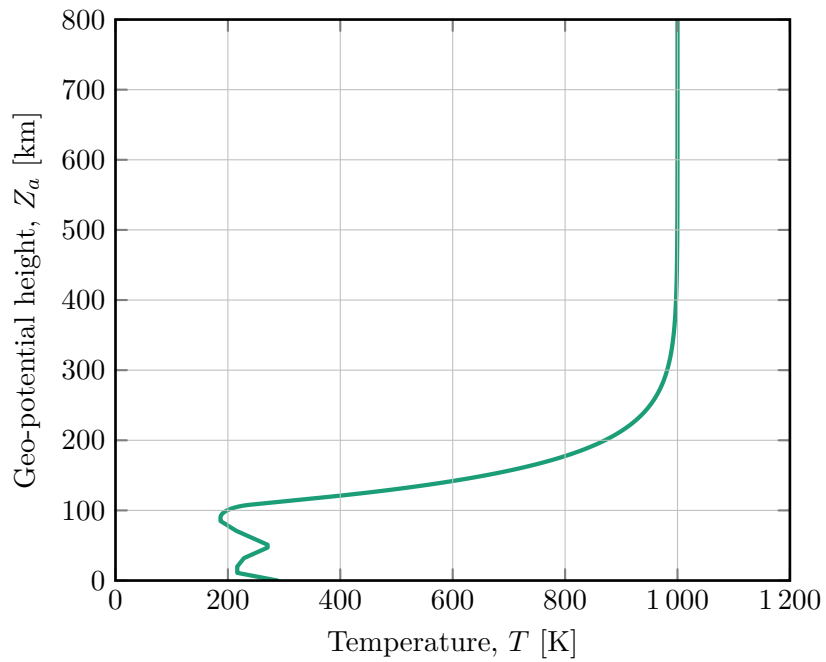


Figure A.5: extended temperature vertical distribution [17].

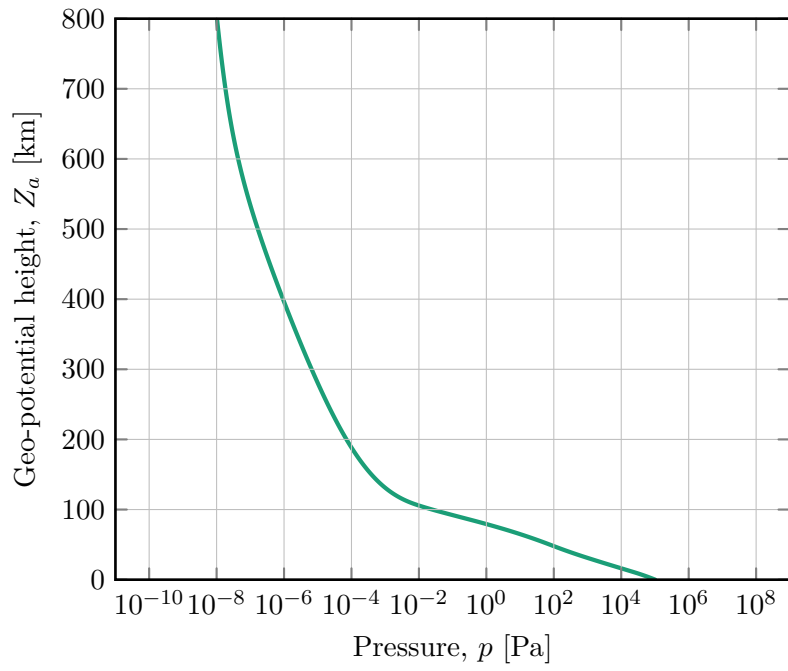


Figure A.6: extended pressure vertical distribution [17].

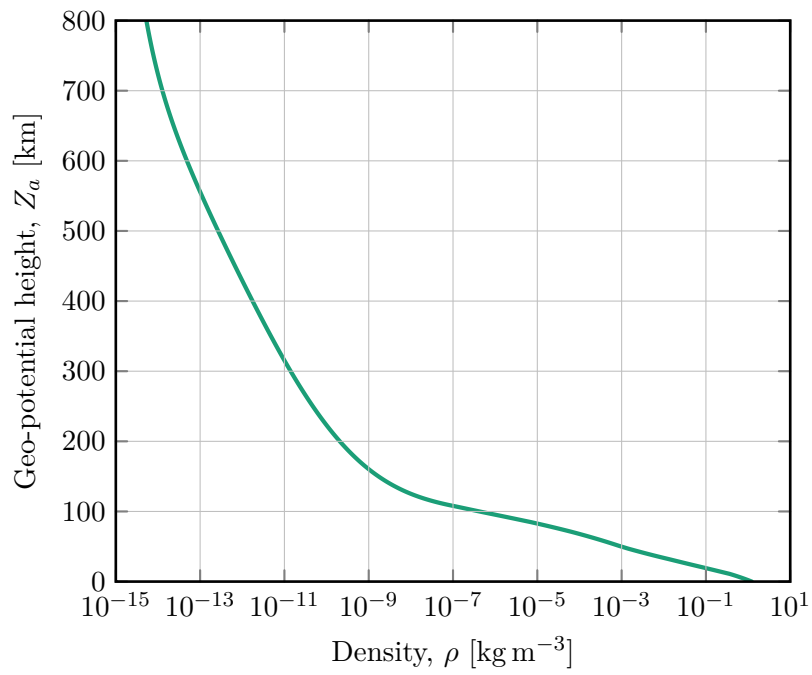


Figure A.7: extended density vertical distribution [17].

Appendix B

Thermochemical properties

In order to provide chemical reaction mechanism and thermodynamic properties of gas species, STAR-CCM+ allows CHEMKIN input files. A full description of the format of the files can be found in [6].

B.1 Chemical mechanism file format

It is divided in three sections:

element list: elements involved in the mixture model;

species list: species involved in the mixture model;

reaction mechanisms: all the chemical reaction involved in the mixture model. The list includes all the coefficient of the Arrhenius modified equation (1.40) for the forward reaction rates.

B.2 Thermodynamic properties

Thermodynamic properties are described using curve fits, all coefficient and temperature ranges are stored in plain text files with specific format [6]. Several authors [11, 15, 16, 4] proposed polynomial that best fit experimental results in terms of thermodynamic properties produced in the NASA Chemical Equilibrium program. In particular from the literature review, thermodynamic data are stored as polynomials with seven or nine coefficients with different temperature ranges.

B.2.1 Seven coefficients polynomials

The polynomials are the following:

$$\begin{aligned} \frac{C_p}{\mathcal{R}}(T) &= a_1 + a_2 T + a_3 T^2 + a_4 T^3 + a_5 T^4 \\ \frac{\mathcal{H}^\circ}{\mathcal{R}T}(T) &= a_1 + \frac{a_2}{2} T + \frac{a_3}{3} T^2 + \frac{a_4}{4} T^3 + \frac{a_5}{5} T^4 + \frac{a_6}{T} \\ \frac{\mathcal{S}^\circ}{\mathcal{R}}(T) &= a_1 \ln T + a_2 T + \frac{a_3}{2} T^2 + \frac{a_4}{3} T^3 + \frac{a_5}{4} T^4 + a_7. \end{aligned} \tag{B.1}$$

B.2.2 Nine coefficients polynomials

The polynomials are the following:

$$\begin{aligned}\frac{C_p}{\mathcal{R}}(T) &= a_1 T^{-2} + a_2 T^{-1} + a_3 + a_4 T + a_5 T^2 + a_6 T^3 + a_7 T^4 \\ \frac{\mathcal{H}^\circ(T)}{\mathcal{R}T} &= -a_1 T^{-2} + a_2 \frac{\ln T}{T} + a_3 + \frac{a_4}{2} T + \frac{a_5}{3} T^2 + \frac{a_6}{4} T^3 + \frac{a_7}{5} T^4 + \frac{b_1}{T} \\ \frac{\mathcal{S}^\circ(T)}{\mathcal{R}} &= -\frac{a_1}{2} T^{-2} + a_2 T^{-1} + a_3 \ln T + a_4 T + \frac{a_5}{2} T^2 + \frac{a_6}{3} T^3 + \frac{a_7}{4} T^4 + b_2.\end{aligned}\quad (\text{B.2})$$

For both seven and nine coefficient fits $\mathcal{H}^\circ(T)$ and $\mathcal{S}^\circ(T)$ are evaluate as follows:

$$d\mathcal{H}^\circ(T) = C_p(T) dT$$

$$d\mathcal{S}^\circ(T) = C_p(T) \frac{dT}{T},$$

so b_1 and b_2 are the constants of integration for the nine coefficient fit whereas a_6 and a_7 for the seven coefficient fit.

B.3 Input file examples

Here are reported a chemical mechanism file and a thermochemical properties file [4].

Chemical mechanism file

```
ELEMENTS
N O E
END
SPECIES
N2 O2 NO N O NO+ E
END
REACTIONS J/KMOL
O2 + 1N = 2O + 1N 1.000000e+22 -1.500000 4.935190e+08
1O + 1O2 = 3O 1.000000e+22 -1.500000 4.935190e+08
1O2 + 1N2 = 2O + 1N2 2.000000e+21 -1.500000 4.935190e+08
2O2 = 2O + 1O2 2.000000e+21 -1.500000 4.935190e+08
1NO + 1O2 = 2O + 1NO 2.000000e+21 -1.500000 4.935190e+08
1N + 1N2 = 3N 3.000000e+22 -1.600000 9.411448e+08
1O + 1N2 = 1O + 2N 3.000000e+22 -1.600000 9.411448e+08
2N2 = 2N + 1N2 7.000000e+21 -1.600000 9.411448e+08
1O2 + 1N2 = 2N + 1O2 7.000000e+21 -1.600000 9.411448e+08
1NO + 1N2 = 2N + 1NO 7.000000e+21 -1.600000 9.411448e+08
1N + 1NO = 1O + 2N 1.100000e+17 0.000000 6.277070e+08
1O + 1NO = 2O + 1N 1.100000e+17 0.000000 6.277070e+08
1NO + 1N2 = 1O + 1N + 1N2 5.000000e+15 0.000000 6.277070e+08
1NO + 1O2 = 1O + 1N + 1O2 5.000000e+15 0.000000 6.277070e+08
2NO = 1O + 1N + 1NO 1.100000e+17 0.000000 6.277070e+08
1O + 1NO = 1N + 1O2 8.400000e+12 0.000000 1.612916e+08
1O + 1N2 = 1N + 1NO 5.700000e+12 0.420000 3.569865e+08
1E + 1N2 = 1E + 2N 3.000000e+24 -1.600000 9.411448e+08
1O + 1N = 1E + 1NO+ 5.300000e+12 0.000000 2.652166e+08
1NO+ + 1N2 = 1NO+ + 2N 7.000000e+21 -1.600000 9.411448e+08
1NO+ + 1O2 = 1NO+ + 2O 2.000000e+21 -1.500000 4.935190e+08
END
```

Thermodynamic properties file

```

THERMO
O2 REF ELEMENT      RUS 890  2  0  0  OG  200.000  6000.000  1000.      1
 3.66096065E+00 6.56365811E-04-1.41149627E-07 2.05797935E-11-1.29913436E-15  2
-1.21597718E+03 3.41536279E+00 3.78245636E+00-2.99673416E-03 9.84730201E-06  3
-9.68129509E-09 3.24372837E-12-1.06394356E+03 3.65767573E+00 0.00000000E+00  4
O      L 1/900  1  0  0  OG  200.000  6000.000  1000.      1
 2.54363697E+00-2.73162486E-05-4.19029520E-09 4.95481845E-12-4.79553694E-16  2
 2.92260120E+04 4.92229457E+00 3.16826710E+00-3.27931884E-03 6.64306396E-06  3
-6.12806624E-09 2.11265971E-12 2.91222592E+04 2.05193346E+00 2.99687009E+04  4
N2 REF ELEMENT      G 8/O2N  2.  0.  0.  0.G  200.000  6000.000  1000.      1
 2.95257637E+00 1.39690040E-03-4.92631603E-07 7.86010195E-11-4.60755204E-15  2
-9.23948688E+02 5.87188762E+00 3.53100528E+00-1.23660988E-04-5.02999433E-07  3
 2.43530612E-09-1.40881235E-12-1.04697628E+03 2.96747038E+00 0.00000000E+00  4
N      L 6/88N  1  0  0  OG  200.000  6000.000  1000.      1
 0.24159429E+01 0.17489065E-03-0.11902369E-06 0.30226244E-10-0.20360983E-14  2
 0.56133775E+05 0.46496095E+01 0.25000000E+01 0.00000000E+00 0.00000000E+00  3
 0.00000000E+00 0.00000000E+00 0.56104638E+05 0.41939088E+01 0.56850013E+05  4
NO     RUS 89N  10  1  0  OG  200.000  6000.000  1000.      1
 3.26071234E+00 1.19101135E-03-4.29122646E-07 6.94481463E-11-4.03295681E-15  2
 9.92143132E+03 6.36900518E+00 4.21859896E+00-4.63988124E-03 1.10443049E-05  3
-9.34055507E-09 2.80554874E-12 9.84509964E+03 2.28061001E+00 1.09770882E+04  4
NO+    RUS 89N  10  1E -1  OG  298.150  6000.000  1000.      1
 2.94587702E+00 1.40325260E-03-4.95503196E-07 7.95948973E-11-4.72076668E-15  2
 1.18244340E+05 6.70644634E+00 3.69301231E+00-1.34229158E-03 2.67343395E-06  3
-1.02609308E-09-6.95610492E-14 1.18103055E+05 3.09126691E+00 1.19166025E+05  4
E electron gas  g12/98E  1.  0.  0.  0.G  298.150  6000.000  1000.      1
 2.50000000E+00 0.00000000E+00 0.00000000E+00 0.00000000E+00 0.00000000E+00  2
-7.45375000E+02-1.17208122E+01 2.50000000E+00 0.00000000E+00 0.00000000E+00  3
 0.00000000E+00 0.00000000E+00-7.45375000E+02-1.17208122E+01 0.00000000E+00  4
END

```


Bibliography

- [1] John D. Anderson. *Hypersonic and High-Temperature Gas Dynamics, Third Edition*. American Institute of Aeronautics and Astronautics, Inc., Jan. 2019. DOI: [10.2514/4.105142](https://doi.org/10.2514/4.105142).
- [2] Frederick S. Billig. “Shock-wave shapes around spherical-and cylindrical-nosed bodies.” In: *Journal of Spacecraft and Rockets* 4.6 (June 1967), pp. 822–823. DOI: [10.2514/3.28969](https://doi.org/10.2514/3.28969).
- [3] Carlo Brunelli. “Thermochemical Models for Hypersonic Regime”. MA thesis. Politecnico di Torino, Corso di laurea magistrale in Ingegneria Aerospaziale, 2021.
- [4] Alexander Burcat and Branko Ruscic. *Third millenium ideal gas and condensed phase thermochemical database for combustion (with update from active thermochemical tables)*. Tech. rep. Argonne National Lab.(ANL), Argonne, IL (United States), 2005.
- [5] Domenic D’Ambrosio. *Fluidodinamica nel volo spaziale - Lecture Notes*. AY 2022-2023. 2023.
- [6] Reaction Design. “CHEMKIN A Software Package for the Analysis of Gas-Phase Chemical and Plasma Kinetics”. In: *no. September* (2000), pp. 1–181.
- [7] Salvatore Esposito. “Numerical simulation of high-speed and high temperature reacting flows using a commercial CFD software”. MA thesis. Politecnico di Torino, Corso di laurea magistrale in Ingegneria Aerospaziale, 2021.
- [8] Enrico Fermi. *Termodinamica*. Bollati Boringhieri, 1972. ISBN: 9788833951829.
- [9] Dmitry Garanin. *Statistical physics*. May 2021. URL: https://www.lehman.edu/faculty/dgaranin/Statistical_Thermodynamics/Statistical_physics.pdf.
- [10] Bernard Grossman. *Fundamental Concepts of Real Gasdynamics*. Version 3.09. Jan. 2000. URL: https://www.aoe.vt.edu/content/dam/aoe_vt_edu/programs/graduate/forms/lectnotes3-09A11101812.pdf.
- [11] Roop N. Gupta et al. “A review of reaction rates and thermodynamic and transport properties for an 11-species air model for chemical and thermal nonequilibrium calculations to 30000 K”. in: (1990).
- [12] L.P. Harrison. “Relation Between Geopotential and Geometric Height”. In: *Robert List, Sixth Editions* (1951), pp. 217–219.
- [13] Dale L. Johnson et al. “Reference and standard atmosphere models”. In: *10th Conference on Aviation, Range, and Aerospace Meteorology*. 2002.
- [14] Eric Jones, Travis Oliphant, Pearu Peterson, et al. *SciPy: Open source scientific tools for Python*. 2001–. URL: <http://www.scipy.org/>.
- [15] R. Kee, F. Rupley, and J. Miller. *The Chemkin Thermodynamic Data Base*. Tech. rep. Mar. 1990. DOI: [10.2172/7073290](https://doi.org/10.2172/7073290).

- [16] Bonnie J. McBride, M.J. Zehe, and S. Gordon. *NASA Glenn coefficients for calculating thermodynamic properties of individual species* NASA. tech. rep. TP-2002, 2002.
- [17] National Oceanic and Atmospheric Administration. “US standard atmosphere, 1976”. In: *Technical Report* (1976).
- [18] International Civil Aviation Organization. *Manual of the ICAO Standard Atmosphere: extended to 80 kilometres (262 500 feet)*. Vol. 7488. International Civil Aviation Organization, 1993.
- [19] Chul Park, Richard L. Jaffe, and Harry Partridge. “Chemical-Kinetic Parameters of Hyperbolic Earth Entry”. In: *Journal of Thermophysics and Heat Transfer* 15.1 (Jan. 2001), pp. 76–90. DOI: [10.2514/2.6582](https://doi.org/10.2514/2.6582).
- [20] Carlos Alberto Rocha Pimentel and Annibal Hetem Jr. “Computation of air chemical equilibrium composition until 30000K - Part I”. in: *Journal of Aerospace Technology and Management* 3.2 (2011), pp. 111–126. ISSN: 2175-9146. DOI: [10.5028/jatm.2011.03021011](https://doi.org/10.5028/jatm.2011.03021011).
- [21] Ji-Wei Qian, Hai-Li Zhang, and Ming-Yao Xia. “Modelling of Electromagnetic Scattering by a Hypersonic Cone-Like Body in Near Space”. In: *International Journal of Antennas and Propagation* 2017 (2017), pp. 1–11. DOI: [10.1155/2017/3049532](https://doi.org/10.1155/2017/3049532).
- [22] Alfio Quarteroni, Riccardo Sacco, and Fausto Saleri. *Matematica numerica*. Springer Science & Business Media, 2010.
- [23] Siemens Digital Industries Software. *Simcenter STAR-CCM+ User Guide v. 2206*. Version 2206.0001 Build 17.04.008. Siemens 2022.
- [24] Roger A. Svehla. *Transport coefficients for the NASA Lewis chemical equilibrium program*. Tech. rep. 1995.
- [25] Theodore A. Talay. *Introduction to the Aerodynamics of Flight*. Tech. rep. 1975.
- [26] Walter G. Vincenti. *Introduction to physical gas dynamics*. Krieger, 1975, p. 538. ISBN: 0882753096.